Galerkin Models Enhancements for Flow Control

Gilead Tadmor[†], Oliver Lehmann[†],
Bernd R. Noack[‡], and Marek Morzyński[§]

[†]Electrical & Comp. Engineering Department, Northeastern University, Boston, MA 02115, USA, tadmor@coe.neu.edu, olehmann@coe.neu.edu

[‡]Institute Pprime, CNRS – Universityé de Poitiers – ENSMA, UPR 3346, Département Fluides, Thermique, Combustion, CEAT, 43, rue de l'Aérodrome, F-86036 Poitiers cedex, France, bernd.noack@univ-poitiers.fr

[§]Poznań University of Technology, Institute of Combustion Engines and Transportation, PL 60-965 Poznań, Poland, marek.morzynski@put.poznan.pl

Abstract Low order Galerkin models were originally introduced as an effective tool for stability analysis of fixed points and, later, of attractors, in nonlinear distributed systems. An evolving interest in their use as low complexity dynamical models, goes well beyond that original intent. It exposes often severe weaknesses of low order Galerkin models as dynamic predictors and has motivated efforts, spanning nearly three decades, to alleviate these shortcomings. Transients across natural and enforced variations in the operating point, unsteady inflow, boundary actuation and both aeroelastic and actuated boundary motion, are hallmarks of current and envisioned needs in feedback flow control applications, bringing these shortcomings to even higher prominence. Building on the discussion in our previous chapters, we shall now review changes in the Galerkin paradigm that aim to create a mathematically and physically consistent modeling framework, that remove what are otherwise intractable roadblocks. We shall then highlight some guiding design principles that are especially important in the context of these models. We shall continue to use the simple example of wake flow instabilities to illustrate the various issues, ideas and methods that will be discussed in this chapter.

1 Introduction

The essence of feedback control is the ability to utilize realtime sensing, decision making and actuation, to manipulate the unsteady dynamics of a system subject to disturbances, uncertainties and time variations in the

operating regime over a wide range of time scales. One of a multitude of pertinent examples that come to mind is the aerodynamic control of a small unmanned air vehicle (UAV / MAV): Indeed, the UAV may have to track far more complex flight trajectories, and face changes in wind speed and orientation, let alone the impact of irregular gusts on aerodynamic forces, that are far higher, in relative terms, than in the case of larger aircraft. This example therefore brings into sharp relief the significance of unsteadiness in feedback control applications that are the subject matter of the yet nascent field of feedback flow control.

Models used in feedback design and implementation reflect the need to reconcile the conflicting demands of precision, time horizon and dynamic envelope, on the one hand, and complexity restrictions imposed by analytic design methods and feasible realtime computations, on the other hand. An ensemble of mathematically rigorous methods to address this balancing act has been developed within mainstream linear systems theory: With a high fidelity, high order model as a starting point, operator theoretic model reduction procedures are associated with provable error bounds that quantify the tradeoff between simplicity, precision and closed loop performance (Antoulas, 2005; G. Obinata, 2000; Sánchez-Peña and Sznaier, 1998). The feasibility of that level of rigor is largely lost in complex, nonlinear systems. In fact, even the computations required by linear reduced order models, e.g., the solution of Lyapunov and Riccati equations, become a formidable task at very high nominal dimension, requiring an appeal to simulation based approximations (Rowley, 2005). Adaptation of linear methods to nonlinear systems, analytical methods based on differential-geometric, energy and stochastic dynamical systems considerations, are often based on asymptotic convergence arguments, heuristics and, at best, on local error bounds (Nijmeijer and van der Schaft, 1990; Rowley et al., 2003; Mezić, 2005; Homescu et al., 2005; Gorban et al., 2006; Schilders et al., 2008).

The combined effects of nonlinearity, high dimension and the rich dynamic repertoire of fluid mechanical systems, bring the tension between model precision, dynamic envelope and simplicity demands to an extreme. This tension has lead to the evolution of low order models, identified directly from experimental or simulation models, as alternatives to the top-down, model reduction approach. Notable examples include black box linear models (Cattafesta et al., 2008), low order Galerkin models (Holmes et al., 1998), and more sporadically, Lagrangian vortex models (Protas, 2008). Yet these alternative approaches lack a rigorous supportive theory that explicitly quantifies the tradeoff between model fidelity and its complexity. Indeed, despite decades of efforts, low order models of natural and actuated fluid flow systems often fail to meet the needs of viable engineering design.

Following on the authors' previous two chapters, we maintain our focus on Galerkin models, and direct the reader to those chapters for a discussion motivating this focus. Our purpose here is to further elucidate the root causes for pronounced shortcomings and failures of prevalent low order Galerkin modeling methods, and to use these observations as a basis for the development of an extended framework of Galerkin models on nonlinear manifolds. Specifically, we shall review inherent conflicts between the traditional Galerkin paradigm and the requirements of flow control applications, which give rise to persistent failures, and develop the proposed framework, expressly, to remove these inconsistencies. Finally, we will highlight essential guidelines for the utilization of the new paradigm in flow control design. The discussion will cover aspects of mean field theory, turbulence models, mode deformation, actuation models and forced and elastic boundary motion.

Nomenclature and formalism. Unless otherwise stated, the mathematical formalisms and nomenclature used in this chapter follow those set in the appendix and used in our previous chapter, by Noack et al. To facilitate reading we shall nonetheless remind the reader, of some of these conventions when using them.

2 Benchmark Model Systems

We shall use two model systems to illustrate the discussion in this chapter: The laminar wake flow behind a two dimensional cylinder at the Reynolds number $Re = 100$, will continue to be used as the main running example. The separated, turbulent flow over a two dimensional airfoil at a high angle of attack, at $Re = 10^6$, will be used as a supplementary example, to illustrate peculiar aspects of high frequency actuation. This section reviews the geometry, the postulated actuators, and some basic facts regarding the dynamics of these two examples. It also serves as a reminder of some of our basic nomenclature.

2.1 The Cylinder Wake

The two dimensional flow in the wake of a circular cylinder is an extensively studied canonical configuration. A systematic analysis of the instability of the steady flow and of the nature of a characteristic periodic attractor were first introduced in the celebrated work of von Kármán (von Kármán and Rubach, 1912), a century ago, with numerous subsequent studies in diverse natural and actuated contexts, continuing to the present day. The general interest and our own selection of this configuration stem from the

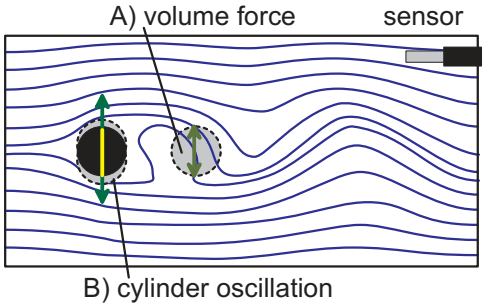

Figure 1. The actuated cylinder wake: The cylinder is represented by the black disk. The downstream circle and arrows indicate the location and orientation of a volume-force actuator. The vertical arrows across the cylinder represent controlled vertical oscillations as an alternative, second form of actuation. Streamlines represent a snapshot of the natural flow.

fact that it is one of the simplest possible examples of the bifurcations from potential to vortical flow, at $Re \approx 4$, and then, to periodic instability with the emergence of vortex shedding and the von Kármań vortex street, at $Re \approx 47$ (Noack and Eckelmann, 1994; Williamson, 1996; Barkley, 2006).

2.2 The Actuated Cylinder Wake Configuration

Figure 1 depicts the key elements of this example. As in previous discussions, the incoming flow and the transverse direction are aligned with the x and y coordinates, respectively. The cylinder is represented by the black disk, in that figure:

$$\Omega_D = \{\mathbf{x} \in \mathcal{R}^2 \ : \ \|\mathbf{x}\| \leq 1/2\}. \tag{1}$$

The flow is represented by streamlines over the area of the computational domain surrounding the cylinder:

$$\Omega = \{\mathbf{x} = (x, y) \in \mathcal{R}^2 \setminus \Omega_D \ : \ x \in [-5, 15], \ y \in [-5, 5], \ x \notin \Omega_D\}. \tag{2}$$

As in the previous chapter, the velocity field is $\mathbf{u} = (u, v)$. Length and velocity are normalized with respect to the cylinder diameter and the horizontal incoming flow velocity U. We consider this configuration at the Reynolds number of $Re = 100$, well above the transition to instability and yet well within the laminar regime.

Periodic vortex shedding leads to often undesirable mechanical vibrations and a generic control objective is to attenuate this instability. Figure 1 includes two forms of actuation that can be used to that end:

One is a vertical volume-force, defined over a downstream disk Ω_{vf}:

$$\begin{aligned} \mathbf{f}(\mathbf{x},t) &= b(t)\,\mathbf{g}(\mathbf{x})\,, \quad \text{where} \\ \mathbf{g}(\mathbf{x}) &= \begin{cases} (0,1) & \mathbf{x} \in \Omega_{vf} \\ (0,0) & \text{otherwise,} \end{cases} \\ \Omega_{vf} &= \{\mathbf{x} \in \mathcal{R}^2 \,:\, \|\mathbf{x}-(0,2)\| \leq 1\}\,, \end{aligned} \tag{3}$$

The volume force may be viewed as mimicking an electro-hydrodynamic (EHD) actuator (D'Adamo et al., 2009). Volume force representations are also commonly used as a simple way to include boundary actuation, such as pulsating jets and zero-net-flux actuators (Glezer and Amitay, 2002) in both CFD and reduced order models (Ahuja et al., 2007; Joe et al., 2008). We shall revisit this point in the discussion of outstanding modeling challenges. The discussion of volume force actuation will refer to a number of studies by our group, including Gerhard et al. (2003); Noack et al. (2004b); Tadmor et al. (2004); Noack et al. (2004a); Tadmor and Noack (2004); Lehmann et al. (2005); Luchtenburg et al. (2006); Tadmor et al. (2010).

To attenuate vortex shedding, actuation policies will be designed to dissipate the kinetic energy of the oscillatory flow field as an opposing force. Actuation will therefore be periodically modulated, taking the form

$$b(t) = B\cos\left(\psi(t)\right). \tag{4}$$

Under such a policy, the oscillations phase ψ is assigned by a feedback controller to apply a decelerating force on the oscillatory vertical component of the flow field $\mathbf{u}$ over Ω_{vf}. The actuation frequency $\dot{\psi}$ must therefore match the shedding frequency.

The second form of forcing shown in Figure 1 is the vertical oscillation of the cylinder. Once again, this is a simple example of a broad array of dynamic fluid body interactions that range from controlled boundary motion to elastic deformations and disturbance driven boundaries, under diverse scenarios of engineered and natural systems. The particular example of the oscillatory-actuated cylinder has been studied by our team, in Noack et al. (2004b); Tadmor et al. (2004); Noack et al. (2004a); Tadmor and Noack (2004), and by this volume's co-author, S. Siegel and collaborators, as described in Siegel et al. (2008).

A postulated sensor is also shown in Figure 1. The sensor measures one or two components of the velocity field, and represents one of several

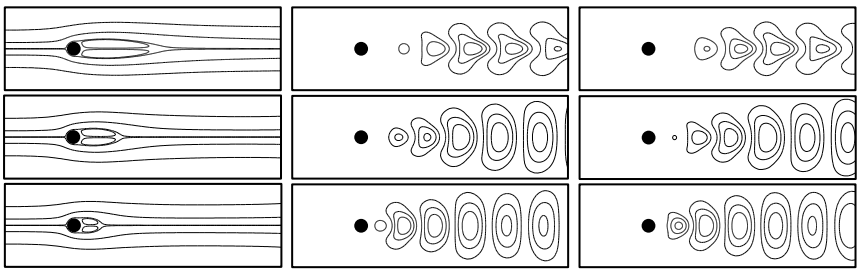

Figure 2. Least order local representations of the unsteady cylinder wake flow at $Re = 100$, from a small perturbation the unstable, steady solution $\mathbf{u}_s$ (top row), through a mid-transient period (mid-row), to the natural attractor (bottom row). From left to right: The mean flow and a mode-pair resolving flow unsteadiness at the dominant, vortex shedding frequency.

standard physical implementations, including hot wire sensors and, as in an increasing number of studies, a real time digital particle image velocimetry (Yu et al., 2006) or laser Doppler anemometry. Sensor readings will provide a representation of a realistic feedback flow control implementation.

2.3 Dominant Coherent Structures of the Natural Flow

The transition to instability at $Re_c \approx 47$ is a supercritical Hopf bifurcation: Considering small fluctuations from the steady solution, $\mathbf{u}_s$, the real part of a complex conjugate pair of eigenvalues of the linearized NSE becomes positive once $Re > Re_c$, giving rise to an oscillatory instability and the inception of periodic vortex shedding. The exponential growth of these oscillatory fluctuations saturates as the flow settles at a periodic attractor. As will be further elaborated in § 6, at least 94% of the TKE[1] can be resolved by an operating-point-dependent mode-pair, throughout the natural transient from the steady solution to the attractor (Noack et al., 2003; Lehmann et al., 2005; Morzyński et al., 2007). These local modes and the local mean flow can be computed as slowly varying, distributed Fourier coefficients of the flow field, a perspective we shall also elucidate in short order. In this particular case, the same modes can be computed by application of the proper orthogonal decomposition (POD) procedure, reviewed in the

[1] As defined in the previous chapter, the TKE is the period-averaged turbulent kinetic energy of the unsteady flow.

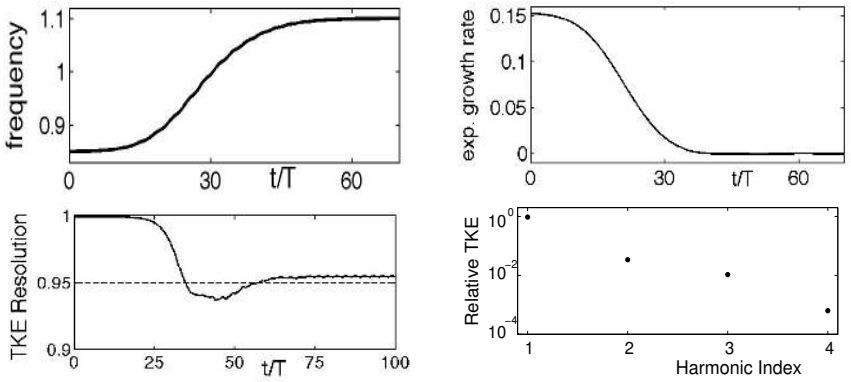

Figure 3. Dynamic characteristics of the cylinder wake flow at $Re = 100$, as they vary along the natural transient from the steady solution to the attractor: The instantaneous shedding frequency (top, left), the instantaneous exponential growth rate of the fluctuation amplitude (top, right), and the feasible TKE resolution with an expansion by a single mode pair (bottom, left). Attractor TKE levels of the first 4 mode-pairs (8 modes), resolving the first 4 harmonics of the shedding frequency, normalized by the TKE at the leading harmonic, are also shown (bottom, right).

previous chapter, to a single vortex shedding period[2].

Figure 2 depicts[3] the mean fields and the dominant mode-pair at the beginning of the natural transient, at a mid-point, and following the convergence to the natural attractor. Figure 3 shows the feasible TKE resolution by a single mode-pair and the gradually changing shedding frequency, along the natural transient. It also provides the distinct TKE levels of each of the first four harmonics of the shedding frequency over the attractor. Figures 2 and 3 highlight two complementary properties of the flow: On the one hand, key quantitative properties of the flow change substantially along the transient: The mean flow's near wake recirculation bubble is drastically reduced as the flow approaches the attractor, the vortical structures of the leading two modes move closer to the cylinder, the characteristic wave-length of these vortices reduces and the shedding frequency grows by nearly 25%. A single mode-pair would therefore provide a far poorer resolution of the entire transient, when compared with what is feasible with operating-point-

[2]The property that POD modes are each associated with distinct frequencies is generic only when the flow is dominated by a single frequency and its harmonics.

[3]Here and throughout, velocity fields are represented by streamlines.

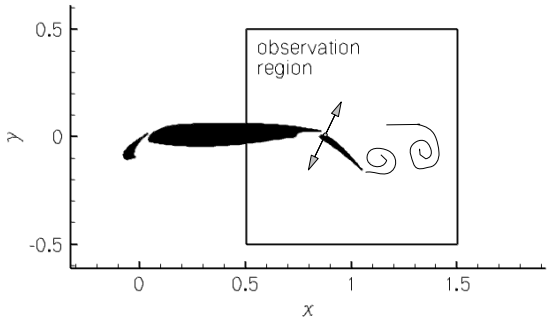

Figure 4. A sketch of the three element high-lift configuration and the observation region for the model. Periodic excitation ($\leftrightarrow$) is implemented at the upper part of the trailing edge flap.

dependent expansions. For example, the attractor POD modes resolve less than 50% of the early transient's TKE (Noack et al., 2003). The flip side of this observation is that the overall qualitative nature of the flow, including the topology of the mean flow and the leading modes, the dominance of a single frequency, etc., are preserved, and their quantitative manifestations change gradually. Both these observations are generic and characterize natural and actuated non-bifurcating transients in fluid flow systems.

2.4 A High Lift Configuration

Figure 4 shows a simplified, two dimensional representation of generic wing extensions, used by transport airplanes to increase lift during takeoff and landing. it includes the main wing section, a leading edge slat and a trailing edge flap. The incompressible flow is considered at $Re = 10^6$, where velocity and length are scaled with respect to the incoming flow velocity U and the wing chord length c, measured when the high lift mechanism is retracted. The chord lengths of the slat and flap are $c_{sl} = 0.158\,c$ and $c_{fl} = 0.254\,c$, and their deployed deflection angles are 26.5° and 37°, respectively. The angle of attack of the main wing section is 6°. At these conditions the flow separates only from the trailing edge flap. The two-way arrow in Figure 4 represents on oscillating jet that is used as the control actuator, with the purpose to reattach the flow to the flap and thus, increase

the lift gain. The actuated jet is simulated by imposing a flow velocity, orthogonal to the airfoil, and is located at $0.04\,c$ from the flap's leading edge. Some additional technical details will be provided during discussion and the complete description can be found in (Luchtenburg et al., 2009).

This configuration has been the subject of several experimental and numerical flow control studies the Berlin Institute of Technology and our group, including (Günther et al., 2007; Schatz et al., 2007; Kaepernick et al., 2005; Luchtenburg et al., 2009). We shall use this example only in an open loop mode. The imposed periodic velocity will be the open loop counterpart of (4):

$$b(t) = B\cos(\omega_a t)\,, \tag{5}$$

where ω_a is the actuation frequency and B the amplitude of actuation.

2.5 The Natural and the Actuated Flows

The natural, massively separated flow around and behind the flap is characterized by alternating shedding of the leading and trailing edge vortices. The average shedding frequency is $\omega_n = 1.875$ (equiv. $St_n = 0.32$) and the fluctuation peak TKE area is in the wake.

The open loop actuated jet, in this example oscillates at the frequency $\omega_n = 3.75$ (equiv. $St_a = 0.6$), with the maximal momentum coefficient $C_\mu = 4 \times 10^{-3}$. Actuation leads to a substantial reattachment of the flow, a near complete attenuation of shedding at ω_n, the emergence of a new periodic attractor, locked-in to the actuation frequency ω_a, and, indeed, a 19% increase of the average lift coefficient. The actuated fluctuations are concentrated above and near the trailing edge flap.

Kinematically, once again, both the natural and the actuated attractors are well resolved, each, each by a single POD mode pair. Figure 5, taken from (Luchtenburg et al., 2009), shows the mean flow, the first POD mode and a generic snapshot of the respective natural and the actuated attractors.

3 Low Order Galerkin Models: Some Added Concepts

This section sets the ground for the main developments, including the extension of the Galerkin framework, in § 4, § 5, § 6 and § 7, and the discussion of actuation and control design, in § 8. This review begins with a reminder of the basic ingredients of the Galerkin model. It continues with a discussion of the triple Reynolds decomposition (TRD) in relation to Galerkin models, and of an interpretation of that decomposition in terms of harmonic

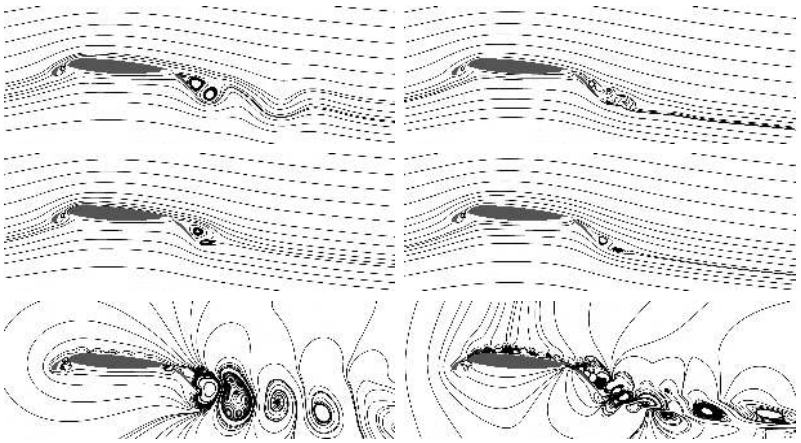

Figure 5. Comparison of a natural (left) and the actuated (right) attractors of the separated flow over the deployed rear flap of the high lift configuration example. Visualized flow fields include characteristic snapshots (top), the mean flows (center) and instantaneous fluctuation (bottom) of the two respective attractors, as detailed in Luchtenburg et al. (2009).

Galerkin expansions. A review of basic concepts of power and energy dynamics completes this set of preliminaries. To motivate the rather lengthy but essential preparatory work, we interrupt the presentation, early on, with a simple illustrative example of the gamut of failures one may encounter when applying the existing Galerkin paradigm to transient modeling.

3.1 The Constitutive First Principles Model

For ease of reference we display again the incompressible Navier-Stokes equations (NSE), the constitutive model underlying the entire discussion:

$$\begin{aligned} \partial_t \mathbf{u} &= \mathcal{N}(\mathbf{u}) + \mathbf{f} = -\nabla \cdot (\mathbf{u} \otimes \mathbf{u}) - \nabla p + \nu \Delta \mathbf{u} + \mathbf{f}, \\ \nabla \cdot \mathbf{u} &= 0. \end{aligned} \tag{6}$$

Low order Galerkin models were developed as efficient computational tools to analyze fixed points and, later on, attractors of partial differential equations (PDEs), such as the NSE. The Galerkin framework was therefore traditionally designed for handling steady domain geometry and boundary conditions. In fluid dynamics contexts, an increasing interest in cases where both these restrictions fail is an outgrowth of generic flow control applica-

tions, e.g., boundary actuators by jets, suction and membranes, active and elastic walls, flapping flight and wind gusts. being able to incorporate these challenges in a systematic modeling framework is a central component of the discussion of this chapter.

The distributed force field, $\mathbf{f}$, may represent an actuation, such as the volume force $\mathbf{f} = b\mathbf{g}$ in (3), where the signal $b(t)$ represents the control command. Boundary forcing is not represented by terms in (6), but rather, they are formulated as time varying inputs into the domain of the infinitesimal generated of the semi-flow, associated with a controlled PDE (Lasiecka and Triggiani, 2000).

3.2 The Galerkin Modeling Framework

The Galerkin model is determined by a choice of a base flow, $\mathbf{u}^B$, defining the origin of a state space hyperplane, and of an expansion mode set $\{\mathbf{u}_i\}_{i\geq 1} \subset \mathcal{L}^2(\Omega)$. The Galerkin approximations of the velocity and the force fields in a fluid dynamic system are then

$$\begin{array}{rcl} \mathbf{u}(\mathbf{x},\, t) & = & \mathbf{u}^B(\mathbf{x}) + \sum_{i\geq 1} a_i(t)\mathbf{u}_i(\mathbf{x}), \\ \mathbf{f}(\mathbf{x},\, t) & = & \mathbf{f}^B(\mathbf{x}) + \sum_{i\geq 1} f_i(t)\mathbf{u}_i(\mathbf{x}), \end{array} \tag{7a}$$

where the generic case of zero-mean steady state forcing means that $\mathbf{f}^B = 0$. The time coefficients $a_i(t)$ and $f_i(t)$ are defined by the projection of the flow field, $\mathbf{u}(\mathbf{x},\, t)$, and the force field, $\mathbf{f}(\mathbf{x},\, t)$, on the expansion hyperplane. When the expansion set is orthonormal (e.g., when $\mathbf{u}_i$ are POD modes), the projection formulae reduce to the inner products

$$a_i = (\mathbf{u},\, \mathbf{u}_i)_\Omega, \qquad f_i = (\mathbf{f},\, \mathbf{u}_i)_\Omega.$$

When $\mathbf{f}$ is a modulated volume force such as (3) we have $f_i(t) = g_i\, b(t)$ where g_i are defined by the time invariant projections of $\mathbf{g}(\mathbf{x})$ and the modulation signal $b(t)$ represents the control command. (Notice that this formulation includes multivariable control, where both $\mathbf{g}(\mathbf{x})$, hence g_i, and $b(t)$ are vector valued, and "$g_i\, b(t)$" stands for the Euclidean inner product.)

The Galerkin dynamical system is the compression of the constitutive NSE to the approximation hyperplane. It comprises of ordinary differential equations, governing the time evolution of the coefficients a_i, and is obtained by the projection of the NSE (6) on the approximation hyperplane. Thus, with an orthonormal expansion, we have

$$\begin{array}{rcll} \dot{a}_i & = & (\partial_t \mathbf{u},\, \mathbf{u}_i)_\Omega & \\ & = & (\mathcal{N}(\mathbf{u}),\, \mathbf{u}_i)_\Omega + (\mathbf{f},\, \mathbf{u}_i)_\Omega & \\ & = & c_i + \sum_{j\geq 1} l_{ij}a_j + \sum_{j,l\geq 1} q_{ijk}a_j a_k + f_i, \quad i \geq 1. & \end{array} \tag{7b}$$

An, ideal, infinite set of incompressible modes that forms a complete orthonormal sequence in $\mathcal{L}^2(\Omega)$ leads to an exact model, which is equivalent to the NSE. In the context of feedback flow control, however, one's interest is rather in the other extreme, i.e., in the lowest possible model order: The term *least order* will thus be understood in reference to designated quantitative and qualitative system properties that the model needs to resolve. For example, in the context of the cylinder wake stabilization problem, these properties will include the instability of the steady solution, existence of a periodic attractor, the TKE growth rate along natural and actuated transients between $\mathbf{u}_s$ and the attractor, and the vortex shedding frequency along such transients and over the attractor. Additionally, the model should be able to correctly represent the actuation force and the sensor signal.

We recall the following fundamental Galerkin model requirements, made to ensure that any flow field generated by (7) satisfies both the incompressibility and boundary conditions:

- Both the base flow and the modes are divergence-free:

$$\nabla \cdot \mathbf{u}^B = 0, \quad \nabla \cdot \mathbf{u}_i = 0, \quad i \geq 1.$$

- The base flow $\mathbf{u}^B$ absorbs the boundary conditions (in particular, only steady boundary conditions are allowed).
- The modes $\mathbf{u}_i$ satisfy homogeneous boundary conditions.

Our discussion will highlight the way these requirements conflict with key modeling needs in generic flow control applications, and delineate the changes needed in the Galerkin paradigm to remove such conflicts.

3.3 A Simple Example of an Utter Failure

The litany of definitions and technicalities occupying the remainder of this section provide the foundation for our subsequent extension of the Galerkin framework. As a motivation we present first a brief, illustrative preview, using the cylinder wake flow to highlight the sever modeling issues that the traditional Galerkin modeling framework gives rise to.

As a matter of basic dynamic principles, a dynamic model capable to resolve oscillatory fluctuations requires at least two states. In particular, a meaningful Galerkin model of the unsteady cylinder wake flow requires at least two modes. As mentioned earlier, this lower bound is kinematically attainable over the natural attractor, where at least 94% of the TKE is resolved by a Galerkin approximation that employs the attractor's mean flow, denoted $\mathbf{u}_{*,0}$, as the base flow, and a single mode-pair (e.g., the leading POD modes), to resolve the fluctuations. As shown in Noack et al. (2003),

the Galerkin projection of the NSE on the chosen expansion is[4] a linear system of the form:

$$\frac{d}{dt}\begin{bmatrix} a_1 \\ a_2 \end{bmatrix} = \begin{bmatrix} \sigma & -\omega \\ \omega & \sigma \end{bmatrix} \begin{bmatrix} a_1 \\ a_2 \end{bmatrix}. \tag{8}$$

The excellent kinematic approximation and the simplicity of this dynamical model certainly make it very appealing. Alas, this model suffers from severe flaws, listed right below, that make it of little, if any use.

Instability. The Galerkin projection yields the values of the growth rate $\sigma \approx 0.05$ and the frequency $\omega \approx 1.1$ in (8). The predicted frequency is a good approximation of the shedding frequency. However, with $\sigma > 0$, (8) is linearly anti-stable, which precludes the existence of an attractor, i.e., the key characterization of this flow configuration.

Poor transient prediction. The model also grossly mis-predicts the early transient dynamics, near the unstable steady solution, $\mathbf{u}_s$: The correct growth rate of small perturbations from $\mathbf{u}_s$ is $\sigma_s \approx 0.44$, i.e., it is nearly nine folds larger than the Galerkin projection value of σ. The early transient shedding frequency is < 0.9, much smaller than the nominal ω.

Model structure inconsistency. Accepting the validity of the NSE, model parameter mismatch is often attributed to aspects of low order models, such as the truncation of the energy cascade to neglected, higher order modes. A common approach to remedy poor dynamic predictions is to employ a posteriori parameter estimation from simulation or experimental data. This procedure, known in our field as *calibration*, is based on the implicit assumption that the NSE-based structure of the dynamical systems is correct, and that the desired predictive power will be achieved once coefficients are appropriately adjusted, e.g., ensuring stability by adding identified eddy viscosities (Aubry et al., 1988; Rempfer, 1991). Figure 3 refutes this assumption: The substantial drift in both the exponential growth rate and in the shedding frequency along the transient is a property of the exact NSE solution. Therefore no constant values of the coefficients σ and ω can match the entire natural transient!

[4] To be precise, (8) is the *phase-averaged Galerkin system: Due to the slight difference between the oscillation amplitudes of the first and second POD modes, the oscillations in the* (a_1, a_2) *plane would be along an ellipse, rather than a circle. The model* (8) *is obtained by averaging the model coefficients over all rotational changes of coordinates.*

Modal expansion inconsistency. The inherent inconsistency of the dynamical system structure with the entire transient is paralleled by the Galerkin approximation: As seen in Figure 2, the flow structures that dominate early transients, starting at small perturbations of the steady solution, are substantially different from their counterparts over the attractor. The implications on feedback flow control of using the same expansion throughout the transient can be severe: A Galerkin approximation of the early transient with an expansion based on the attractor's mean, $\mathbf{u}_{*,0}$, and on attractor POD modes is guaranteed to fail in the near wake. Likewise, predictions based on an approximation by $\mathbf{u}_s$ and the stability eigenmodes will be misleading as the flow approaches the attractor. As mentioned earlier, the quality of TKE resolution, in both cases, drops to as low as 50%, when the flow state is considered away from the nominal operating condition at which the modes were obtained. These discrepancies can become manifest both in state estimation by dynamic observers and in the anticipated impact of actuation, based on any fixed pair of expansion modes. Poor closed-loop performance will then be inevitable (Gerhard et al., 2003; Lehmann et al., 2005; Luchtenburg et al., 2006).

Failure to predict an attractor. The observation above highlighted the failure at modeling the entire transient. Here we note that the shortcomings of the model persist even when one's interest is restricted to a single operating point, e.g., the generic focus on small fluctuations from the attractor: Calibrating the growth rate to the observed marginal stability value of $\sigma = 0$, the model becomes a representation of an ideal linear oscillator, consistent with the attractor's periodic orbit. Yet this model has no preferred oscillation amplitude and therefore cannot recover from disturbance-induced drift. That is, the existence of periodic orbits does not translate to the existence of a true attractor.

Inconsistency with moving boundaries. The inclusion of actuation requires adding a control term to the model, reflecting the effect of the actuated force field. The description of the cylinder wake benchmark includes two forms of actuation: A volume force and cylinder oscillations. The inclusion of the former is, at least conceptually, straightforward. That is not the case when actuated cylinder oscillations are considered. One difficulty is due to the fact that some points in the computational domain are alternately occupied by a solid body (the cylinder) and by moving fluid. The Galerkin projection of the NSE is ill defined at these points, and the model is not be capable to produce meaningful dynamic predictions in their neighborhood. A second difficulty is due to the fact that, since boundary motion does not

involve a body force, it does not lead to a first principles based control term in the Galerkin system.

As the discussion of this chapter unfolds, we shall demonstrate that the difficulties we have just identified are not unfortunate peculiarities of a specific example. Rather, they are the results of generic inconsistencies between the very structure of the traditional Galerkin model and of modeling practices. The existence of many successful Galerkin models is typically the results of implicit or explicit structural corrections. Even then, the dynamic envelope and operational range of low order Galerkin models are mostly severely limited. Our goal is to expose these generic inconsistencies and to propose solutions at the structural level. The technical discussion in this section, starting with the triple Reynolds decomposition, right below, provide the necessary tools to do so.

3.4 The Triple Reynolds Decomposition (TRD)

The discussion of impediments to the success of standard low order Galerkin models and of suggested remedies will employ the concepts and notations of the TRD, which is formalized in Eq. (B.9) of Appendix B.3. For convenience we present this formalism here, including both the standard and the triple Reynolds decomposition:

$$\mathbf{u} = \mathbf{u}^B + \mathbf{u}' = \mathbf{u}^B + \mathbf{u}^C + \mathbf{u}^S. \tag{9}$$

The middle expression in (9) is the standard Reynolds decomposition of the velocity field $\mathbf{u}$ as the sum of a *base flow* $\mathbf{u}^B$ and an *unsteady fluctuations* field $\mathbf{u}'$. Associated with this decomposition is the concept of the *fluctuation energy*

$$K' := \frac{1}{2}\overline{\|\mathbf{u}'\|^2_\Omega}, \tag{10}$$

where the bar indicates the ensemble average. In the generic ergodic case, ensemble and time averages are equivalent, the latter providing the computationally accessible option we shall use in this chapter. The *turbulent kinetic energy*, and the abbreviation *TKE* are identified with K'. We alert the reader to the fact that this notation is a slight modification of the nomenclature listed in the appendix and used in the previous chapter, where the TKE is denoted simply by K, i.e., without a prime. The reason for this change is our explicit reference to the *total kinetic energy* of the flow field, including the non-oscillatory base flow, which we shall denote by K:

$$K := \frac{1}{2}\overline{\|\mathbf{u}\|^2_\Omega}. \tag{11}$$

The TRD is shown following the second equality in (9). Here the unsteady fluctuation field $\mathbf{u}'$ is partitioned into a *coherent velocity field* $\mathbf{u}^C$ and a remainder $\mathbf{u}^S$. The coherent component $\mathbf{u}^C$ is understood as the part of $\mathbf{u}$ that one is interested to resolve by a low order Galerkin approximation. The superscript notation of $\mathbf{u}^S$ is motivated by the conceptual parallel to the stochastic flow component that is represented in CFD simulations only indirectly, by subgrid, turbulence models. We will categorize state-related modeling issues by their relations to each of the three components of (9).

As an illustration, in a two states attractor POD approximation of the cylinder wake flow, the base flow is the attractor's mean flow, and the coherent fluctuations are defined by the projection of $\mathbf{u}' = \mathbf{u} - \mathbf{u}^B$ on the dominant POD mode pair:

$$\mathbf{u}^B := \mathbf{u}_{*,\,0} := \overline{\mathbf{u}} \;\text{ and }\; \mathbf{u}^C := \sum_{i=1}^{2} a_i \mathbf{u}_i \;\text{ with }\; a_i := (\mathbf{u}',\, \mathbf{u}_i)_\Omega\,, \quad i = 1, 2.$$

The remainder, $\mathbf{u}^S$, comprises of higher frequency components of the flow.

3.5 Harmonic Modes and Harmonic Expansions

Here we provide an explicit mathematical definition of the three components of the Reynolds decomposition.

As the unsteady flow component that is sought to be resolved by a low order Galerkin approximation, $\mathbf{u}^C$ is implicitly defined in terms of certain ranges of length-scales and time-scales. In this chapter we focus on frequency bandwidth characterizations of $\mathbf{u}^C$. That focus is motivated by the observation that the dynamics of interest in phase-dependent feedback flow control studies are invariably dominated by a finite set of distinct, slowly varying frequencies. This description applies, in particular, to the two illustrating examples we have introduced in § 2.

Dynamical systems featuring a distinct set of slowly varying frequencies match each frequency with a pair of states. It therefore appears prudent to construct the reduced order model of frequency-specific expansion modes, to begin with. In that case, the Galerkin expansion provides an explicit definition for $\mathbf{u}^B$, $\mathbf{u}^C$ and $\mathbf{u}^S$ in terms of participating frequencies:

$$\begin{aligned} \mathbf{u} \;=\; & \underbrace{\mathbf{u}_* + A_0\,\mathbf{u}_0}_{\mathbf{u}^B} \\ & + \underbrace{\textstyle\sum_{i=1}^{N_h} A_{2i-1}\cos(\phi_i)\mathbf{u}_{2i-1} + A_{2i}\sin(\phi_i)\mathbf{u}_{2i}}_{\mathbf{u}^C} \\ & + \underbrace{\textstyle\sum_{i=N_h+1}^{\infty} A_{2i-1}\cos(\phi_i)\mathbf{u}_{2i-1} + A_{2i}\sin(\phi_i)\mathbf{u}_{2i}}_{\mathbf{u}^S}\,, \end{aligned} \tag{12}$$

where the distinct participating frequencies are $\frac{d}{dt}\phi_i = \omega_i$. In what follows we add some needed details on the technical assumptions made regarding the components of (12), on ways to compute them, on the meaning of the equality in this expansion, and indeed, on its utility.

Starting with formalisms, the flow fields $\mathbf{u}_i$ are assumed to be normalized, $\|\mathbf{u}_i\|_\Omega = 1$. This way $\{\mathbf{u}_i\}_{i\geq 1}$ is viewed as playing the role of a Galerkin expansion set, and the Galerkin expansion is defined by the scalar coefficients $a_{2i-1} := A_{2i-1}\cos(\phi_i)$ and $a_{2i} := A_{2i}\sin(\phi_i)$. In particular, w.l.o.g., we require that $A_i \geq 0$, $i \geq 1$. In preparation for the discussion of mean field models, in § 4, the 0^{th} mode in (12), defining the slowly varying base flow, $\mathbf{u}^B$, includes a constant component, denoted $\mathbf{u}_*$ and a slowly time varying component, $A_0\mathbf{u}_0$. Following common practice, one may define the fixed component $\mathbf{u}_*$ as either a steady NSE solution, $\mathbf{u}_s$, or as the mean flow of a studied attractor, which we denote by $\mathbf{u}_{*,0}$, throughout this chapter.

We shall adopt the convention that the participating frequencies are organized in an ascending order, $\omega_i < \omega_{i+1}, \ldots$. In the particular case in which these frequencies are commensurate, when the flow is dominated by a single base frequency and by its harmonics, $\omega_i = i\,\omega$, then (12) is a temporal Fourier expansion and the distributed coefficients of that expansion are $A_i\mathbf{u}_i$. Regardless of whether the participating frequencies are commensurate or not, we postulate that the flow component $\mathbf{u}^C$ that we want resolved by the Galerkin model is defined by the lower frequencies, ω_i, $i = 1, \ldots, N_h$. The high frequencies ω_i, $i > N_h$, are included merely in order to formalize the definition of $\mathbf{u}^S$. These frequencies are not used in computational realizations, but they can be clearly selected in a way that ensures the possibility of an equality in the restriction of (12) to time windows $[t - \frac{1}{2}t_p,\, t + \frac{1}{2}t_p]$, $t \geq \frac{1}{2}t_p$, for some fixed $t_p \geq 2\pi/\omega_1$.

The definitions above are obvious in "steady state", i.e., when the frequencies ω_i, expansion modes $\mathbf{u}_i$ and amplitudes A_i are time invariant. What makes (12) useful in transient flows, as well, is the assumption that the flow field $\mathbf{u}$ is band limited, allowing only slow time variations in these harmonic characteristics. We interpret this assumption in terms of of a time scale $\tau \gg 2\pi/\omega_1$ (equivalently, $\tau/t_p \gg 1$) and the following smooth time dependencies:

$$\mathbf{u}_i(\mathbf{x},\, t/\tau), \quad A_0(t/\tau), \quad \omega_i(t/\tau). \tag{13}$$

By this assumption, the expansion modes remain essentially constant over the short time windows $[t-\frac{1}{2}t_p,\, t+\frac{1}{2}t_p]$, and the infinite sum equality in (12) may be interpreted in the $\mathcal{L}^2(\Omega\times[t-\frac{1}{2}t_p,\, t+\frac{1}{2}t_p])$ sense, over such intervals. The truncated series for $\mathbf{u}^B + \mathbf{u}^S$ is then a smooth, periodically dominated function of time, justifying the point-wise, mid-window interpretation of the original $\mathcal{L}^2(\Omega \times [t - \frac{1}{2}t_p,\, t + \frac{1}{2}t_p])$ approximation.

We note Models based on slowly varying harmonic coefficients are commonplace, e.g., *dynamic phasor* models in power engineering (DeMarco and Verghese, 1993; Lev-Ari and Stanković, 2008; Tadmor, 2002). The use of harmonic mode sets and *harmonic balancing* has been motivated in flow applications as an effective and relatively simple computational approach to system identification of otherwise complex phenomena, such as separated flows (Tadmor et al., 2008), vortex breakdown (Mishra et al., 2009), and aeroelastic fluid-body interactions (Attar et al., 2006).

The harmonic modes at the time t are computed by the straightforward but generally oblique projection of the time function

$$r \mapsto \mathbf{u}(\,\cdot\,, r) - \mathbf{u}_* \,:\, \left[t - \frac{t_p}{2},\, t + \frac{t_p}{2}\right] \mapsto \mathcal{L}^2(\Omega)$$

on the temporal expansion set $\{1,\, \cos(\phi_i),\, \sin(\phi_i),\;\; i \geq 1\} \subset \mathcal{L}^2\left[t - \frac{t_p}{2},\, t + \frac{t_p}{2}\right]$. In the particular case of commensurate frequencies, where $\omega_i = i\,\omega$, these modes are computed by the standard Fourier series formulae, with $t_p = 2\pi/\omega$:

$$\tilde{\mathbf{u}}_0(\mathbf{x},\, t) = \frac{1}{t_p} \int\limits_{t-\frac{t_p}{2}}^{t+\frac{t_p}{2}} \mathbf{u}(\mathbf{x},\, r)\, dr, \quad \mathbf{u}_0 := \frac{1}{\|\tilde{\mathbf{u}}_0\|_\Omega} \tilde{\mathbf{u}}_0, \tag{14a}$$

and for $i = 1, 2, \ldots,$

$$\tilde{\mathbf{u}}_{2i-1}(\mathbf{x},\, t) := \frac{2}{t_p} \int\limits_{t-\frac{t_p}{2}}^{t+\frac{t_p}{2}} \mathbf{u}(\mathbf{x},\, r)\, \cos(i\omega\, r)\, dr, \;\; \mathbf{u}_{2i-1} := \frac{1}{\|\tilde{\mathbf{u}}_{2i-1}\|_\Omega} \tilde{\mathbf{u}}_{2i-1}, \tag{14b}$$

$$\tilde{\mathbf{u}}_{2i}(\mathbf{x},\, t) := \frac{2}{t_p} \int\limits_{t-\frac{t_p}{2}}^{t+\frac{t_p}{2}} \mathbf{u}(\mathbf{x},\, r)\, \sin(i\omega\, r)\, dr, \quad \mathbf{u}_{2i} := \frac{1}{\|\tilde{\mathbf{u}}_{2i}\|_\Omega} \tilde{\mathbf{u}}_{2i}. \tag{14c}$$

To maintain notational simplicity, the remainder of this discussion is presented for the case of harmonically related frequencies. We note that the only difference in the general case is in the need to compute the temporal correlation of the temporal basis, and use the inverse of that matrix to "de-correlate" the modes.

Although convergence to an exact equality in the infinite expansion (12) is guaranteed by standard harmonic analysis, an important distinction of the harmonic modes is that spatial orthogonality is not generic. Nonetheless, we

shall now demonstrate that these modes share useful advantages of spatially orthogonal modes.

One such advantage is the simplicity of the computation of the time coefficients, $a_i(t)$, by a straightforward extension of the projection formulae for spatially orthogonal expansion sets, i.e. $a_i = (\mathbf{u},\, \mathbf{u}_i)_\Omega$, which is no longer valid in its original form. The harmonic time coefficients a_i are completely determined by the amplitudes A_i The latter are computed by the Fourier series based spatio-temporal projections on the base functions $\mathbf{u}_{2i-1}(\mathbf{x})\cos(\phi_i(t))$ and $\mathbf{u}_{2i}(\mathbf{x})\sin(\phi_i(t))$ in $\mathcal{L}^2\left(\Omega \times \left[t - \frac{t_p}{2},\, t + \frac{t_p}{2}\right)\right)$. Specifically:

$$\begin{aligned} A_{2i-1}(t/\tau) &= \frac{2}{t_p}\int_{t-\frac{t_p}{2}}^{t+\frac{t_p}{2}} (\mathbf{u}(\,\cdot\,, r),\, \mathbf{u}_{2i-1}(\,\cdot\,, t/\tau))_\Omega \cos(\phi_i(r))\, dr \\ &= \frac{2}{t_p}\int_{-\frac{t_p}{2}}^{\frac{t_p}{2}} (\mathbf{u}(\,\cdot\,, t+r),\, \mathbf{u}_{2i-1}(\,\cdot\,, t/\tau))_\Omega \cos(\phi_i(t+r))\, dr \end{aligned} \tag{15a}$$

$$\begin{aligned} A_{2i}(t/\tau) &= \frac{2}{t_p}\int_{t-\frac{t_p}{2}}^{t+\frac{t_p}{2}} (\mathbf{u}(\,\cdot\,, r),\, \mathbf{u}_{2i}(\,\cdot\,, t/\tau))_\Omega \sin(\phi_i(r))\, dr \\ &= \frac{2}{t_p}\int_{-\frac{t_p}{2}}^{\frac{t_p}{2}} (\mathbf{u}(\,\cdot\,, t+r),\, \mathbf{u}_{2i}(\,\cdot\,, t/\tau))_\Omega \sin(\phi_i(t+r))\, dr \end{aligned} \tag{15b}$$

A second appealing property is the Pythagorean property of the TKE. The *modal energy* (for $i \geq 1$, the *modal TKE*) at the time t is the period averaged kinetic energy of the respective mode:

$$K_0(t/\tau) := \frac{1}{2}\|A_0(t/\tau)\,\mathbf{u}_0(\,\cdot\,, t/\tau)\|_\Omega^2 = \frac{1}{2}A_0(t/\tau)^2,$$

$$K_{2i-1}(t/\tau) := \frac{1}{2t_p}\int_{t-\frac{t_p}{2}}^{t+\frac{t_p}{2}} \|a_{2i-1}(r)\mathbf{u}_i(\,\cdot\,, t/\tau)\|_\Omega^2\, dr$$

The latter term is simplified as follows:

$$\begin{aligned} K_{2i-1}(t/\tau) &:= \frac{1}{2t_p}\int\limits_{t-\frac{t_p}{2}}^{t+\frac{t_p}{2}} a_{2i-1}(r)^2\,dr\ \underbrace{\|\mathbf{u}_i(\,\cdot\,,t/\tau)\|_\Omega^2}_{=1} \\ &= \frac{1}{2t_p}\int\limits_{t-\frac{t_p}{2}}^{t+\frac{t_p}{2}} (A_{2i-1}(t/\tau)\cos(\phi_i(r)))^2\,dr \\ &= \frac{A_{2i-1}(t/\tau)^2}{4\,i\,\pi}\int\limits_{\phi_i(t)-i\,\pi}^{\phi_i(t)+i\,\pi} \cos(i\,\omega\,r)^2\,dr \\ &= \frac{1}{4}A_{2i-1}(t/\tau)^2. \end{aligned}$$

Likewise we obtain

$$K_{2i}(t/\tau) = \cdots = \frac{1}{4}A_{2i}(t/\tau)^2.$$

Having selected an index set $\mathcal{I} \subset \mathbb{N}_0$ and denoted

$$\mathbf{u}^{\mathcal{I}} = \sum_{i\in\mathcal{I}} a_i\,\mathbf{u}_i,$$

the temporal orthogonality of the distinct components of a harmonic expansion with a single base frequency now leads to the desired equality, which is a distributed version of Plancharel's theorem according to which

$$K^{\mathcal{I}}(t/\tau) := \frac{1}{2t_p}\int\limits_{t-\frac{t_p}{2}}^{t+\frac{t_p}{2}} \|\mathbf{u}^{\mathcal{I}}(\,\cdot\,,r)\|_\Omega^2\,dr$$

becomes

$$
\begin{aligned}
K^{\mathcal{I}}(t/\tau) &= \tfrac{1}{2t_p}\int_{t-\frac{t_p}{2}}^{t+\frac{t_p}{2}} \left(\mathbf{u}^{\mathcal{I}}(\,\cdot\,,r)\,,\mathbf{u}^{\mathcal{I}}(\,\cdot\,,r)\right)_\Omega\, dr \\
&= \tfrac{1}{2t_p}\int_{t-\frac{t_p}{2}}^{t+\frac{t_p}{2}} \left(\sum_{i\in\mathcal{I}} a_i(r)\mathbf{u}_i(\,\cdot\,,t/\tau)\,,\sum_{i\in\mathcal{I}} a_j(r)\mathbf{u}_j(\,\cdot\,,t/\tau)\right)_\Omega dr \\
&= \sum_{i,j\in\mathcal{I}} (\mathbf{u}_i,\,\mathbf{u}_j)_\Omega\;\tfrac{1}{2}\,\overline{a_i(t+\cdot)a_j(t+\cdot)} \\
&= \underbrace{\frac{1}{2}A_0(t/\tau)^2}_{\text{if } 0\in\mathcal{I}} + \sum_{1\le i\in\mathcal{I}} \tfrac{1}{4}A_i(t/\tau)^2 \\
&= \underbrace{K_0(t/\tau)}_{\text{if } 0\in\mathcal{I}} + \sum_{1\le i\in\mathcal{I}} K_i(t/\tau)^2
\end{aligned}
\tag{16}
$$

It is noted that this version of the Pythagorean rule exceeds what is generically valid for standard, spatially orthogonal Galerkin expansion, where it is valid only for K' and its components, but generally *not* for the total kinetic energy. It is also noted that while (16) does not extend as an exact equality when the various frequencies are not harmonically related, an arbitrarily good approximation is achievable when the t_p is selected sufficiently large.

It is easy to see that should a Krylov-Bogoliubov phase averaging hypothesis be applicable, the oscillation amplitudes and the TKE become a functions of the frequency alone and can be determined by the instantaneous state of the Galerkin approximation. Thus

$$
A_{2i-1} = A_{2i}, \quad \text{and} \quad K_{2i-1} = K_{2i} = \frac{1}{4}A_{2i-1}^2 = \frac{1}{4}\left(a_{2i-1}^2 + a_{2i}^2\right). \tag{17}
$$

The cylinder wake flow is an example of a case where the Krylov-Bogoliubov hypothesis is a good approximation of the exact dynamics (Noack et al., 2003; Tadmor et al., 2010).

3.6 The Harmonically Dominated Galerkin System

Time variations in the modes $\mathbf{u}_i$ and the frequencies ω_i will be assumed negligible, or recoverable from an exogenous, measurable parameter, which we shall discuss in § 6. The components of the time evolution of the Galerkin coefficients that need to be included in a reduced order dynamical system are thus those involving the slowly varying amplitudes A_i and the locally linear evolution of the phases ϕ_i. That is, we consider a polar coordinates counterpart of the Galerkin system.

The phase equations are straightforward:

$$\dot{\phi}_i = \omega_i, \quad i = 1, \ldots, N_h. \tag{18a}$$

We present the computation of the time derivatives of A_i only for commensurate frequencies, allowing us to appeal to the Fourier coefficient formulae (15). For the time being we also assume that short time variations in $\mathbf{u}_i$, $i \geq 1$, are negligible, deferring treatment of faster modal variations to § 6. Then,

$$\begin{aligned}
\tfrac{d}{dt} A_{2i-1}(t/\tau) &= \tfrac{d}{dt} \tfrac{2}{t_p} \int_{-\frac{t_p}{2}}^{\frac{t_p}{2}} (\mathbf{u}(\,\cdot\,, t+r),\, \mathbf{u}_{2i-1})_\Omega \cos(\phi_i(t+r))\, dr \\
&= \tfrac{2}{t_p} \int_{-\frac{t_p}{2}}^{\frac{t_p}{2}} \tfrac{d}{dt} \left((\mathbf{u}(\,\cdot\,, t+r),\, \mathbf{u}_{2i-1})_\Omega \cos(\phi_i(t+r)) \right)\, dr \\
&= \tfrac{2}{t_p} \int_{-\frac{t_p}{2}}^{\frac{t_p}{2}} (\partial_t\, \mathbf{u}(\,\cdot\,, t+r),\, \mathbf{u}_{2i-1})_\Omega \cos(\phi_i(t+r))\, dr \\
&\qquad -i\,\omega \tfrac{2}{t_p} \int_{-\frac{t_p}{2}}^{\frac{t_p}{2}} (\mathbf{u}(\,\cdot\,, t+r),\, \mathbf{u}_{2i-1})_\Omega \sin(\phi_i(t+r))\, dr \\
&= \tfrac{2}{t_p} \int_{-\frac{t_p}{2}}^{\frac{t_p}{2}} (\mathcal{N}(\mathbf{u}(\,\cdot\,, t+r) + \mathbf{f}(\,\cdot\,, t+r),\, \mathbf{u}_{2i-1})_\Omega \cos(\phi_i(t+r))\, dr \\
&\qquad\qquad -\omega_i\, (\mathbf{u}_{2i},\, \mathbf{u}_{2i-1})_\Omega\, A_{2i}.
\end{aligned}$$

Likewise,

$$\begin{aligned}
\tfrac{d}{dt} A_{2i-1}(t/\tau) &= \tfrac{2}{t_p} \int_{-\frac{t_p}{2}}^{\frac{t_p}{2}} (\mathcal{N}(\mathbf{u}(\,\cdot\,, t+r) + \mathbf{f}(\,\cdot\,, t+r),\, \mathbf{u}_{2i-1})_\Omega \sin(\phi_i(t+r))\, dr \\
&\qquad\qquad +\omega_i\, (\mathbf{u}_{2i},\, \mathbf{u}_{2i-1})_\Omega\, A_{2i-1}.
\end{aligned}$$

We note that the only difference in the case where incommensurate frequencies are involved is the need for a left division of the vector formed by these expressions by a slowly varying correlation matrix.

For later reference and in order to stress the simple structure of these equations we rewrite them in a compressed form, in terms of the modified

frequencies

$$\tilde{\omega}_i := \omega_i \ (\mathbf{u}_{2i-1},\, \mathbf{u}_{2i})_\Omega \,.$$

Then:

$$\begin{aligned} \tfrac{d}{dt} A_{2i-1} + \tilde{\omega}_i \, A_{2i} \ &= \ \text{the } \cos(\phi_i) \text{ phasor of } \ (\mathcal{N}(\mathbf{u}) + \mathbf{f},\, \mathbf{u}_{2i-1})_\Omega \,, \\ \tfrac{d}{dt} A_{2i} - \tilde{\omega}_i \, A_{2i-1} \ &= \ \text{the } \sin(\phi_i) \text{ phasor of } \ (\mathcal{N}(\mathbf{u}) + \mathbf{f},\, \mathbf{u}_{2i})_\Omega \,. \end{aligned} \tag{18b}$$

The left hand side terms of (18b) adhere to the generic form of *dynamic phasor models* (DeMarco and Verghese, 1993; Tadmor, 2002; Lev-Ari and Stanković, 2008). Dynamic phasor models are widely used in power engineering, where they were introduced to predict the slowly varying transients of the harmonic coefficients (termed dynamic phasors) of AC voltages and currents. The right hand side terms in (18b) are affine-plus-quadratic expressions in the amplitudes A_i. These equations therefore adhere to the general pattern of Galerkin models.

It is noted that the presence of the $\tilde{\omega}_i$-proportional terms on the left hand side of (18b) gives rise to an oscillatory homogeneous dynamics at the frequency $\tilde{\omega}_i$. Therefore, validity of the underlying hypothesis that the amplitudes A_i are slowly varying means that these terms are either small, e.g., when $\mathbf{u}_{2i-1} \perp \mathbf{u}_{2i}$, or that they are (nearly) cancelled by the right hand side terms of (18b).

We revisit the two modes POD expansion and the Galerkin system (8), as the simplest illustration of (18). Due to the particular structure of the cylinder wake flow, it has the non-generic property that the two dominant POD modes are also harmonic modes at the shedding frequency, over the attractor. Given the scope and objective of this example, we are satisfied with the fact that flow state trajectories initiated at small perturbations of attractor states are well approximated as

$$\begin{aligned} \mathbf{u}(\mathbf{x},\, t) \ &= \ \mathbf{u}_{*,\,0}(\mathbf{x}) + a_1(t)\mathbf{u}_1(\mathbf{x}) + a_2(t)\mathbf{u}_2(\mathbf{x}) \\ &= \ \mathbf{u}_{*,\,0}(\mathbf{x}) + A_1(t/\tau)(\cos(\phi(t))\mathbf{u}_1(\mathbf{x}) + \sin(\phi(t))\mathbf{u}_2(\mathbf{x})), \end{aligned} \tag{19a}$$

and ignore the issue of the merit (or lack of merit) of (8) for dynamic predictions. Let us consider now the ingredients of (18) in this example:

• The fact that the harmonic modes we use are POD modes means that they are spatially orthogonal. Thus, in this example, $\tilde{\omega}_1 = 0$ in (18).

• The fact that (8) is the Galerkin projection of the NSE over the expansion (19a) means that:

$$\begin{aligned}(\mathcal{N}(\mathbf{u}_{*,0}+a_1\mathbf{u}_1+a_2\mathbf{u}_2,\,\mathbf{u}_1)_\Omega &= \sigma a_1-\omega a_2\\ &= A_1\,(\sigma\,\cos(\phi)-\omega\,\sin(\phi)),\end{aligned}\tag{19b}$$

$$\begin{aligned}(\mathcal{N}(\mathbf{u}_{*,0}+a_1\mathbf{u}_1+a_2\mathbf{u}_2,\,\mathbf{u}_2)_\Omega &= \sigma a_2+\omega a_1\\ &= A_1\,(\sigma\,\sin(\phi)+\omega\,\cos(\phi)).\end{aligned}\tag{19c}$$

The $\cos(\phi)$ phasor of the right hand side of (19b) is $\sigma\,A_1$, and the $\sin(\phi)$ phasor of the right hand side of (19c), is $\sigma\,A_2$. Thus, (8) gives rise to a dynamic phasor model, comprising of the equations

$$\frac{d}{dt}A_i=\sigma\,A_i,\quad i=1,2.\tag{20}$$

This model isolates and highlights the exponential instability of the oscillation amplitude under (8).

3.7 Interim Comments

The preceding discussion provided an explicit interpretation of the TRD in terms of harmonic expansions and dynamic phasors. The focus of the discussion has been on periodically dominated flows. The same focus will be maintained throughout this chapter. It is noted however that the rationale and definitions of Galerkin expansions in terms of harmonically specific modes extend, mutatis mutandis, to flows that involve multiple, non-commensurate frequencies, on which we commented in the text.

While harmonic modes are generically *not* mutually orthogonal in the state space $\mathcal{L}^2(\Omega)$, Galerkin expansions by harmonic modes do retain useful properties of Galerkin expansions with spatially orthogonal mode sets. Those properties include simple projection formulae to compute time coefficients of distinct modes, the equality of the TKE stored in the i^{th} mode to the respective Galerkin state TKE, and the pythagorean law by which the total TKE of a harmonic expansion is the sum of the respective modal TKE levels.

An explicit TRD interpretation as a frequency band partition of the flow field is provided by the (generalized) harmonic expansion: The base flow, the coherent unsteadiness and the unresolved flow field represent the slowly varying mean flow, the intermediate bandwidth and the high bandwidth components of the harmonic expansion.

A side benefit of the formalism (12) that will prove extremely useful later on, is that the continuity of the harmonic modes with respect to gradual

changes in the flow provide a simple and consistent framework to represent the continuous deformation of dominant coherent structures along transients (Lehmann et al., 2005; Morzyński et al., 2007). This enables to maintain a relatively small expansion set without any loss in model accuracy. Defining counterpart concepts of deformable mode sets is a far greater challenge in the POD framework, due to the lack of a firm generic dependence between indices of POD modes and intrinsic dynamic characteristics, such as frequencies and phases, as illustrated in Tadmor et al. (2007a, 2008); Mishra et al. (2008, 2009). We shall revisit this issue when we discuss mode deformation, in § 6.

Till then, the discussion of *mean field models* in § 4, and of *turbulence subgrid models*, in § 5, will be based on the use of time invariant mode sets. The one exception will be the 0^{th} harmonic mode, which is the core of the Galerkin mean field theory.

3.8 Dynamic Power Balancing

As in any physical system, the time evolution of the energy content of distinct components state components, e.g., K^B, K^C and K^S, is key to understanding the dynamics of a fluid flow system. The last component of the preliminaries concerns these concepts which we discuss first in the context of exact NSE model, and then in the Galerkin model.

Dynamic Power Balancing: NSE Definitions The dynamic law governing the time evolution of the TKE, K', is derived from the NSE (Noack et al., 2002, 2005, 2008). We use the following nomenclature to refer to the contributions of distinct components of the (actuated) NSE to the *energy supply rate* (i.e., the *power*) in the flow:

$$\frac{d}{dt}K' \;=\; P + D + C + T + F + G\,, \tag{21}$$

where P, D, C, T, F, G are the respective *production*, *dissipation*, *convection*, *transfer*, *pressure* and *actuation* components of the power $\frac{d}{dt}K'$, and are defined as:

$$P \;=\; -\overline{(\mathbf{u}',\, \nabla\cdot(\mathbf{u}'\otimes\mathbf{u}^B))_\Omega}\,, \tag{22a}$$

$$C \;=\; -\overline{(\mathbf{u}',\, \nabla\cdot(\mathbf{u}^B\otimes\mathbf{u}'))_\Omega}\,, \tag{22b}$$

$$T \;=\; -\overline{(\mathbf{u}',\, \nabla\cdot(\mathbf{u}'\otimes\mathbf{u}'))_\Omega}\,, \tag{22c}$$

$$D \;=\; \frac{1}{Re}\overline{(\mathbf{u}',\, \Delta\,\mathbf{u}')_\Omega}\,, \tag{22d}$$

$$F = -\overline{(\mathbf{u}',\, \nabla p')_\Omega}\,. \tag{22e}$$

$$G = \overline{(\mathbf{u}',\, \mathbf{f})_\Omega}\,, \tag{22f}$$

The power provided by the actuation force field $\mathbf{f}$ is included for later reference and will not be discussed in this section. With a continued focus on periodically dominated systems, averaging at the time t is carried over the period $\left[t - \frac{t_p}{2},\, t + \frac{t_p}{2}\right]$. Effects on the supplied power of changes in any of the harmonic modes, and in any of the amplitudes A_i, are assumed negligible.

As we have already demonstrated, the total energy of periodically dominated flows is the sum of the modal contributions, i.e., $K = \sum_i K_i$. When computing power terms in the context of the Galerkin system, we shall therefore focus on modal contributions. Modal power contributions can be derived from (22). For example, the combined contributions of the $(2i-1)^{st}$ and $(2j-1)^{st}$ modes to the production power component is computed by substituting $A_0\,\mathbf{u}_0$ for $\mathbf{u}^B$ and $A_{2i-1}\cos((2i-1)\,\omega\, r)\,\mathbf{u}_{2i-1}$ and $A_{2j-1}\cos((2i-1)\,\omega\, r)\,\mathbf{u}_{2j-1}$ for $\mathbf{u}'$ in (22a). This leads to the following expression:

$$\begin{aligned} -A_{2i-1}A_{2j-1}A_0 \Big(&(\mathbf{u}_{2i-1},\, \nabla\cdot(\mathbf{u}_{2j-1}\otimes\mathbf{u}_0))_\Omega \\ &+ (\mathbf{u}_{2j-1},\, \nabla\cdot(\mathbf{u}_{2i-1}\otimes\mathbf{u}_0))_\Omega \Big)\cdot \\ &\cdot\overline{\cos((2i-1)\omega\,\cdot)\cos((2j-1)\omega\,\cdot)} \\ = \; -\delta(i-j)\,\tfrac{1}{2}\,&(\mathbf{u}_{2i-1},\, \nabla\cdot(\mathbf{u}_{2i-1}\otimes\mathbf{u}_0))_\Omega\; A_0\, A_{2i-1}^2 \\ = \; -\delta(i-j)\,2\sqrt{2}\,&(\mathbf{u}_{2i-1},\, \nabla\cdot(\mathbf{u}_{2i-1}\otimes\mathbf{u}_0))_\Omega\; \sqrt{K_0}\, K_{2i-1}. \end{aligned} \tag{23}$$

Similar expressions are obtained, by an obvious analogy, for the modal contributions to the remaining power components.

Dynamic Power Balancing: Galerkin System Definitions As discussed in previous chapters, the inner product terms following the last two equalities in (23) are the Galerkin projection definitions of coefficients of the Galerkin system (7b). The same will hold for the modal contributions to other power components. In other words, the total modal power contributions are *equivalently* computed in terms of the time coefficients in the ideal, infinite Galerkin system. Motivated by our concentration on the Galerkin

system, we continue our analysis with a focus on the Galerkin formulation:

$$\frac{d}{dt}K_i = \frac{d}{dt}\frac{1}{2}\overline{a_i^2} = c_i\overline{a_i} + \sum_{j=1}^{\infty} l_{ij}\,\overline{a_i a_j} + \sum_{j,k=1}^{\infty} q_{ijk}\,\overline{a_i a_j a_k} + g_i\,\overline{a_i\,b}. \qquad (24)$$

Considering harmonic Galerkin expansions, let us examine each of the terms in (24):

The contribution of the constant terms vanishes.

$$c_i\overline{a_i} = 0.$$

This is a consequence of the sinusoidal nature of a_i for $i \geq 1$.

Only the diagonal linear terms make a nonzero power contribution. This is simply a restatement of Plancharel's theorem. Thus,

$$Q_i := \sum_{j=1}^{\infty} l_{ij}\,\overline{a_i a_j} = \frac{1}{2}\,l_{ii}\,A_i^2 = 2\,l_{ii}\,K_i, \quad Q' = \sum_{i=1}^{\infty} Q_i, \quad Q = Q_0 + Q'. \quad (25)$$

This expression includes the combined contribution of the production, convection and dissipation to the modal power. We say that the i^{th} mode is *productive* when $l_{ii} > 0$, that it is *dissipative* when $l_{ii} < 0$, and term the marginal case, where $l_{ii} = 0$, as *neutral*. Productive modes are typically a dominant component of $\mathbf{u}'$. They are therefore included in $\mathbf{u}^C$ and in the expansion mode set of the Galerkin model. Modes spanning $\mathbf{u}^S$, are invariably dissipative.

It is noted that the annihilation of off-diagonal linear terms by windowed time averages remains a good approximation well beyond the periodically dominant case. For example, assuming that a POD model is obtained over a statistically representative interval, the time coefficients will remain orthogonal over sufficiently long time windows.

Triadic energy exchanges represent the transfer power in the NSE and their cumulative contributions are conservative (lossless). This means that the sum total of the rate of energy exchanges between any three modes through the quadratic terms of the Galerkin system is zero. Denoting the (order dependent) rate of energy supplied by the j^{th} and k^{th} modes to the i^{th} mode by

$$T_{ijk} = q_{ijk}\overline{a_i a_j a_k}, \qquad (26)$$

the lossless nature of the triadic exchanges is a formal consequence of the equality

$$q_{ijk} + q_{ikj} + q_{ikj} + q_{jik} + q_{jki} + q_{kij} + q_{kji} = 0.$$

Evaluating each T_{ijk} is generally an unsolved problem. Indeed, this issue is at the core of what continues to keep the problem of turbulence closure a Grand Challenge, even as we enter a second century of relentless efforts to address it. The difficulty in the general case arises from the lack of explicit expressions for phase relationships between the oscillations in the three modes. For completeness we shall shortly discuss a simple axiomatic finite time thermodynamics (FTT) framework that we proposed in Noack et al. (2008), as an approximate solution, tailored specifically for Galerkin systems. However, in the particular but important class of periodically dominated flows, on which we focus here, an explicit computation is possible. Starting with the products $a_j(t)a_k(t)$, one has:

$$a_j(t)a_k(t) = \tfrac{1}{2}A_j(t/\tau)A_k(t/\tau)\cdot$$
$$\cdot\begin{cases} \cos(\phi_j-\phi_k)+\cos(\phi_j+\phi_k) & \begin{matrix} j=2\ell-1 \\ k=2m-1 \end{matrix} \\ \cos(\phi_j-\phi_k)-\cos(\phi_j+\phi_k) & \begin{matrix} j=2\ell \\ k=2m \end{matrix} \\ \sin(\phi_j+\phi_k)+\sin(\phi_j-\phi_k) & \begin{matrix} j=2\ell \\ k=2m-1 \end{matrix} \\ \sin(\phi_j+\phi_k)-\sin(\phi_j-\phi_k) & \begin{matrix} j=2\ell-1 \\ k=2m\,. \end{matrix} \end{cases} \tag{27}$$

Multiplying by a_i and taking period averages, as in (26), we obtain:

$$\begin{aligned} T_{ijk} &= q_{ijk}\overline{a_i a_j a_k} \\ &= \sigma_{ijk}\begin{cases} \tfrac{1}{4}q_{ijk}A_iA_jA_k = 2q_{ijk}\sqrt{K_iK_jK_k} & i=|j\pm k| \\ 0 & else\,. \end{cases} \end{aligned} \tag{28}$$

where $\sigma_{ijk}=\pm 1$ depending on i,j,k. Summing over all pertinent input pairs, the net TKE flow rate to the i^{th} mode is

$$T_i = \sum_{\substack{j,k \\ i=|j\pm k|}} 2\,\sigma_{ijk}\,q_{ijk}\sqrt{K_iK_jK_k}\,. \tag{29}$$

We defer the discussion of the actuation power to § 8. Ideally, the contribution of the pressure term to the power balance in the Galerkin system is zero. In cases where that is not the case, this term is approximated by the linear and quadratic terms of the Galerkin system, and is therefore subsumed by the terms discussed right above.

A Finite Time Thermodynamics Variant The analytic form of the transfer terms in (28)-(29) relied heavily on the near periodicity assumption, which provided for the phase relations (27). The the lack of such models in more general cases motivated our development of the axiomatic framework of *finite time thermodynamics (FTT)* (Noack et al., 2008). The FTT axioms lead to an identical formulation of the contributions of linear Galerkin system terms, in (25). The FTT estimates of triadic energy exchange rates are of the form:

$$\widehat{T}_{ijk} = \chi_{ijk}\sqrt{K_i K_j K_k}\,\left(1 - \frac{3K_i}{K_i + K_j + K_k}\right). \tag{30}$$

This form indicates that the respective phases of modal oscillations will be aligned in a way that, on average, energy will flow "downhill", i.e., from TKE rich to low TKE modes. The expressions (30) match (28) when the rational scaling term in (30) is nearly constant. That happens, e.g., when the modal TKE levels are rapidly decaying, making the scaling term equal to either 1, 0, -0.5 or -2.

3.9 Closing Comments

The following comment is made in anticipation of the review of mean field models in § 4, below. Discussions of the kinetic energy in the flow and of its time variations, including those by the present authors in Noack et al. (2002, 2005, 2008, 2010); Tadmor et al. (2010), is typically focused on the unsteady component of the flow, ideally $\mathbf{u}'$, and on its energy content, the K'. In anticipation of the discussion of Galerkin mean field models, in § 4, it is useful to highlight the implications of the preceding analysis on the non-oscillatory base flow, and on the triadic energy exchanges between the base flow and the fluctuations:

$$q_{0jj}\overline{a_0 a_j^2} = q_{0jj} A_0\, A_j^2 = 2q_{0jj}\sqrt{K_0}\, K_j, \tag{31}$$

This expression is analogous to the Reynolds stress term

$$\overline{(\mathbf{u}^B,\, \nabla\cdot(\mathbf{u}'\otimes\mathbf{u}'))_\Omega}\,, \tag{32}$$

which is left out in the TKE focused (21), is obvious. This parallel, and the importance of the *bilateral* energy transfer between fluctuating modes and the base flow, is the basis of the Galerkin mean field theory that we we shall discuss next.

4 Broadband Galerkin Models: Mean Field Models

With an eye on low and least order models suitable for the design of flow control, the sections spanning the remainder of this chapter, elaborate on the challenges mentioned in the review of the spectacular failure of (8). The first category of modeling challenges and solutions that we discuss occupies this section and the following § 5. It can be broadly explained in terms of the TRD (9), its explicit harmonic realization (12), and the trilateral energy flow between $\mathbf{u}^B$, $\mathbf{u}^C$ and $\mathbf{u}^S$.

With $\mathbf{u}^C$ at the focus of attention, and with a usual concentration on observed steady state dynamics, traditional low order Galerkin models use an attractor's mean flow as a time invariant definition of $\mathbf{u}^B$. Slow variations in the base flow, and small structures that we conceptually aggregate in $\mathbf{u}^S$, are both truncated and ignored. The adverse effects of this practice, including the potential for utter failures, such as we have seen in the case of (8), were explained In the seminal article by Aubry et al. (1988). Using the vocabulary of the present discussion, the exposition highlighted the need to include at least a lumped representation of the dynamic energy exchanges between $\mathbf{u}^C$, $\mathbf{u}^B$ and $\mathbf{u}^S$, to regain the stabilizing effects of changes in the base flow and of energy transfer to turbulence, in the exact NSE solution.

The methods proposed by Aubry et al. (1988) defined the beginning of efforts, continued to the present day, to effectively represent the contributions of truncated flow structures in a way that is simple enough to meet sought complexity bounds. Directly or indirectly, investigations alongare particularly Widely applicable solutions are yet to be developed.

The purpose of this section is to seek insight into the problem from an analysis the very structure of the underlying physical mechanisms, at the NSE and the Galerkin levels. That analysis will then reveal the root causes of observed difficulties in structural inconsistencies in the traditional framework, and guide us in the systematic development of viable alternatives. The first part of the discussion addresses the need for and the form of mean field representations, and the second part addresses the issue of turbulence modeling.

4.1 The Need for a Mean Field Model: An NSE Perspective

The discussion of mean field representations summarizes key components of the expositions in Noack et al. (2003); Tadmor et al. (2010), where the interested reader will find additional details.

Let us apply the filters on the right hand sides of (14) to the entire NSE.

The averaging of (14a) yields the familiar Reynolds averaged equation:

$$\partial_t \mathbf{u}^B + \nabla \cdot \left(\mathbf{u}^B \otimes \mathbf{u}^B\right) + \overline{\nabla \cdot (\mathbf{u}' \otimes \mathbf{u}')} = -\nabla p^B + \nu \Delta\, \mathbf{u}^B, \tag{33a}$$

where the time derivative $\partial_t \mathbf{u}^B$ scales with $1/\tau$ and is commonly ignored. The Reynolds averaged equation highlights the impact of the fluctuations $\mathbf{u}'$ on the base flow, via the slowly varying Reynolds stress $\overline{\nabla \cdot (\mathbf{u}' \otimes \mathbf{u}')}$.

The dynamical system explanation of this effect, via the Reynolds averaged equation, is complemented by an energy flow interpretation, which was discussed right above. That is, the Reynolds stress is the term responsible for the energy flow rate (32) between $\mathbf{u}'$ and $\mathbf{u}^B$.

An appeal to the combined higher order harmonic filters in (14b) and (14c), would similarly yield a high-pass filtered harmonic counterpart of the Reynolds equation:

$$\begin{aligned} \partial_t \mathbf{u}' + \nabla \cdot \left(\mathbf{u}^B \otimes \mathbf{u}'\right) + \nabla \cdot \left(\mathbf{u}' \otimes \mathbf{u}^B\right) \\ + \nabla \cdot (\mathbf{u}' \otimes \mathbf{u}')' = -\nabla p' + \nu \Delta\, \mathbf{u}', \end{aligned} \tag{33b}$$

where the prime $'$ indicates the high-pass filtered component of a time function. Thus $\nabla \cdot (\mathbf{u}' \otimes \mathbf{u}')'$ is the high-pass filtered component of $\nabla \cdot (\mathbf{u}' \otimes \mathbf{u}')$, and the term $\nabla \cdot \left(\mathbf{u}^B \otimes \mathbf{u}^B\right)$ is eliminated by a high-pass filter. A critical observation, in this equation, is that the component of (33b) that is linear in $\mathbf{u}'$ includes the base flow dependent terms $\nabla \cdot \left(\mathbf{u}^B \otimes \mathbf{u}'\right) + \nabla \cdot \left(\mathbf{u}' \otimes \mathbf{u}^B\right)$. Changes in $\mathbf{u}^B$ will therefore modify the linear growth rate of the $\mathbf{u}'$.

Here too, the stabilizing mechanism is reflected by a power term, which is the counterpart of (32) in (33b). That term is

$$\overline{(\mathbf{u}',\, \nabla \cdot (\mathbf{u}^B \otimes \mathbf{u}') + \nabla \cdot (\mathbf{u}' \otimes \mathbf{u}^B))_\Omega}, \tag{34}$$

Once again, it captures the energy transfer rate between the base flow and the fluctuations. The conservatism of this flow rate means that (34) has the negative value of (32).

This bilateral interdependence is precisely what enables the transition from an unstable steady solution to a marginally stable attractor in the NSE solution: Small perturbations of the steady solution experience high production rate. As the base flow approaches the attractor's mean, that rate declines, and with it, the growth in K', saturating over the attractor.

This mechanism explains the structural failure of (8), where a constant base flow is used and where the said change in the production rate cannot take place. A detailed examination of the dynamic energy balancing along the transient in the cylinder wake example, verifying this explanation, can

be found in Tadmor et al. (2010). That analysis demonstrates that, *regardless of the precision of the Galerkin approximation of* $\mathbf{u}'$, a substitution of the slowly varying $\mathbf{u}^B$ by a fixed field, e.g. by the steady NSE solution or by the attractor's mean flow, will lead to a drastic mis-match of energy production and dissipation along the natural transient. For example the use of the attractor's mean field leads to the non-physical prediction of decay of small fluctuations from the steady solution.

The conclusion at this point is therefore that, in order to provide a close approximation of modal energy production and consumption, a reduced order model must account for the interactions between the fluctuations and a (slowly varying) dynamic mean field.

4.2 Simple Galerkin-Reynolds Mean Field Models

The preceding analysis exposes the sources of observed model failures in both energy flow and dynamical system terms. By the same token, it also suggests a clear solution path: Just as the NSE comprises of the bilaterally interacting (33a) and (33b), a least order Galerkin model should include approximations of both these NSE components. The coherent flow $\mathbf{u}^C$ and the fluctuations equation (33b) are already addressed by the standard Galerkin modeling framework of (7). A Galerkin-Reynolds equation needs to be added to the model, targeting the time variations in the base flow component $\mathbf{u}^B = \mathbf{u}_* + a_0\,\mathbf{u}_0$ in (12), and serving as the counterpart of the Reynolds averaged NSE (33a).

The previous chapter by Noack et. al. suggested a very simple recipe for a least order Galerkin approximation of base flow variations

$$\mathbf{u}^B \approx \mathbf{u}_{*,\,0} + a_\Delta \mathbf{u}_\Delta. \tag{35a}$$

in terms of a single *shift mode*:

$$\mathbf{u}_\Delta := \frac{1}{\|\mathbf{u}_s - \mathbf{u}_{*,\,0}\|_\Omega}\,(\mathbf{u}_s - \mathbf{u}_{*,\,0})\,, \tag{35b}$$

were we return to the erstwhile interpretation of $\mathbf{u}_* = \mathbf{u}_{*,0}$ as the time-independent attractor's mean flow. By this definition, $a_\Delta = 0$ over the attractor and $a_{\Delta,s} < 0$ near the steady solution. This definition arises naturally when one is focused on the dynamic envelope of the flow between an unsteady attractor and an unstable fixed point. As shown in Lehmann et al. (2005); Tadmor et al. (2010), the relative TKE error in (35), in the cylinder wake example, is $\leq 30\%$. The term *shift mode* was coined in Noack et al. (2003) to indicate the role of mean field variations in determining the rate of energy shifted from the base flow to the attractor. The cylinder wake version of the shift mode (35b) is depicted in Figure 6.

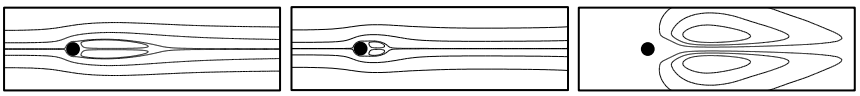

Figure 6. The shift mode as defined in (35b) for the cylinder wake flow (right). For ease of reference we present here again the steady solution (left) and the mean of the attractor flow (center).

Extensions are readily obtained in cases where a wider dynamic envelope renders the approximation (35) insufficient. One example, continuing the empirical approach underlying this chapter, is to approximate the trajectory of the 0^{th} harmonic component of the transient flow, $a_0\mathbf{u}_0 = \mathbf{u}^B - \mathbf{u}_*$, over the dynamic envelope of interest, e.g., using a POD basis. The incremental base flow is captured by period averaging $\mathbf{u}^B - \mathbf{u}_*$ for a choice of $\mathbf{u}_*$, the base flow at a nominal operating point (e.g., an attractor). Alternatives with a stronger first principle flavor appeal to evaluation(s) of the local orientation of the mean field correction, as defined by the local period-averaged NSE. Such definitions require also an approximation of the fluctuation field, $\mathbf{u}'$, e.g., by a (local or global) Galerkin expansion. Details can be found in Tadmor et al. (2010) (cf. Tadmor et al. (2007b, 2008)). We shall revisit and extend these ideas in our discussion of nonlinear manifold embedding and parameterized Galerkin models on nonlinear manifolds, in § 6.

To illustrate the transformative power of these idea we apply the least order approximation (35) to the failing example of the two state cylinder wake model (8). The least order Galerkin expansion of the cylinder wake flow that approximates time variations of both $\mathbf{u}^C$ and $\mathbf{u}^B$ employs the modes $\{\mathbf{u}_i\}_{i=1}^2$, as in (8), and the shift mode from (35b), $\mathbf{u}_\Delta$. The Galerkin projection on this extended basis substitutes the faulty (8) by a three equations Stewart-Landau system, comprising of two components, derived in Noack et al. (2003): The new, Galerkin-Reynolds equation, is a counterpart of (33a):

$$\frac{d}{dt}a_\Delta = -\sigma^B\, a_\Delta \,+\, \beta^B \left(a_1^2 + a_2^2\right). \tag{36a}$$

The Galerkin-Reynolds stress counterpart is the term $\beta^B \left(a_1^2 + a_2^2\right) = 2\beta^B K$. The Galerkin counterpart of the fluctuations equation (33b) is a nonlinear variant of (8):

$$\frac{d}{dt}\begin{bmatrix} a_1 \\ a_2 \end{bmatrix} = \begin{bmatrix} \sigma^C - \beta^C a_\Delta & -(\omega + \gamma a_\Delta) \\ \omega + \gamma a_\Delta & \sigma^C - \beta^C a_\Delta \end{bmatrix} \begin{bmatrix} a_1 \\ a_2 \end{bmatrix}. \tag{36b}$$

The constant coefficients β^B, β^C, σ^C and σ^B, and the constant term c, in

this model, are all positive.

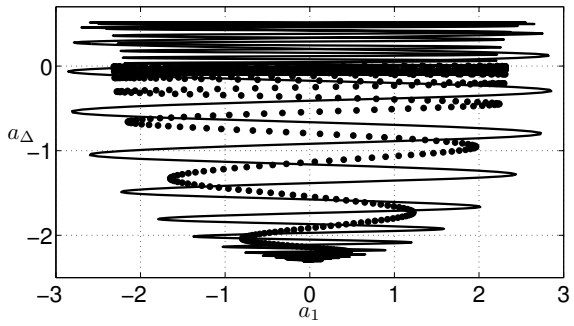

Figure 7. Natural transient of a DNS simulation (dotted line) and the three states Galerkin model (36), that includes the two leading attractor POD modes and the shift mode (35b) (solid curve). The added shift mode enables the recovery of key qualitative aspects of the NSE solution, including the existence of an attractor and the paraboloid manifold connecting the steady solution, $\mathbf{u}_s$, with the attractor. Reasons for the quantitative difference between the Galerkin and the NSE predictions include the lack of adequate turbulence representation, which will be discussed next, and mode deformation, which is the subject of § 6.

When compared with the faulty two states model (8), the effect of the added shift mode and the Galerkin-Reynolds equation in (36) is no less than dramatic. The model now supports the the existence of *both* a marginally stable attractor, where $a_\Delta = \sigma^C/\beta^C$ and $a_1^2 + a_2^2 = (c + \sigma^B a_\Delta)/2\beta^B$, and a linearly unstable fixed point, a counterpart of $\mathbf{u}_s$, where $a_1 = a_2 = 0$, $a_\Delta = -c/\sigma^B$, and where the positive fluctuation growth rate is $\sigma^C - \beta^C a_\Delta = \sigma^C + \beta^C c/\sigma^B > 0$. As shown in Figure 7, this new least order model captures key dynamic qualitative features the NSE solution, as well as a decent, albeit imperfect approximation of the paraboloid transient manifold that is defined by the projection of the NSE solution on the expansion modes. In fact, this approximation is a substantial improvement over the prediction achievable by Galerkin model that employs four times as many modes in the expansion of $\mathbf{u}^C$, but does not (explicitly) includes a mean field representation, other than by trace components in the POD modes (Deane et al., 1991; Noack et al., 2003). The residual mismatch is nonetheless conspicuous: The oscillations amplitude is over-predicted, both throughout

the transient and over the attractor, while the growth rate near the fixed point is under-predicted. Our task in the following sections is to identify and remove the key structural obstacles that cause model inaccuracies such as this.

5 Broadband Galerkin Models: Subgrid Models

Continuing with the discussion of neglected scales, that we begun in the previous section, we now turn our attention from the adverse effects of suppressing $\mathbf{u}^B$ to the impact of neglecting $\mathbf{u}^S$.

5.1 The Need for Subgrid Models

The language of dynamic energy balancing continues to be central. TKE production, i.e., the extraction of energy from $\mathbf{u}^B$, occurs in the most dominant modes which are therefore included in $\mathbf{u}^C$. Any remaining modes in the expansion set that defines $\mathbf{u}^C$, and the entire $\mathbf{u}^S$, are dissipative. TKE dynamics balances the net production and dissipation with the growth or decay rate of modal energies. As follows from our previous discussion of energy dynamics, the conduits for triadic intermodal energy flow are formed by the quadratic term of the NSE, and by its representation by the quadratic terms of the ideal, infinite Galerkin system. The suppression of these conduits, when the dissipative modes spanning $\mathbf{u}^S$ are truncated, therefore creates a non-physical imbalance between energy production and dissipation. That imbalance leads to a net over-prediction of the TKE in the Galerkin system. This includes the modes aggregated in $\mathbf{u}^C$, and when a mean field model is included, in the combined modes spanning $\mathbf{u}^B$ and $\mathbf{u}^C$. In the extreme, the imbalance may lead to global instability.

This phenomenon is manifest in both of the models we have previously considered for the cylinder wake flow:

The two states model (8). The instability of this model is the consequence of the suppression of all the quadratic terms, hence all the conduit for intermodal energy exchanges. This includes both conduits that lead to energy balance with the base flow and those that allow energy flow to modes capturing higher temporal harmonics. With no component capable to drain the TKE generated by the first two modes, the TKE level of $\mathbf{u}^C$ grows at an exponential rate.

The three states model (36). The Galerkin-Reynolds stress $\beta^B(a_1^2 + a_2^2)$, in (36a), and the quadratic terms $-\beta^C\, a_\Delta\, a_i$, in (36b), create lossless energy

links between $\mathbf{u}^C$ and $\mathbf{u}^B$. Their presence eliminates the possibility of global instability and enables an energy balance over an attractor. Nonetheless, the suppression of quadratic terms linking the dominant frequency with modes representing higher harmonics causes the energy absorbed by those modes, in the exact NSE solution, to remain trapped in the three states representing $\mathbf{u}^B + \mathbf{u}^C$. The resulting over prediction by the Galerkin model of both the transient and attractor amplitudes features prominently in Figure 7.

The significance of the distorting effects of truncated energy cascades in low order Galerkin models was brought to attention by the aforementioned article by Aubry et al. (1988). The solution approach suggested in that article is to correct the energy imbalance by increasing the kinematic viscosity ν with an added *eddy viscosity* ν_t. The added dissipation is set to balance the rate by which energy is transferred from $\mathbf{u}^C$ to $\mathbf{u}^S$ over the NSE attractor. Distinct *modal eddy viscosities* $\nu_{t\,i}$ were introduced shortly thereafter (Rempfer, 1991), motivated by difficulties to tune a single ν_t. Mounting examples of tuning difficulties continue to accumulate since.

We use the cylinder wake example to elucidate structural reasons for these difficulties and to motivate the class of solutions we shall present shortly. To simplify the discussion we exploit some particular properties of the cylinder wake flow. First, a Krylov-Bogoliubov phase averaging hypothesis, whereby $A_{2i-1} = A_{2i}$ for all $i = 1, 2 \ldots$ is nearly accurate (Noack et al., 2003). The fact that modal TKE levels in the first several harmonics decline geometrically, with a factor of some 20-30 folds and higher between successive harmonics, allows additional simplifications. Considering the ideal, infinite Galerkin system (7b) and the explicit expressions (27), for $i = 1, \ldots, 4$, we then have the following restrictions on pertinent quadratic terms:

- For $i \in \{1, 2\}$, non-negligible quadratic terms $q_{ijk} a_j a_k$ can only be those where either
  - $j \in \{1, 2\}$ and $k \in \{3, 4\}$
  - $j \in \{3, 4\}$ and $k \in \{1, 2\}$
  - $j \in \{1, 2\}$ and $k = 0$,
  - $j = 0$ and $k \in \{1, 2\}$,

Likewise, using the convention that a_0 is the coefficient of the 0^{th} harmonic, namely, the shift mode coefficient, we have:

- For $i \in \{3, 4\}$, non-negligible quadratic terms $q_{ijk} a_j a_k$ can only be those where $j, k \in \{1, 2\}$.

These observations will be used to estimate the rate of energy transfer from $\mathbf{u}^C$ to $\mathbf{u}^S$, denoted T^{SC} in two ways: One estimate will be based directly

on the dynamic equations. The other will be based on a postulated eddy viscosity model.

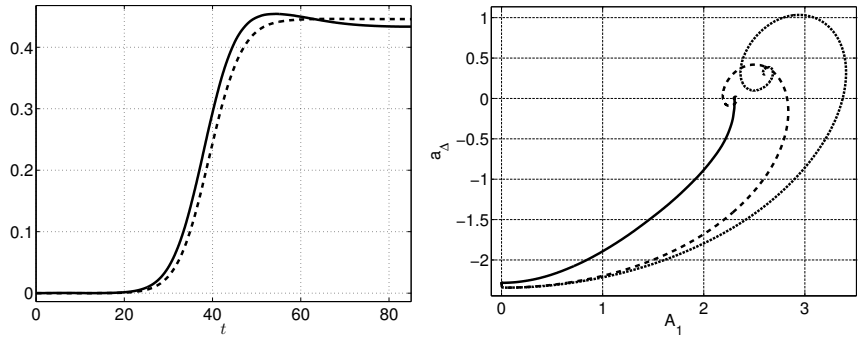

Figure 8. The proposed turbulence model is evaluated in a three states Galerkin model of the cylinder wake flow, comprising of the leading attractor POD mode pair and the shift mode (35b). The second harmonic amplitude A_3 is used as a surrogate for $a_S = \sqrt{K^S}$. The projection of the exact NSE solution (solid curve, left), is well approximated by the estimate obtained by slaving A_3 to A_1^2, as in (37) (there, dashed). The effect of including this turbulence model in the Galerkin system is illustrated by transient plots in the $(A_1,\, a_\Delta)$ plane. The bold line continues to represent the exact NSE solution. The dissipation coefficient of the turbulence model (dashed curve) is determined by energy balance over the attractor, whereas the remaining coefficients are derived by the Galerkin projection of the NSE. The advantage of adding the turbulence model is evident in eliminating the over-prediction of the attractor amplitude and in reducing the transient overshoot of the original three states Galerkin model (dotted curve). That said, the remaining transient overshoot is nonetheless significant. It is the result of mode deformation, as will be discussed in § 6.

A direct estimate of T^{SC}. By the simplifications, above, the differential equations governing a_i, $i \in \{3, 4\}$, comprise linear (and stable) homogeneous parts and sinusoidal quadratic forcing terms at amplitudes that are proportional to $A_1^2 = A_2^2\,(= 2K_1 = 2K_2)$. Consequently, $A_3 = A_4$ is linearly slaved to A_1^2. A time scale separation between the response times in the first and second harmonics allows to approximate this property in algebraic, rather than dynamic terms:

$$A_3 = \kappa A_1^2. \tag{37}$$

This dependence can be seen in the left plot, in Figure 8.

The conclusion concerning $q_{ijk}a_j a_k$ with $i \in \{3,4\}$ is that the TKE transfer rate from $K^C := K_1 + K_2 = \frac{1}{2}A_1^2$ to $K^S \approx K_3 + K_4 = \frac{1}{2}A_3^2$ is captured by

$$T^{SC} = \sum_{i=3}^{4}\sum_{j,k=1}^{2} q_{ijk}\overline{a_i\, a_j\, a_k} =: \lambda A_1^2 A_2 = \underbrace{\lambda\kappa}_{=:\frac{1}{4}\upsilon} A_1^4 \;=\; \upsilon\, K_1^2. \tag{38}$$

The same conclusion is obtained in complete analogy by evaluation of the terms $q_{ijk}\overline{a_i a_j a_k}$ with $i \in \{1,2\}$, in order to estimate the same energy flow rate.

An eddy viscosity estimate of T^{SC}. A subgrid (modal) eddy viscosity suggests that the suppression of the energy flow from $\mathbf{u}^C$ to $\mathbf{u}^S$ can be compensated by adding dissipative terms of the form $-\nu_t a_i$, $i = 1, 2$, to the first two equations in the Galerkin system. The average rate of TKE loss, i.e., $T^{CS} = -T^{SC}$, due to these terms is

$$\hat{T}^{CS} := \sum_{j=1}^{2} \nu_t \overline{a_j^2} \;=\; \nu_t\; A_1^2 \;=\; 2\,\nu_t\, K_1. \tag{39}$$

To be valid, the eddy viscosity estimate (39) needs to be reconciled with (38). Denoting attractor related values by the subscript "$_*$", the selection of

$$\nu_t := \frac{1}{2}\,\upsilon K_{*\,1} \tag{40}$$

achieves that objective over the attractor. Yet along transients and near $\mathbf{u}_s$, the discrepancy between (39) and (38) grows indefinitely. The root cause for the discrepancy is the very *structure* of the eddy viscosity compensation by a linear dissipative term, instead of the quadratic nonlinearity of the transfer terms in the exact Galerkin system.

Commenting on the discussion to this point, we stress that while the approximate relations (37) and (38) were obtained under conditions that extend beyond the specific example of the cylinder wake, these conditions are not generic. Nonetheless, the illustrated causes for the mismatch between the eddy viscosity estimate and the correct value of T^{SC} are generic indeed. Specifically, the mismatch is due to the generic situation where K^S cannot be estimated at a constant level, and that the actual value of T^{SC}, arising from the sum of pertinent triadic terms $q_{ijk}\overline{a_i a_j a_k}$, cannot be approximated by a term proportional to K_i alone.

5.2 The Structure of Valid Subgrid Models

We seek a consistent, low complexity scheme for adding dissipation to the Galerkin system, in a way that can compensate for the severance of energy flow from $\mathbf{u}^B + \mathbf{u}^C$ to $\mathbf{u}^S$ in the exact model. We shall derive that scheme in two steps: In the first step, termed **the energy balancing step**, we focus on the slower, non-oscillatory dynamics of the energy flow equation (24). Here we shall formulate an added phase invariant dissipative term with the goal of reconciling the energy levels of the truncated system with those of the ideal model, as derived from NSE simulations. In the second step will translate the expressions obtained for the energy dynamics equation to phase dependent correction terms in the truncated Galerkin system (7b).

Energy Balance. The truncated energy conduits from $\mathbf{u}^C$ to $\mathbf{u}^S$ are the triadic terms that involve at least one unresolved mode in (24):

$$T_i^S := \sum_{\substack{j,k\geq 1 \\ \max\{j,k\}>N}} q_{ijk}\overline{a_i a_j a_k}. \tag{41}$$

The terms contributing to the summation in (41) have been analytically computed in (28) for periodically dominated flows, yielding

$$T_i^S := \frac{1}{4} \sum_{\substack{j,k\geq 1 \\ \max\{j,k\}>N \\ i=|j\pm k|}} \sigma_{ijk}\, q_{ijk} A_i A_j A_k, \quad i=1,\ldots,N, \tag{42}$$

In a more general setting, lacking the rigid phase information of periodically dominant dynamics, an estimate can be based on the FTT terms (30):

$$T_i^S := \sum_{\substack{j,k\geq 1 \\ \max\{j,k\}>N}} \chi_{ijk} A_i A_j A_k \left(1 - \frac{3K_i}{K_i+K_j+K_k}\right). \tag{43}$$

The challenge in a reduced order model that suppresses a detailed resolution of $\mathbf{u}^S$, is that T_i^S needs to be estimated without explicit knowledge of the amplitudes A_j, $j>N$. We shall base our estimates from two variants of a simple axiom, motivated by generic power lows for the distribution of modal energy as a function of the modal frequency:

Axiom 5.1 (A Global Algebraic Power Rule)**.**

$$K^S = \kappa\, (K^C)^\lambda$$

for some $\kappa > 0$ and $\lambda > 1$.

In the cylinder wake example we used the equality $K^C = 2K_1$ and the approximation $K^S = 2K_3$ to show in (37) that this axiom is a good approximation with $\lambda = 2$. Variants may include distinct *effective* modal TKE levels K_i^S, which allows the energy of the turbulence flow field that interacts with $\mathbf{u}_i$ to vary with i. In that case, K^C substituted by K_i and mode-dependent κ_i and λ_i need to be used.

For simplicity we focus first on periodically dominated flows satisfying Axiom 5.1. In that case, the expression (41) is approximated by an expression of the form

$$T_i^S \approx (K^C)^{\frac{\lambda}{2}} A_i \sum_{j=0}^{N} \xi_{ij} A_j, \quad i = 0, \ldots, N. \tag{44}$$

The sum thus approximates contributions of terms in (42) that include a single A_j, $j > N$, in the ideal, infinite system, but neglects the products of two such terms, which are assumed small. The unresolved amplitudes are substituted by $(K^C)^{\frac{\lambda}{2}}$.

The terms T_i^S are added to the truncated energy equation. In nearly periodic, un-actuated systems, that will be

$$\frac{d}{dt} K_i = \sum_{j=1}^{N} 2\, l_{ii}\, K_i + \sum_{\substack{1 \le j,k \le N \\ i = |j \pm k|}} \frac{1}{4} \sigma_{ijk}\, q_{ijk}\, A_i A_j A_k + T_i^S, \tag{45}$$

where $\sigma_{ijk} = \pm$ is determined by which harmonic functions are involved. Using NSE simulations data, the free parameters of the dissipative term, i.e., η_i and ξ_{ij}, are estimated by the requirement that (45) be satisfied by that data. An additional simplification is this formulation is attained by a focus only on energy exchanges between a single resolved mode and $\mathbf{u}^S$, whereby $\xi_{ij} = \delta(i-j)\, \xi_i$.

The Galerkin Subgrid Terms. The translation of a phase invariant estimate of T_i^S in (44) into phase dependent terms in the Galerkin system (7b), will be based on our previous derivation of the translation of terms in (7b) into terms in the Galerkin energy equations (24): The quadratic term $q_{ijk} a_j a_k$, in the former, gives rise to the term $\frac{1}{4}\, q_{ijk}\, A_i\, A_j A_k$ (or $\frac{1}{2}\, q_{ijk}\, A_i\, A_j A_k$ when one index is 0) in the latter. The conclusion, in the reversed translation, the terms T_i^S need to be multiplied by 2, that one copy of A_i should be eliminated, and that the terms A_j should be substituted by

$\mp a_j$, where, once again, the sign is determined by which harmonic functions are involved. Thus, T_i^S from (44) gives rise to Galerkin system terms of the form

$$d_i^S := \frac{1}{2}\sum_{j=0}^{N} \xi_{ij}(K^C)^{\frac{\lambda}{2}}\, a_j. \tag{46}$$

In a simplified version, those terms reduce to *nonlinear modal eddy viscosity* terns

$$d_i^S = \frac{1}{2}\xi_{ij}(K^C)^{\frac{\lambda}{2}}\, a_i =: -\nu_{t,\,i}(K^C)a_i. \tag{47}$$

Considering this approach in the context of the cylinder wake example and the three states model (36), we recall the estimates (37) and thus, (38). The former agrees with Axiom 5.1 with $\lambda = 2$. The latter agrees with the simplified version (47) with $\xi_{11} = \xi_{22} = \upsilon$. The added dissipative terms in (36b) will thus be proportional to $-K^c a_i$. With that subgrid representation added to (36), we obtain the system

$$\frac{d}{dt}\begin{bmatrix} a_1 \\ a_2 \end{bmatrix} = \begin{bmatrix} \sigma^C - \beta^C a_\Delta - \nu_t a_S & -(\omega + \gamma a_\Delta + \zeta a_S) \\ \omega + \gamma a_\Delta + \zeta a_S & \sigma^C - \beta^C a_\Delta - \nu_t a_S \end{bmatrix}\begin{bmatrix} a_1 \\ a_2 \end{bmatrix}. \tag{48a}$$

$$\frac{d}{dt}a_\Delta = -\sigma^B\, a_\Delta \,+\, \beta^B\left(a_1^2 + a_2^2\right) - c, \tag{48b}$$

$$a_S = \kappa\left(a_1^2 + a_2^2\right). \tag{48c}$$

We also note that slaving the shift mode to the fluctuations will make (48b) an algebraic counterpart of (48c). The improvement in the dynamic prediction due to the inclusion of this subgrid model is visualized in the right plot, in Figure 8.

An alternative, substitutes the algebraic dependencies in Axiom 5.1 by dynamic dependencies:

Axiom 5.2 (Global Dynamic Power Rule)**.** The modal TKE level K^S, satisfies

$$\frac{d}{dt}a_S = -\sigma^S a_S + \kappa\,(K^C)^\lambda.$$

for some $\kappa,\ \sigma^C > 0$ and $\lambda > 1$.

Returning to our running example, with the dynamic variant, a fourth dynamic state is added to (36), leading to the system:

$$\frac{d}{dt}\begin{bmatrix} a_1 \\ a_2 \end{bmatrix} = \begin{bmatrix} \sigma^C - \beta^C a_\Delta - \nu_t a_S & -(\omega + \gamma a_\Delta + \zeta a_S) \\ \omega + \gamma a_\Delta + \zeta a_S & \sigma^C - \beta^C a_\Delta - \nu_t a_S \end{bmatrix}\begin{bmatrix} a_1 \\ a_2 \end{bmatrix}. \tag{49a}$$

$$\frac{d}{dt}a_\Delta = -\sigma^B\, a_\Delta \,+\, \beta^B \left(a_1^2 + a_2^2\right) - c, \tag{49b}$$

$$\frac{d}{dt}a_S = -\sigma^S\, a_S \,+\, \kappa \left(a_1^2 + a_2^2\right), \tag{49c}$$

5.3 Closing Comments

Lumped force models: A low order alternative to the binary resolve-or-neglect choice. Low order models are differentiated from detailed models by a clear focus on an application-specific set of dynamic properties that need to be resolved, and by the high premium put on low complexity. The amplitude and phase of certain flow structures, e.g., the amplitudes and phases associated with von Kármán vortices in wake control, the leading and trailing edge vortices in separation control, are examples. This focus labels as "uninteresting" significant portions of the flow's dynamic characteristics, and an inherent dilemma: Neglecting these structures, hence their impact on retained flow structures, hinders effective and accurate dynamic predictions. Including additional states increases complexity and sensitivity, and therefore erodes a model's utility in realtime applications. Motivated by the universal significance and mean field and subgrid representations, we have suggested a third path: Representing the lumped forces effected by neglected structures on retained states. Time scale separations enables to model such impact by few slow states that interact with similarly slow properties, e.g., oscillations amplitudes, of retained states.

An analogy between mean field and subgrid representations. The structure of (49c) in the augmented system (49), and the stabilizing role played by the added state, a_S, in that system, are completely analogous to the structure and of the Galerkin-Reynolds equation (49b) and the role of the shift mode coefficient a_Δ. The same parallelism applies to the algebraic variant, i.e., to (48), and an obvious slaved mean field model counterpart. This similarity is by no means accidental: Although $\mathbf{u}^B$ and $\mathbf{u}^S$ aggregate altogether different frequency ranges and length scales in the flow, the focus in both models is on representations of slow mechanisms for time averaged energy exchanges with $\mathbf{u}^C$. This analogy is easily seen when stated in terms of period averaged energy exchanges between states in ideal harmonic expansions.

The structural analogy to the mean field model may reduce in more complex configurations, when $\lambda \neq 2$ provides the best fit, or when non-periodic flows require an appeal to an FTT representation, based on (43), as explained in the previous chapter, and in more detail, in Noack et al. (2010). Nonetheless, the main ingredients of the big picture will remain essentially

unchanged: The centerpiece of the added viscosity in the i^{th} equation will remain of the form of $-\nu_t(K_1,\ldots,K_N)a_i$. The fundamental difference from the standard linear eddy viscosity approach is the explicit dependence of the positive dissipation coefficient ν_t on the resolved TKE, as a monotonously increasing, algebraic or dynamic function. The viscosity coefficient vanishes at the steady solution, and it grows indefinitely with the growth of K^S. In complete analogy to the state dependent stabilizing effect of the mean field model, this functional dependence reflects the changes in the dissipative effects of turbulence on large coherent structures along the modeled dynamic manifold.

A conceptual departure from the Galerkin framework. The introduction of the mean field model may have constituted a new focus in low order Galerkin models, but did not deviate from the traditional Galerkin framework. In contrast, the Galerkin subgrid framework outlined here introduces a significant conceptual departure from the Galerkin framework. To this point, the state of the Galerkin system state has been the time varying vector $\mathbf{a} = (a_1,\ldots,a_N)$ of coefficients of an approximation of the NSE state $\mathbf{u}$ by a modal expansion (7a). The modeling premise is that the compression of the NSE to the state space hyperplane that is defined by these expansions is a good approximation, and the dynamical system was based on the NSE as the constitutive equation. None of these ingredients applies to (49c): Here a_S is an estimated surrogate for the unresolved TKE component, K^S. The constitutive equation is not the distributed NSE, but the lumped energy dynamics equation (21). A first principles derivation of the coefficients of (49c) and of the added dissipative term in equations governing the unsteady states (49a) now has to be derived by balancing empirical energy flow rates, i.e., balancing (24) with empirical time trajectories of a_i, $i = 1,\ldots,N$, and not by a projection of the NSE.

Is the subgrid model simply a calibration method? Attractor energy flow analysis in Galerkin models was developed in (Rempfer, 1991) and expanded in (Noack et al., 2002, 2005) and is the foundation of our FTT framework (Noack et al., 2008). This useful tool was recently adapted to the analysis of transient dynamics, and played a central role in establishing the necessity of a mean field model by energy flow considerations, in Tadmor et al. (2010). Energy balancing grew to become an important component of what is known as *calibration*, i.e., parameter tuning in low order Galerkin flow models, aiming to compensate for dynamic distortions such as those described here (Manhart, 1998; Tadmor et al., 2004; Tadmor and Noack, 2004; Noack et al., 2005; Couplet et al., 2005; Attar et al., 2006; Galletti

et al., 2007; Cordier et al., 2010; Bourguet et al., 2009; Navon, I. M. Navon).

One may thus argue that once system parameters are calibrated by empirical data, there might not be any need for a subgrid model. For example, in Tadmor et al. (2004); Tadmor and Noack (2004); we have demonstrated that a properly calibrated three states model (36) can provide a near perfect representation of the natural transient. In effect, here the subgrid model is absorbed into (36), exploiting the identical structures of the mean field and the subgrid equations. While that may well be the case in some examples, even then we see a significance in the very understanding of the correct structure of the subgrid model, in general, as well as in the ability to derive a model from constitutive equations. Absent the rigorous hard error bounds one has in linear systems theory, the reliance on the physical fundaments is as important to ensure robustness and reliability of the model, as are, the often very limited empirical validation experiments.

6 Mode Deformation and Models on Nonlinear Manifolds

The very objective of flow control can be stated in terms of the deformation of leading flow structures (Prabhu et al., 2001). Such deformations are also characteristic of short and long term changes in the ambient operating conditions, such as in the incoming flow velocity and orientation, and during any significant transient, whether controlled or in response to disturbances and ambient changes (Prabhu et al., 2001; Lehmann et al., 2005; Morzyński et al., 2007). To be useful in flow control, models must accommodate these changes over the intended dynamic envelope, loosing neither their predictive power, simplicity and robustness. Here we discuss structural issues that stand in the way of meeting these conflicting demands by standard Galerkin flow models, and suggest a framework of Galerkin models on nonlinear manifolds as a promising alternative.

Bifurcations, where small parameter changes lead to abrupt and drastic realignment of the large scale topology of the flow are associated with model discontinuity (Marsden and McCracken, 1976; Guckenheimer and Holmes, 2002; Aref et al., 2007). Most feedback flow control tasks, however, address flow regulation at a level of resolution where one encounters gradual, continuous modification of dynamic and topological characteristics[5].

[5]To further elaborate this point, note that while the supercritical bifurcation in the wake flow at $Re_c \approx 47$ marks a transition to instability and the emergence of a periodic attractor, key flow characteristics are qualitatively preserved and undergo only a gradual quantitative change during that bifurcation: A pair of least-stable (equiv.

These changes preserve *qualitative* topological and dynamic properties but may have significant cumulative *quantitative* effects. So much so, that the representation capability of a Galerkin model derived at a single nominal operating point may be seriously deteriorated over large portions of the desired dynamic range, and with it, the utility of control design, based on that model (Gerhard et al., 2003; Lehmann et al., 2005; Luchtenburg et al., 2006).

Following a summary of key aspects of the effects of mode deformation and a review of possible paths to address them, right below, the purpose of this section is to describe a class of nonlinear Galerkin models, defined over nonlinear manifolds and expressly geared to meet the challenge associated with dynamic deformation of leading flow structures. In § 7 we shall utilize the proposed framework to address yet another outstanding modeling challenge, the representation of flow over unsteady boundary geometries.

Finally, we mention a recent elegant account of similar ideas in Sapsis and Lermusiaux (2009) developed in the context of stochastic nonlinear PDEs.

6.1 Adverse Effects of Deforming Coherent Structures

We highlight three aspects of the adverse cumulative effects of the deformation of dominant flow structures, that we have already briefly mentioned in the previous section, illustrated by properties of the cylinder wake flow.

Poor resolution of the flow field by the Galerkin expansion. To illustrate this issue we revisit our previous observation that the quantitative differences between stability and attractor POD modes, and between an unstable steady NSE solution and the mean flow of an attractor, can both be substantial. As seen in Figure 2, these differences are especially manifest in the near wake of a cylinder, where the recirculation bubble of $\mathbf{u}_s$ is over three times longer than that of the attractor's mean, $\mathbf{u}_{*,0}$. As a consequence,

most unstable) eigenmodes dominates the dynamics of perturbations from $\mathbf{u}_s$, these modes are associated with a complex conjugate pair of eigenvalues of the linearized NSE, and changes in both these modes and eigenvalues are continuous as functions of the Reynolds number. Moreover, while the suppression of mean field representation in the Galerkin model will not entail an instability when $Re < Re_c$, the arguments heretofore regarding the significance of mean field variations to accurate dynamic predictions remain valid, motivating a model of the form (36) or (49) to predict the dynamic response to large initial perturbations, or in the use of dynamic models in branch continuation, as in Mishra et al. (2009). The point we make here is therefore that structure of the model is preserved and the expansion modes undergo only a gradual change, even during changes in flow conditions that entail stability related bifurcations.

if the Galerkin approximation employs $\mathbf{u}_s$ and the modulated two dominant eigenmodes, to resolve the unsteady flow, then attractor oscillations of the significant unsteadiness of the velocity field cannot be adequately resolved within that near wake area that is contained in the recirculation bubble of $\mathbf{u}_s$. Conversely, the use of the attractor mean, $\mathbf{u}_{*,0}$, and of the two leading attractor POD modes, in the Galerkin approximation, will lead to gross over prediction of the oscillations amplitude in the near wake area, at the beginning of the transient leading from $\mathbf{u}_s$ to the attractor. In fact, the TKE resolution, in both cases, will deteriorate to $\leq 50\%$. In this example, this poor resolution compares with the excellent resolution feasible by a locally extracted two modes expansion of the same flow, seen in Figure 3. Figure 5 provides an additional illustration of mode deformation, showing changes between the actuated and the natural attractors of the high lift configuration example.

Poor dynamic predictions. The prediction of dynamic properties of the flow by the Galerkin system, including the growth rate and oscillation frequencies, are determined by the Galerkin projection of the NSE on the expansion hyperplane. The accuracy of the approximation of the NSE by the Galerkin system critically depends on the resolution of the velocity and the acceleration fields by the Galerkin approximation. The level of prediction will therefore deteriorate, away from the operating point at which the model was derived. This fact is vividly illustrated in Figure 3, where we ignore for the moment the overshoot issue, which is caused by the lack of a subgrid model, which we discussed previously. Comparing the trajectories of the exact NSE solution and of the Galerkin model we see that many more periods are needed in the latter to reach comparable changes in the mean field, and eventually, to reach the attractor level. This difference is due to an order of magnitude difference between the Galerkin projection evaluation of σ^B, in (36) and (48), and the real part of the leading eigenvalue of the linearized NSE, at $\mathbf{u}_s$. A careful observation will also reveal the cumulative phase difference between the two trajectories, reflecting a nearly 25% difference between the POD-based Galerkin projection's evaluation of the oscillation frequency, and the imaginary parts of the said eigenvalues. These qualitative changes are quantitatively visualized in the plots of the time variations of the instantaneous vortex shedding frequency and of the exponential growth rate of the fluctuations, along the natural transient of the cylinder wake flow, in Figure 3.

Distorted phase predictions. As will be further elaborated in § 8, the information about the phase of flow oscillations is critical in dissipative

feedback control. Intuitively, in order to stabilize an unsteady flow by TKE dissipation, the actuation must act as an opposition force and oscillate at the same frequency and at an opposing phase to the oscillatory velocity field it aims to attenuate. A correct prediction of both the relevant phase of the flow and thus, of the effective phase of the actuation, are therefore essential to the success of a stabilizing opposition control policy. The loss of resolution of oscillations at the dominant frequency by expansion modes, away from the operating conditions at which these modes were derived, leads to the subsequent deterioration in the model based definition of the correct actuation phase. As a consequence, control will become ineffective; not only may it lose its dissipative effect, but it may actually become destabilizing (Gerhard et al., 2003; Lehmann et al., 2005; Luchtenburg et al., 2006).

Existing Remedies The issues reviewed above are widely recognized roadblocks, and have motivated considerable efforts to mitigate their impact. Approaches to address these issues can be categorized as follows:

Limiting the operational envelope. A simple way to avoid the distortions caused by mode deformation is to stick to the classical restriction of Galerkin models to a single operating point and thus, the narrow validity region of the expansion set, such as near an attractor or a fixed point. Yet this approach gives up on the very purpose of low order models in flow control applications: As stated in the introduction, the essence of feedback control is to enable a system to operate properly through time varying assignments of the operating conditions and in unsteady ambient environments.

Extended mode sets. Representing the obvious flip side of the same idea, mode deformations can be addressed by including in the expansion set modes obtained at multiple operating conditions. This approach has been adapted, in multiple variants by many research groups. In our own work, Noack et al. (2003), we demonstrated that using both the stability and the attractor POD modes, along with the shift mode (35b), the Galerkin system recaptures a nearly exact dynamic representation.

The common denominator in the wide range of proposed versions of this approach, is the goal to minimize the overall size of the extended expansion set. Examples of variants are the double POD (Siegel et al., 2008) and interval based POD (Borggaard et al., 2007), adding modes extracted by sensitivity analysis (Hay et al., 2009), and informing snapshot selection by computed probability densities and uncertainty quantification (Mathelin and Maitre, 2009).

One obvious downside of this approach is an eventual loss on the model

complexity front. A second issue that is perhaps less obvious at first glance, is the possible raise of the numerical sensitivity associated with the design of dynamic observers for the extended state space. This observation too is illustrated by Figure 2: While modes obtained at different points that reflect the continuous deformation of a distinct flow structure, along a transient, may be different enough to cause the obstructions described right above, these modes may still be far from mutually orthogonal, raising the specter of numerical sensitivity in any effort to distinguish between their respective contributions to a single noisy sensor signal.

Online mode set adaptation. To mitigate the proliferation of the expansion set for wide validity envelopes, yet another family of solutions is based on the adaptation of the expansion set on the fly. Examples include an iterative, simulation based search for an optimal state trajectory and an optimal control, or an iterative optimal state estimation, using an adaptive reduced order model, along with a periodic appeal to the NSE. These methods include, e.g., adaptive control methods (Ravindran, 2000), the *trust region* approach (Fahl, 2000; Arian et al., 2000; Bergmann et al., 2007; Bergmann and Cordier, 2008; Chen et al., 2009), and the *episodal POD* technique (Mokhasi and Rempfer, 2008; Mokhasi et al., 2009). The advantage of this class of methods is that the size of the expansion set remains equal to that of a local model, avoiding both the aforementioned issues of complexity and numerical sensitivity, which can be critical in nonlinear dynamic optimization. Yet the need to repeatedly re-derive the modes and model coefficients, as the operating conditions changes, would typically render adaptive low order models far more computationally taxing than their nonadaptive counterparts. So much so, that such procedures become effective, primarily in off line computations, where they still enable substantial computational savings when compared with using the NSE alone.

Offline mode set adaptation. The topic of this section is a third option: The adaptation of the model and mode set using a pre-computed correction scheme. This approach aims to realize the advantages of adaptation and address the hurdles listed above, without sacrificing the potential for realtime implementation. The ingredients of solutions in this class must include a parameterization of the dynamic envelope, a method to utilize sensor readings to determine changes in the operating point, within that envelope, and characterization of changes in the expansion modes and the dynamical system, as a function of the operating point parametrization. Next we shall formalize these ingredients in terms of nonlinear manifold embedding, and a Galerkin dynamical system, defined on that manifold, as an extension to

the affine embedding of the classical Galerkin framework (7). Early versions of these ideas have been presented in Lehmann et al. (2005); Luchtenburg et al. (2006); Morzyński et al. (2007); Stankiewicz et al. (2008). Related work on deformable modes in reduced order models in fluid dynamics can be found in Amsallem and Farhat (2008); Amsallem et al. (2009); Sapsis and Lermusiaux (2009). We also note that concepts of mode deformation and interpolation have long been a mainstay in video processing and in the generation of animation videos, including animation of fluid motion (Chiang et al., 2008; Amanatiadis and Andreadis, 2009). Finally, nonlinear manifold embedding is at the core of center and approximate inertial manifold models, including fluid dynamic and flow control applications (Foias et al., 1988; Foiaş et al., 1988; Holmes, 1985; Du and Gunzburger, 2003; Noack et al., 2003; Kasnakoğlu et al., 2009). The framework presented below bears both similarities and points of departure from the center / inertial manifold formalism that we will highlight in the closing comments, at the end of this section.

6.2 Deformable modes and accurate low order models

Instead of adding modes in order to resolve mode deformation over the entire operating envelope, the proposed solution is to employ a low dimensional parametrization $\alpha \in \mathcal{A}$ of the operating point, allowing the modes to deform as nonlinear functions of α, and the approximation, to take values over a nonlinear manifold, parametrized by α:

$$\mathbf{u}(\mathbf{x},\, t) \,\approx\, \mathbf{u}^B(\mathbf{x},\, \alpha) \,+\, \sum_{i=1}^{N} a_i(t)\, \mathbf{u}_i(\mathbf{x},\, \alpha). \tag{50a}$$

The dimension N of the local tangent space of the nonlinear manifold embedding is lower than that of the linear subspace span by the ensemble of all local tangent spaces of the form (50a), for all $\alpha \in \mathcal{A}$, which is the required dimension of an affine approximation with the same resolution. The difference is reflected in the order of the dynamical system, governing the evolution of the state $\mathbf{a} = [a_i]_{i=1}^N$. This advantage comes at the obvious cost of higher structural complexity. We will revisit this point along the discussion.

To derive the form of the dynamical system component of the model we first observe that the time derivative of the approximation (50a) now includes an $\dot{\alpha}$-proportional force field, in additional to the traditional ex-

pansion by the time derivatives of the coefficients a_i:

$$\begin{aligned} \partial_t \mathbf{u}(\mathbf{x},\, t) \;\; &\approx \;\; \textstyle\sum_{i=1}^{N} \dot{a}_i(t)\mathbf{u}_i(\mathbf{x},\alpha) \\ &\quad + \left(\tfrac{\partial}{\partial\alpha}\mathbf{u}_0(\mathbf{x},\alpha) \;+\; \textstyle\sum_{i=1}^{N} a_i(t)\, \tfrac{\partial}{\partial\alpha}\mathbf{u}_i(\mathbf{x},\alpha) \right) \dot{\alpha}(t). \end{aligned} \tag{50b}$$

The projection of the NSE on (50a) will therefore include both α-dependent coefficients and $\dot{\alpha}$-proportional terms:

$$\begin{aligned} \dot{a}_i = c_i(\alpha) + \textstyle\sum_{j=1}^{N} l_{ij}(\alpha)\, a_j + \sum_{j,k=1}^{N} q_{ijk}(\alpha) a_j a_k \\ + \left(c_i'(\alpha) + \textstyle\sum_{j=1}^{N} l_{ij}'(\alpha) a_j \right) \dot{\alpha}, \quad i = 1, \ldots, N. \end{aligned} \tag{50c}$$

The $\dot{\alpha}$-dependent terms can be neglected when the time constant of changes in the operating condition is small relative to the oscillation period. This is fairly generic during natural transients. It is also a standard requirement in on line adaptation schemes. Yet the significance of including $\dot{\alpha}$-dependent terms is precisely in allowing fast transitions. Conceptually, these terms define a spatially global force field that realizes the effect of the deformation of leading flow structures. In this way, (50) provides a critical enabler to representing intrinsically transient effects, such as the dynamic morphing of a leading edge vortex over a rapidly pitching airfoil into a stagnant separation bubble, hence the hysteresis in lift loss. This effect cannot be captured by the prediction of aerodynamic forces in terms of the state of a traditional, low order Galerkin expansion. As we shall see in the discussion of unsteady boundaries, in § 7, this mechanism is also critical for Galerkin modeling of flow interactions with moving boundaries.

Illustrating these ideas, we have shown (cf. Figure 2) that the topology of both the respective mean fields and of the pairs of local modes representing the oscillatory field, gradually morph from one set of velocity fields to the other along the transient, naturally lending themselves to smooth parametrization. We have also shown (cf. Figure 3) that the unsteady cylinder wake flow is well approximated near any point along the natural transient by a Galerkin expansion, defined by a parametrized representation of the local mean field and a single pair of locally derived modes. The excellent kinematic approximation is paralleled at the dynamic model level by the agreement of the Galerkin projection values of system coefficients with observed dynamic properties of the exact NSE solution for the natural transient of the cylinder wake flow (cf. Figure 9). The Galerkin model employs interpolated modes of the form (52). A practical computational method to explicitly realize the parameterization, including the one showed in Figure 9, will be discussed next.

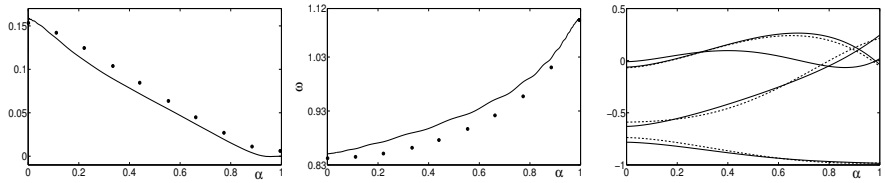

Figure 9. To illustrate the quality of the parametrized Galerkin model, we compare the transient values of $\dot{A}_1/A_1$ along the natural transient of the exact NSE solution (left, solid) with the Galerkin projection evaluation of the expression $\sigma^C - \beta^C a_\Delta$, using the local bases at several intermediate operating points (left, dots). The parametrization is by $\alpha = K_1^{1.5}$. The small positive residual illustrates both the need for a turbulence model and the agreement between the empirical and theoretical observations. A similar comparison is made in the center figure between the observed and predicted shedding frequency. Once again the quality of the approximation is a vast improvement of what is achieved with a single basis. The right figure depicts the interpolation coefficients $b_{i,\,k}(\alpha)$ for $i = 0$ and $i = 1, 2$, when the local bases are defined by the interpolation scheme (52), with $L_0 = 4$ and $L_1 = L_2 = 3$.

6.3 Computational Aspects of Parametrized Mode Sets

The success of nonlinear Galerkin models of the form (50) depends on several key ingredients. Those include the ability to derive a smooth, low sensitivity mapping

$$\alpha \mapsto \mathbf{u}_i(\,\cdot\,,\alpha) \,:\, \mathcal{A} \mapsto \mathcal{L}^2(\Omega), \quad i = 0, 1 \ldots, N.$$

that covers the desired range; the ability to derive a computationally simple and robust approximation of these mappings; and the ability to robustly estimate the parameter α from measurable quantities. Conceptually, there are two interdependent facets to each of these issues. One facet concerns the rate and extent of changes in the leading coherent flow structures along transients, covered by the dynamic envelope. The smoothness and rate of mode deformation along such transients is a measure of the feasibility of the proposed framework, and can be determined by direct analysis of such transients. The other facet concerns the existence of a simple α parametrization of the operating condition.

Parametrize the operating point. Externally determined components of α include the incoming flow velocity and its orientation, the parameters

of pulsatile actuation with slowly varying frequency, amplitude and phase shift relative to a fixed reference frame (time) or to flow oscillations. Also included in this category are parameters of a varying boundary geometry, ranging from flapping flight through membrane actuators, to elastic fluid body interactions. As noted earlier, the discussion of moving boundaries is deferred to § 7. State dependent parameter components need to be robustly estimated from measured surrogates. Examples include the TKE of the unsteady flow, the TKE captured in a frequency band, and the dominant oscillations frequency and the choice should be driven by minimizing the numerical sensitivity of dynamic estimation from sensor data.

The examples we used to illustrate the discussion, above, were all restricted to relatively slow deformations and straightforward parametrization. That said, our studies experimental and simulation based studies of 2D and 3D wake stabilization, in Lehmann et al. (2005); Pastoor et al. (2008), demonstrate the ability of the suggested framework to produce easily, robustly implementable and effective control strategies. In the cylinder wake example, Lehmann et al. (2005), both the shift mode coefficient a_Δ and the instantaneous TKE can be used to parametrize the operating point and both can be inferred from appropriately positioned point-wise flow velocity sensing. In the experimental 3D bluff body stabilization, Pastoor et al. (2008), an even simpler, implicit parametrization underlies a phase feedback that depends on the incoming flow velocity and the phase of vortex shedding from a single lip of the bluff body. A very similar phase feedback strategy, successfully applied to the dynamic state estimates and feedback control of shear layer vortices, in Pastoor et al. (2005), and to separation control of the flow over an airfoil at a high AOA, in Joe et al. (2008); Joe and Colonius (2010).

The dynamics of operating point parametrization. A central outstanding challenge is the potential for *dynamic* interconnections between measurable parameters and deformable flow structures. As an illustration, consider the *dynamic stall* phenomenon (McCroskey, 1982). The dynamic nature of the deformation of dominant flow structures that determine the aerodynamic forces over a rapidly pitching airfoil is at the essence of this phenomenon. To account for the dynamic dependence of lift and drag on the angle of attack (AOA), Theodersen's classic model incorporates the pitch rate into a functional representation of these forces. Later extensions, e.g., McCroskey (1982); DeLaurier (1993); Goman and Khrabrov (1994); Peters et al. (2007)), include in the lift model a simple dynamic system representation of the dependence of aerodynamic forces on the AOA. The goal is to account for such phenomena as the substantial delay in the gradual

changes of the lift, following the end of a pitching motion, i.e., when the AOA is already constant. Despite some experimental demonstration in the cited articles, our experience[6] clearly shows that the this type of models is very sensitive to changes in the characteristics of the pitching maneuvers. The approach proposed in this chapter is to regain robustness by basing the said dynamic model on the key physical aspects that come to play: Forces generated by the moving boundary, which will be discussed in the following section, and the dynamics mode deformation. By this approach, a successful model will be able to correctly couple the parametrization (50a) of mode deformation by α, with an identified auxiliary model that determines α dynamically, in terms of the AOA and other characteristics of the ambient flow. This remark will be further clarified by our next discussion of moving and bending boundaries.

The form and computation of deformable modes. The simplest option is to use (local) linear approximations:

$$\begin{aligned} \mathbf{u}_i(\mathbf{x},\, \alpha) \;&\approx\; \mathbf{u}_{*,i}(\mathbf{x}) \,+\, \kappa_i(\alpha)\mathbf{u}_{\Delta,\,i}(\mathbf{x}), \\ \partial_\alpha \mathbf{u}_i(\mathbf{x},\, \alpha) \;&\approx\; (\partial_\alpha \kappa_i(\alpha))\, \mathbf{u}_{\Delta,\,i}(\mathbf{x}). \end{aligned} \tag{51a}$$

Here $\mathbf{u}_{*,i}$ is the value of the i^{th} mode at a nominal operating point, such as over an attractor, and $\mathbf{u}_{\Delta,\,i}$ approximates the gradient (or the Jacobian, when α is vector valued) $\partial_\alpha \mathbf{u}_i$. The nonlinearity of the dependence on α is absorbed in the mappings $\alpha \mapsto \kappa_i$. As in the case of the shift mode definition, (35b), the simplest way to define the approximate gradients $\mathbf{u}_{\Delta,\,i}$ is via

$$\mathbf{u}_{\Delta,\,i} := \frac{1}{\|\mathbf{u}_{*,i} - \mathbf{u}_{s,i}\|_\Omega} \left(\mathbf{u}_{*,i} - \mathbf{u}_{s,i}\right), \quad , i = 0, 1, \ldots N, \tag{51b}$$

where the attractor is the selected nominal operating point and the steady solution defines the maximal intended range of the approximation. The evaluation of the interpolation coefficients κ_i as functions of $\alpha \in \mathcal{A}$ can then be identified and tabulated from transient numerical or experimental data. Figure 10 illustrates these ideas with depictions of $\mathbf{u}_{\Delta,\,i}$, $i = 1, 2$, calculated for the natural transient of the cylinder wake flow. The figure thus complements Figure 6 which showed $\mathbf{u}_\Delta := \mathbf{u}_{\Delta,\,0}$.

Refined approximations are achievable by a projection of POD approxi-

[6] Here we refer to observation made during joint experimental work with D. R. Williams and associates on flow control of a pitching 3D airfoil Williams et al. (2009).

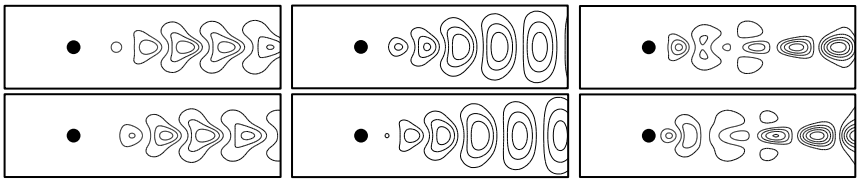

Figure 10. The "shift modes" in a least order approximation of the deforming mode pair that resolves the shedding frequency along the natural transient of the cylinder wake flow. The two shift modes, as defined in (51b), are depicted in the right column. For ease of reference we present here again the corresponding stability eigenmodes, (left column), resolving the 1^{st} harmonic near the steady solution, and the mode pair that resolves that harmonic over the attractor (center column).

mations of each of the "trajectories" $\alpha \mapsto \mathbf{u}_i$ onto the unit sphere in $\mathcal{L}^2(\Omega)$:

$$\mathbf{u}_i(\,\cdot\,,\alpha) \approx \sum_{\ell=1}^{L_i} \tilde{a}_{i,\ell}(\alpha)\mathbf{u}_{i,\,\ell}, \quad \sum_{\ell=1}^{L_i} \tilde{a}_{i,\ell}^2 \equiv 1. \tag{52}$$

The application of this option to the natural transient of the cylinder wake flow is illustrated in Figure 9, depicting the flow fields $b_{i,\,\ell}$ in POD approximations (52) of $\mathbf{u}_i$, $i = 0, 1, 2$. The smoothness of the α dependencies illustrate the robustness and simplicity of these approximations. An illustration focused on the 0^{th} harmonic can be found in Tadmor et al. (2010).

The expressions (51) represent the interpolation of $\mathbf{u}_i(\,\cdot\,,\alpha)$ between evaluations at the two ends of a transient. Yet another natural refinement is thus the interpolation between sampled values of $\mathbf{u}_i(\,\cdot\,,\alpha)$ at multiple intermediate points. This approach, in conjunction with POD modeling, gave rise to the use of geodesic curves over the Grassmann manifold of orthonormal bases, e,g., in Amsallem and Farhat (2008); Amsallem et al. (2009). The use of geodesic interpolation, formalized in Edelman et al. (1998), is common in image and video processing. Since the geodesic is defined in terms of the interpolation hyperplane, rather than individual base vectors, it requires an additional of extracting the explicit basis realization. The advantage of the POD based interpolation (52) over the interpolation approach is that as a POD approximation, (52) optimizes the approximation with respect to bounds on the number of representative flow fields $\mathbf{u}_{i,\ell}$, using the entire data regarding the α-dependence of the expansion modes. In contrast, the starting point of an interpolation scheme is the a priori selection of these fields, as determined by the interpolation points.

While geodesic interpolation over a Grassmann manifold concerns the entire interpolation plane, the hierarchical significance of expansion modes, indicated by their index, is a fundamental albeit implicit tenet of the Galerkin framework. There is therefore an advantage to parametrization approaches that retain the index references to the modes. The harmonic expansion has this advantage, as modes are identified by both the harmonic number and the phase alignment with respect to a common phase trajectory and slowly varying frequencies. An advantage of harmonic modes over POD modes is the instability of the indexing with respect to changes in the operating points: POD approximations can experience significant state space rotations between modes representing similar energy levels in response to small variations in the operating point.

6.4 Closing Comments

Parametrized modes vs. higher dimension. Our first comment revisits the important distinction between higher state dimension and the inclusion of a dependence on the parameter α. This is called for because, at a first glance, an approximations such as (52) may appear as equivalent to the use of the larger expansion set, $\{\mathbf{u}_{i,\,\ell}\}_{\ell=1}^{L_i}{}_{i=1}^{N}$, which is precisely what we tried to avoid, in the first place. We therefore recall that the coefficients $\tilde{a}_{i,\ell}(\alpha)$ in the parametrization (52) are not states of the dynamical system. As functions of α, these coefficients are determined either by an external input, including control commands and the ambient conditions, or as functions of the Galerkin system state, $\mathbf{a} = [a_i]_{i=1}^N$. In the latter case, this slaving of $\{\tilde{a}_{i,\ell}\}_{i,\ell}$ is conceptually analogous to the slaving of higher modes to few dominant modes in center and approximate inertial manifold models. The distinction is that here, the goal is the resolution of mode deformation between operating points, and not the not the resolution of smaller and faster structures, as in center and approximate inertial manifold models.

Parametrized modes vs. center and inertial manifold models. Expanding on this point, the center / approximate manifold approximation of the flow field (and generally, the exact state of the high order system), is by expansions of the form

$$\mathbf{u} = \mathbf{u}_* + \sum_{i=1}^{N} a_i \mathbf{u}_i + \sum_{i=N+1}^{N+M} \tilde{a}_i(\mathbf{a})\mathbf{u}_i,$$

where $\mathbf{a} = [a_i]_{i=1}^N$ is the state of the low order Galerkin system, $\mathbf{u}_i$, $i = N+1, \ldots, N+M$, are the slaved modes of a higher order model, resolving finer spatial and temporal resolution.

In contrast, when the formalism of (52) is used, the flow field reconstruction in the proposed framework is

$$\begin{aligned} \mathbf{u} &= \mathbf{u}_* + \textstyle\sum_{i=1}^{N} a_i \mathbf{u}_i(\alpha) \\ &= \mathbf{u}_* + \textstyle\sum_{i=1}^{N} a_i \sum_{\ell=1}^{L_i} \tilde{a}_{i,\ell}(\alpha) \mathbf{u}_{i,\ell}, \\ \alpha &= f(\mathbf{a}, \mathit{inputs}). \end{aligned} \tag{53}$$

What changes is therefore the purpose of using $\sum_{i=1}^{N} L_i > N$ modes, which is the resolution of mode deformation, rather than smaller scales. The two approaches are therefore complementary, rather than overlapping.

Analytic construction of the parametrized expansion set. The ability to compute the deforming expansion modes by direct appeal to the NSE and stability eigenmodes, as an alternative to the empirical / post processing approach we described earlier, is an interesting observation, previously pursued in relation to base flow corrections (Tadmor et al., 2007b, 2010). This approach is based by an extension of the use of the Reynolds equation and a close variant can be found in the aforementioned independent and elegant study by Sapsis and Lermusiaux (2009). A brief outline of key aspects of the procedure is presented here for harmonic expansions.

A useful observation. The computations is greatly facilitated by the observation that the local deformation of the mode $\mathbf{u}_i$ must be orthogonal to that mode. The reason is simply the fact that the normalized modes vary over the unit sphere in $\mathcal{L}^2(\Omega)$, whereby the correction term, which is proportional to the tangent vector $\partial_\alpha \mathbf{u}_i$, must be orthogonal to the sphere at $\mathbf{u}_i$:

$$\partial_\alpha \mathbf{u}_i \perp \mathbf{u}_i. \tag{54}$$

Expansions of small fluctuations from $\mathbf{u}_s$: Small fluctuations from a fixed point are approximated by eigenmode expansions

$$\mathbf{u} = \mathbf{u}_s + A_0 \mathbf{u}_0 + \sum_{i=1}^{N_h} A_i (\cos(\phi_i)\mathbf{u}_{2i-1} + \sin(\phi_i)\mathbf{u}_{2i}). \tag{55}$$

Here N_h is the number of frequencies we aim to resolve and $\{\mathbf{u}_{2i-1}\}_{i=1}^{N_h}$ are the respective stability eigenmodes, at $\mathbf{u}_s$ is the fixed point. The linear mean field correction mode, $\mathbf{u}_0$, is the eigenvector for the largest real eigenvalue. It may be difficult to compute when that eigenvalue represents fast decay. In that case $A_0 = 0$ and $\mathbf{u}_0$ can be ignored when very small fluctuations are considered. To simplify this brief discussion, we shall nonetheless

assume that $\mathbf{u}_0$ is known. The rationale presented here will allow the reader to extend the observations we make to the case where we use $\mathbf{u}_0 = 0$ near $\mathbf{u}_s$.

Generalized Reynolds averaged equations. Let us recall the spatio-temporal projections we used in the discussion of harmonic expansions, in § 3.

The period averaged projection of the NSE on the expansion (55) is the Reynolds equation, (33a). That equation determines the (quadratically dominated) algebraic relationships between A_0 and A_i, $i = 1, \ldots, N_h$. However, as A_1 is increased, so will the residuum in the period averaged NSE. That residuum can be corrected by correcting both A_0 and $\mathbf{u}_0$, i.e., by defining

$$\begin{aligned} &A_0(\alpha_s + \delta\alpha\partial_\alpha)\mathbf{u}_0(\alpha_s + \delta\alpha\partial_\alpha) \\ &\qquad \approx A_0(\alpha_s)\mathbf{u}_0(\alpha_s) + (\partial_\alpha A_0\mathbf{u}_0(\alpha_s) + A_0(\alpha_s)\partial_\alpha\mathbf{u}_0)\ \delta\alpha, \end{aligned}$$

where α_s is the parameter value at the steady solution and $\delta\alpha$ reflects the change in the operating condition. The orthogonality property (54) allows us to partition the residuum equation into two independent linearized equations, one for the component of the mean field correction that is aligned with $\mathbf{u}_0(\alpha_s)$, yielding the amplitude correction $\partial_\alpha A_0$, and one for the component orthogonal to $\mathbf{u}_0(\alpha_s)$, yielding the orientation $\partial_\alpha\mathbf{u}_0$ of the $\dot{\alpha}$-proportional mode deformation.

As in the computation of Fourier coefficients, (14), sinusoidally weighted period averages distill the NSE components that are pertinent to each participating frequency and phase. In precisely the same manner, and by precisely the same rationale as for the 0^{th} harmonic, right above, these weighted averages create equations that define the dependence of the incremental amplitudes and modes as functions of $\delta\alpha$. That is, they allow us to solve for $\partial_\alpha A_i$ and for $\partial_\alpha\mathbf{u}_i$, for all i. Moreover, a Galerkin projection of the NSE, using the corrected modes and amplitudes, will yield the corrected value of the dominant frequency $\omega(\alpha_s + \delta\alpha)$.

Incremental marching. There is no conceptual difference between the computation of $\partial_\alpha A_i$ and $\partial_\alpha\mathbf{u}_i$, near α_s, and between the computation of such increments near any other operating point. Key to this observation is the fact that the computations are based on period averaging, whether near α_s or near any other value of α. The conclusion is that expansion modes, coefficients and frequency can (ideally) be computed along the entire operational range in terms of solutions of a succession of incremental equations.

7 Galerkin Models for Flows in Unsteady Geometry

Fluid interactions with moving and deforming boundaries are part and parcel of key fluid mechanics issues, from flow control challenges in engineered systems through bio-flyers and swimmers, to plants. Familiar examples in engineered systems include damaging vibrations in turbine engines (Russell, 1950; Hall et al., 2006; Boyce, 2006), wind turbines (Andersen et al., 2007; Barlas and van Kuik, 2009; Wilson et al., 2009; Berg et al., 2009), helicopter blades (Leishman, 2006) and civil infrastructure (Clark et al., 2004; Strømmen, 2006; Stathopoulos and Baniotopoulos, 2007), full-structure bending and torsional forces on light, high-altitude long-endurance (HALE) flying wings, such as DARPA's Vulture and NASA's ill-fated Helios (Noll et al., 2007; Patil, 2007; Raghavan and Patil, 2010), and both damaging flatter and buffeting and the currently pursued potential for lift enhancement and drag reduction by active aero/hydroelastic and boundary actuation mechanisms (Theodorsen, 1935; Livne, 2003; Ho et al., 2003; Kamakoti and Shyy, 2004; Clark et al., 2004; Ansari et al., 2006; de C. Henshaw et al., 2007; Kota et al., 2009; Carruthers et al., 2007; Liang et al., 2006; Lopez and Sarigul-Klijn, 2010; Dong et al., 2010). Equally interesting, elastic fluid body interactions are central to bio-swimmers and bio-flyers (Pendleton, 2000; Ho et al., 2003; Fish and Lauder, 2006; Carruthers et al., 2007; Kato and Kamimura, 2008; Lauga and Powers, 2009; Dong et al., 2010; Shyy et al., 2010), and even plant-wind interactions (de Langre, 2008). In addition to their critical roles in crisply encapsulating an accessible understanding of the physics of fluid-body interactions, and in the design of feedback controllers, low order models are increasingly sought as computational tools, used to accelerate numerical simulations in these highly demanding configurations (Schuster et al., 2003; FFAST, 2010). This section addresses the conceptual challenge of a consistent definition of LOGMs for these flow configurations, and the means to compute such models.

7.1 A Galerkin Modeling Conundrum and Existing Solutions

In applications such as the examples listed above, the Galerkin modeler faces yet another, seemingly insurmountable conceptual conundrum: Unsteady geometry requires that (Eulerian) global expansion modes satisfy at once the mutually exclusive dynamic properties of body and of fluid, over subdomains that are alternately occupied by body and by fluid. This inherent contradiction precludes the physical credibility and consistency that are at the very foundation of the Galerkin approach to model reduction. Here we review existing approaches and set the ground for a solution path.

Most prevalent solution categories. Reviewing today's state of the art (Dowell and Hall, 2001; Livne, 2003; Schuster et al., 2003; Clark et al., 2004; Peters et al., 2007; Demasi and Livne, 2009; Silva et al., 2009), most existing solutions may be broadly classified in one of two general categories:

In one category, low oscillation amplitudes justify a sole focus on the generated acceleration forces acting on the fluid at the boundary. Boundary displacements and domain variations are ignored, the ambiguity regarding the governing dynamic laws is eliminated, and the Galerkin method can be used in its traditional form. Methods that employ linearized elasticity models are quintessential examples of this approach.

The primary focus of methods of the second category is on the elastic body. Fluid dynamic representation is reduced to low order models of aerodynamic forces, induced by the flow. Tracing to Theodorsen (1935), such models may postulate potential flows, with or without a periodic train of vortices over an airfoil, and or claibrate aerodynamic forces by harmonic balancing. Methods in this category provide effective computational and analytical tools in (nearly) steady or in predictably periodic flows.

These broad-brush descriptions do not do ample justice to the rich and diverse pools of ideas in each of the two categories. Nonetheless, they provide a "birds-eye view" of the limitations of both, when the targeted fluid-body system displays large scale, unsteady, transient dynamics.

Actuation modes. Yet a third direction, applicable primarily to rigid body motion, is based on two complementary ideas:

(i) Transition to body-locked coordinates. This is straightforward in an external flow around a single moving rigid body. Resulting variations of far field geometry are viewed as negligible and handled by domain truncation to a uniform, time invariant subdomain.

(ii) An unsteady coordinate change induces an unsteady addition to the velocity field, including the boundary velocity. The unsteady velocity at the boundary is absorbed by a modulated Galerkin expansion, using (incompressible) *actuation / boundary modes* $\mathbf{u}_{act,\,i}$, so that the velocity field

$$\mathbf{u} - \mathbf{u}_{act} := \mathbf{u} - \sum_{i=1}^{N_{act}} b_i \mathbf{u}_{act,\,i}, \tag{56}$$

is steady along the boundary. When this correction follows a transition to a steady domain, then $\mathbf{u} - \mathbf{u}_{act}$, has the properties required by the traditional Galerkin framework: A steady domain with steady boundary conditions.

We illustrate these ideas, right below, with two simple examples: The oscillating cylinder (Noack et al., 2004b; Tadmor et al., 2004; Siegel et al., 2008; Liberge and Hamdouni, 2010), and the rotating cylinder (Graham et al., 1999a,b; Bergmann et al., 2005, 2007). Other pertinent examples include the lid-driven cavity (Fitzpatrick et al., 2005), and the flow around a heaving and pitching airfoil (Lewin and Haj-Hariri, 2005; Stankiewicz et al., 2008). Finally, we mention also actuation modes arising in the context of an unsteady inflow which does not involve boundary motion, but does invoke very similar ideas (Kasnakoğlu et al., 2008). We shall revisit these examples throughout this section.

$*$ *The vertically oscillating cylinder.* Referring to the description in § 2, we use α to denote the instantaneous vertical coordinate of the center of the cylinder, whereby the unsteady domain is

$$\Omega(\alpha) = \{\mathbf{x} = (x, y) \in [-5,\, 15] \times [-5,\, 5],: \, \|(x, y - \alpha\| \geq 1/2\,\},$$

and the point-wise parametrization of the boundary is

$$\Omega'(\alpha) = \left\{ \mathbf{x}_b(\alpha,\, \kappa) := 1/2 \begin{pmatrix} \cos(\kappa) \\ \sin(\kappa) \end{pmatrix} + \alpha \begin{pmatrix} 0 \\ 1 \end{pmatrix}, \quad \kappa \in [0,\, 2\pi) \right\}.$$

Moving to a body locked coordinates, the cylinder center is used as origin. Vertical fluctuations of the upper and lower boundaries, now located at $y = \pm 5 + \alpha$, are ignored and $\Omega_c := \Omega(0)$ is used as a fixed computational domain. Ignoring the far field unsteady boundary is justified since the spatial development of flow unsteadiness near the upper and lower boundaries is negligible.

The transition to a body locked coordinates induces a global addition of a vertical velocity $-\dot{\alpha} \binom{0}{1}$. This addition cancels the original vertical velocity of points along Ω'_c, where a standard zero velocity boundary condition now holds. Yet the added unsteadiness is felt away from the cylinder, and in particular, the far field boundary velocity is now unsteady. The actuation mode used to cancel this unsteadiness in Noack et al. (2004b); Tadmor et al. (2004), is depicted in Figure 11 (left plot). It is a viscus potential flow around the cylinder, with a vertical unit amplitude inflow.

$*$ *The rotating cylinder.* This effects of cylinder rotation on lift, drag, and wake stability have been studied extensively in both experimental and numerical studies (Hu et al., 1996; Mittal and Kumar, 2003; Lo Jacono et al., 2008). Flow control studies (Graham et al., 1999a,b; Bergmann et al., 2005, 2007; Bergmann and Cordier, 2008) employed low order Galerkin models

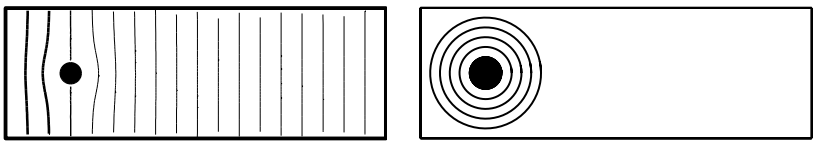

Figure 11. Left: An actuation mode $\mathbf{u}_{act}$ for the vertically oscillating cylinder is defined as a potential flow with a vertical inflow. Right: An actuation mode for the rotating cylinder is a potential vortex flow with a zero far field azimuthal velocity.

and required a method to address boundary unsteadiness. The solution proposed by these authors is the use of an actuation mode depicted in the right plot, in Figure 11, formed as a potential vortex flow, driven by the rotating cylinder with a no-slip boundary condition, and a zero azimuthal velocity on a larger, concentric circle. Notice that while this example involves an unsteady boundary, the geometry of the flow domain is steady, to begin with.

Lagrangian- ulerian methods and deformable grids. Shortcomings of the actuation / boundary modes approach include the lack of systematic guidelines for generating actuation modes and, more significantly, a quantum leap in the challenge of the transition to steady coordinates of elastic and multiple bodies. To address the latter, a number of pioneering studies (Epureanu et al., 2002; Anttonen et al., 2003, 2005; Feng and Soulaïmani, 2007; Liberge et al., 2008) endeavored to adapt Eulerian-Lagrangian dynamic mesh adaptation methods, that are commonly used in CFD models of aeroelasticity (Batina, 1990; Farhat et al., 1998; Blom, 2000; Schuster et al., 2003; Ishihara and Yoshimura, 2005; Hsu and Chang, 2007; Xie et al., 2007; Braun et al., 2008; Roszak et al., 2009). The objective in these methods is to continuously deform the fluid simulation's grid, in a way that agrees with the deforming fluid-body interface and that obeys pertinent geometric properties, including incompressibility. Identifying the flows state not with the Eulerian location but rather, with the index of a Lagrangian grid point, these methods achieve the equivalent of a transition to a canonical computational domain. An analogy of the deforming fluid domain to the boundary-driven equilibrium of an elastic body allows the developer of a numerical method to draw on a vast body of knowledge in theoretical and numerical solid mechanics. Developments along these lines are still vibrant, not only in CFD and computational elasticity (Bijelonja et al., 2006; Persson and Peraire, 2009) but also in other areas of applied geometry, notably, in diverse areas of computer graphics (Hong et al., 2006; Irving et al., 2007;

Adams et al., 2008; Diziol and Bayer, 2009).

Our objective in this section is to review a broadly applicable methodology that integrates these ideas with the observation underlying the actuation modes approach, regarding the two ingredients of a successful solution: The transition to a steady computational domain, where the ambiguity between body and fluid is removed, and the cancellation of residual unsteady velocity at the boundary, to enable the space-time separation of variables, at the essence of the Galerkin paradigm. In what follows we use two subsections to derive the characteristics of each of these two components, preparing for the subsequent constructive integration of the two. Setting the ground for these technical discussions, we begin with a brief review of basic formalism and assumptions that will be used, and introduce the concept of the *complete flow domain*, for flows over unsteady boundaries.

7.2 Canonical Embedding Preliminaries

Nomenclature and assumptions. To simplify notations, throughout this section we use $\alpha \in \mathcal{A}$ *only* to define a smooth *point-wise* parametrization of the boundary[7] $\Omega'(\alpha)$ of the compact domain $\Omega(\alpha)$. That is, we assume that boundary points are defined by a smooth function $\mathbf{x}_b(\alpha, \kappa) \in \Omega'(\alpha)$, where κ is a local coordinates parametrization (in the differential geometric sense) of the boundary curve or surface, for each α.

The boundary $\Omega'(\alpha)$ may include both walls of bodies immersed in, or bounding the flow, and free, far field inflow and outflow boundaries of the studied domain. Restricting this discussion to incompressible flows, we assume that the volume (or area) of $\Omega(\alpha)$ is constant, and independent of α. Where needed, the constant volume assumption can be easily enforced by α-dependent far field, inflow and outflow boundaries.

The velocity conditions along the boundary include steady or unsteady inflow and outflow conditions, and *no-penetration* and *no-slip* conditions along body walls. The latter require that, along these sections, fluid velocity must agree with wall velocity.

We treat α as an exogenous input. Control mechanisms and elastic fluid-body interactions are represented by feedback laws, determining α.

The augmented domain and velocity field. While the ambiguity regarding the applicable dynamic rule at points in space that are alternately

[7] We bear in mind, however, that the need to parametrize mode deformations may only rise in the presence of deforming boundaries, and that viable models should incorporate parametrization of mode deformation, as discussed in § 6.

occupied by fluid and structure is clear, we argue that essentially the same ambiguity exists throughout the spatial domain: The dynamic rule at a point $\mathbf{x}$ is determined by the location of $\mathbf{x}$ relative to the boundary. A complete description of a point in the domain thus requires the specification of the pair $(\mathbf{x},\, \alpha)$, whereby the *complete flow domain* is the manifold:

$$\mathcal{M}_\Omega := \{(\mathbf{x}\,, \alpha) \,:\, \alpha \in \mathcal{A},\ \mathbf{x} \in \Omega(\alpha)\,\}. \tag{57}$$

Vector fields over $\mathcal{M}_\Omega$ comprise of pairs $(\mathbf{u}, \nu)$, so that

$$\frac{d}{dt}(\mathbf{x},\, \alpha) = (\mathbf{u},\, \upsilon). \tag{58}$$

The concept of the complete domain, $\mathcal{M}_\Omega$, will enable the use of compact and unambiguous formalism, throughout this discussion. For example, in stating the prescribed wall velocity, by (58).

Should we develop LOGMs over $\mathcal{M}_\Omega$***?*** The derivation of expansion modes by the methods considered heretofore requires a succession of snapshots of the flow. Among other issues (e.g., the nonlinearity of $\mathcal{M}_\Omega$) we note that a LOGM for the flow over $\mathcal{M}_\Omega$ stipulates that a snapshot is a vector field $(\mathbf{u}, \nu)$, which needs to be defined for all $(\mathbf{x},\, \alpha) \in \mathcal{M}_\Omega\mathcal{M}_\Omega$. Yet the time trace of a simulation or an experiment defines the fluid velocity $\mathbf{u}(\,\cdot\,, t)$ as a vector field over $\Omega(\alpha(t))$, for the single value of $\alpha(t)$. This gap can be closed in a way that conceptually parallels what will be described here. Considering the complexity of this option, however, our choice is to limit the use of the augmented domain and vector fields to the notational and conceptual simplifications they will enable along the discussion. LOGMs will be developed more traditionally, either over a canonical computational domain, or equivalently, in an Eulerian-Lagrangian setting, over an unsteady grid in the physical domain, as will be explained below.

7.3 Canonical Embedding for Deforming Boundaries

Admissible embedding in a canonical computational domain. The transition to a steady (canonical) computational domain, Ω_c, is made by an *admissible mapping*, ψ,

$$\psi \,:\, (\mathbf{x},\, \alpha) \mapsto (\mathbf{x}_c,\, \alpha) \,:\, \mathcal{M}_\Omega \mapsto \Omega_c \times \mathcal{A}, \tag{59}$$

which is required to satisfy the following basic properties:

• ψ is a diffeomorphism. This is clearly necessary to enable an unambiguous correspondence between the flow over the physical domain and its

representation over the canonical domain.

• For each α, $\psi(\Omega'(\alpha),\, \alpha) = (\Omega'_c,\, \alpha)$. Thus, a coordinate parametrization of Ω'_c is defined by $\kappa \mapsto \psi(\mathbf{x}_b(\alpha,\, \kappa),\, \alpha)$, for each $\alpha \in \mathcal{A}$.

• For each α, the induced mapping

$$\mathbf{x} \mapsto \mathbf{x}_c \,:\, \Omega(\alpha) \mapsto \Omega_c$$

is incompressible (isocheric).

The velocity field over the canonical domain. Invoking (58), an admissible mapping ψ induces a mapping of velocity fields over the physical domain to velocity fields over the canonical computational domain, via:

$$\begin{aligned} \Psi(\mathbf{u},\, v,\, \mathbf{x},\, \alpha) &= \left(\tfrac{d}{dt}\psi(\mathbf{x},\, \alpha),\, \psi(\mathbf{x},\, \alpha)\right) \\ &= \left(\left(J_{\mathbf{x}_c,\mathbf{x}}\,\mathbf{u} + J_{\mathbf{x}_c,\alpha} v,\, v\right),\, \psi(\mathbf{x},\, \alpha)\right), \end{aligned} \tag{60a}$$

where

$$J := \left[\begin{array}{cc} J_{\mathbf{x}_c,\mathbf{x}} & J_{\mathbf{x}_c,\alpha} \\ 0 & I \end{array}\right] := \left[\begin{array}{cc} \partial_{\mathbf{x}}\mathbf{x}_c & \partial_\alpha \mathbf{x}_c \\ 0 & I \end{array}\right] \tag{60b}$$

is the Jacobian of ψ. The requirement that ψ be diffeomorphic guarantees that $J_{\mathbf{x}_c,\mathbf{x}}$ is invertible, and that both this Jacobian and its inverse are smooth functions of $(\mathbf{x},\, \alpha)$. The inverse mapping has a similar form:

$$\begin{aligned} \Psi^{-1}(\mathbf{u}_c,\, v,\, \mathbf{x}_c,\, \alpha) &= \left(\tfrac{d}{dt}\psi^{-1}(\mathbf{x}_c,\, \alpha),\, \psi^{-1}(\mathbf{x}_c,\, \alpha)\right) \\ &= \left(\left(J^{-1}_{\mathbf{x}_c,\mathbf{x}}\,\mathbf{u}_c - J^{-1}_{\mathbf{x}_c,\mathbf{x}}\, J_{\mathbf{x}_c,\alpha} v,\, v\right),\, (\mathbf{x},\, \alpha)\right). \end{aligned} \tag{60c}$$

The mapping Ψ translates boundary conditions in the physical and the velocity of the boundary motion, reflected by $\nu = \dot{\alpha}$, into boundary velocity conditions over the canonical domain.

An auxiliary flow. An admissible mapping ψ is associated with an auxiliary Lagrangian (particle) flow over the manifold $\mathcal{M}_\Omega$: $\forall \alpha,\, \beta \in \mathcal{A}$,

$$\mathcal{S}(\beta, \alpha) := \psi^{-1}(\,\cdot\,, \beta) \circ \psi(\,\cdot\,, \alpha) \,:\, (\Omega(\alpha),\, \alpha) \rightleftarrows (\Omega(\beta),\, \beta). \tag{61}$$

The smooth invertibility of ψ implies that $\mathcal{S}$ is a diffeomorphic and incompressible (isocheric) deformation of the physical domain, depending smoothly on α.

The requirement that the boundary be invariant under ψ means that $\mathcal{S}$ gives rise to a diffeomorphic flow over the boundary:

$$\mathcal{S}_b(\beta, \alpha) \,:\, (\Omega'(\alpha),\, \alpha) \rightleftarrows (\Omega'(\beta),\, \beta), \tag{62a}$$

such that

$$\forall \alpha,\, \beta \in \mathcal{A}, \quad \mathcal{S}_b(\beta, \alpha) = \mathcal{S}(\beta, \alpha)\,|_{(\Omega'(\alpha),\, \alpha)}. \tag{62b}$$

The Lagrangian particle flow $\mathcal{S}$ induces a corresponding flow of velocity fields, in complete analogy to (60):

$$\mathcal{T}(\beta, \alpha) := \Psi^{-1}(\,\cdot,\, , \dot{\beta},\, \cdot\,, \beta)\Psi(\,\cdot,\, , \dot{\alpha},\, \cdot\,, \alpha) \tag{63}$$

This definition leads to consistent concepts of algebra and analysis by which snapshots of the velocity field over one boundary configuration can be compared to, and algebraically co-manipulated with snapshots over another boundary configuration. The, presence of the canonical domain is kept implicit, and the governing equation, the NSE, remains unchanged!

A focus on $\mathcal{S}$. The following observation allows us to consider the construction of ψ and Ψ, indirectly, in terms of $\mathcal{S}$ and $\mathcal{T}$:

Observation 7.1. *An admissible mapping ψ generates an ensemble of admissible, diffeomorphically equivalent maps $\{\psi_\beta\}_{\beta\in\mathcal{A}}$:*

$$\psi_\beta(\mathbf{x},\, \alpha) := \mathcal{S}(\beta, \alpha)(\mathbf{x},\, \alpha) \in \Omega(\beta) \times \{\beta\}. \tag{64}$$

Consequently, ψ also generates an ensemble of mappings $\{\Psi_\beta\}_{\beta\in\mathcal{A}}$, which correspond to $\{\psi_\beta\}_{\beta\in\mathcal{A}}$ in complete analogy to the definition (60) *of Ψ in terms of ψ. There is therefore no loss of generality in assuming that $\Omega_c = \Omega(\beta)$, for any fixed $\beta \in \mathcal{A}$, using ψ_β and Ψ_β in the roles of ψ and Ψ.*

A "spring analogy" construction of $\mathcal{S}$: Basic steps. Lagrangian-Eulerian methods, mentioned on p. 61, offer a natural option for the construction of $\mathcal{S}$. Given the extensive literature on these methods, and ongoing efforts invested in their continued improvement, we see no need or point to expend on a favorite variant. This discussion is therefore limited to a conceptual outline of generic key steps, right below, to be followed by highlight of possible points of departure from CFD considerations and implementations of spring-analogy algorithms:

• A point β is selected as the *origin* in the parameter set $\mathcal{A}$. In principle this selection is arbitrary, but as we shall comment later, it may be advantageous to select the parameter reflecting the elastic boundary in a relaxed state.

• A grid $\mathbf{X} := \{\mathbf{x}_i\}_{i=1}^{N_g} \subset \Omega(\beta)$, is selected to meet the desired resolution of a LOGM at the parameter value β. For later reference, we denote the

sub-grid of boundary points as $\mathbf{X}_b := \{\mathbf{x}_{b,\,j}\}_{j=1}^{N_{b,g}} \subset \Omega'(\beta)$.

• Boundary deformation, as α varies, translate to variations in $\mathbf{X}_b$. The initial selections of $\mathbf{x}_{b,\,j}$, for the parameter value β, therefore immediately extend to the definition of boundary grid points as functions of α. Thus

$$\mathbf{X}_b(\alpha) := \{\mathbf{x}_{b,\,j}(\alpha)\}_{j=1}^{N_{b,g}} \subset \Omega'(\alpha), \qquad \alpha \in \mathcal{A}. \tag{65}$$

• An algorithm for smooth, incompressible mesh adaptation defines the deformation of $\mathbf{X}$ in response to changes in $\mathbf{X}_b(\alpha)$, as α varies. Thus

$$\mathbf{X}(\alpha) := \{\mathbf{x}_i(\alpha)\}_{i=1}^{N_g} \subset \Omega(\alpha), \qquad \alpha \in \mathcal{A}. \tag{66}$$

The incompressibility of the deformation is interpreted by the requirement that the volume of the grid cell represented by $\mathbf{x}_i(\alpha)$ is independent of α.

• The flow $\mathcal{S}$ is defined by the mappings $\mathbf{X}(\alpha_1) \mapsto \mathbf{X}(\alpha_2)$, $\alpha_i \in \mathcal{A}$.

• The flow $\mathcal{T}$ maps velocity fields over $\Omega(\alpha_1)$ to a velocity fields over $\Omega(\alpha_2)$, as a function of α_i and $\dot{\alpha}_i$, as detailed in (63).

• To extract expansion modes for a LOGM from velocity field snapshots $\{\mathbf{u}(\,\cdot\,, t)\}_{t\in\mathcal{I}}$, these snapshots need to be evaluated (interpolated) at the Lagrangian grid points $\mathbf{x}_i(\alpha)$, and viewed as functions of the Lagrangian grid points (identified by the indices, i). This way, the mapping $\mathcal{T}$ enables the linear algebra of velocity fields from different snapshots, that can now be used in mode extraction methods, such as POD.

Note that in the discrete setting, the index j of a boundary point $\mathbf{x}_{b,\,j}(\alpha)$, is a discrete analogue of the parameter κ in a continuous description. Note also that the inflow and outflow boundary sections are generically steady. Thus, the generic boundary conditions for Lagrangian motion of grid points over this sections are independent of α.

The "spring analogy" construction of $\mathcal{S}$: Cautionary comments. It is important to highlight differences between CFD and LOGMs needs, and the essential implications of these differences on the implementation of adaptive mesh algorithms.

• The very large grids used in CFD simulations necessitate the spatial and temporal *localization* of mesh adaptation methods. Jumps and readjustments that may occur as a consequence, are viewed as a matter of course.

Consistency of the association of the instantaneous grid as a function of boundary configuration, is not required. In contrast, in order to be able to derive a viable parametrized LOGM, the essential property of (66) is that it is defined *globally*, both in space and as a function of α, and the simplicity, smoothness and robustness of this definition, held at a premium. At the same time, the far sparser grids that suffice for LOGM computations, make this type of grid definition feasible. An import of a mesh adaptation algorithm, "as is", from a CFD context to LOGM use, is therefore very likely not to enable the desired definitions of $\mathcal{S}$ and $\mathcal{T}$.

• A recurrent issues in the discussions of elasticity-based mesh adaptation concerns the adverse effects of over-stretching of the grid, such as in response to a rotational motion. Considering the simple example of a rotating cylinder, attaching boundary points of a grid formed as material points of a fictitious elastic body, to points along the boundary of the physical domain, i.e., the rotating cylinder and the steady far field boundary, will cause the elastic material to stretch in an infinite spiraling motion. This stretching will lead to loss of grid continuity and to numerical singularity. By the same token, this scenario also illustrates a situation in which the use an adaptive mesh is not only difficult, but, is utterly unnecessary, and is easily substituted by the simple and robust implementation of an actuation / boundary mode, as discussed earlier.

What we have shown in the discussion leading to the outline of the construction of $\mathcal{S}$ and $\mathcal{T}$, amounts to the observation that, when successful, that procedure can fully address the transition to a canonical domain, where fluid velocity obeys steady boundary conditions. Yet the simple example of the rotating cylinder demonstrates that the success of the outlined constructions is not guaranteed, highlighting grid stretching due to rotational motion, as a major culprit. That example reminds us of the second ingredient of the envisioned approach: The use of actuation modes. Our next step is to suggest a simple means to define actuation modes, and a way to use them to mitigate the observed shortfall.

The construction of $\mathcal{S}$: Slip conditions and actuation modes. As described above, and as commonly implemented in CFD applications, the elastic body analogy requires a rigid attachment of the fictitious elastic body, represents the fluid domain, to the physical domain's boundary. That requirement ensures that the mapping of fluid velocity to the Lagrangian grid, will remain consistent with the inflow, outflow, no-penetration and no-slip conditions.

Considering the difficulty illustrated by the rotating cylinder example,

we note that its rout-cause is the wall-tangent velocity, imposed by the no-slip condition. We also note that the no-slip condition has no bearing on geometry variations. The solution path outlined here is to use grid deformation *only* in order to track the unsteady geometry, as implied by the no-penetration conditions. In this framework, the boundary grid points in $\mathbf{X}_b(\alpha) = \{\mathbf{x}_{b,\,j}(\alpha)\}_{j=1}^{N_{b,\,g}}$ are allowed to slide along the walls of immersed bodies, but are held locked to the far field boundaries. Actuation modes will be used in a subsequent step, to absorb residual wall-tangent velocity, as in (56). As an aside, we note that the need to absorb residual boundary velocity may exist not only due to boundary motion, but also due to unsteady inflow velocity, whether as a control mechanism or a disturbance.

Comments & alternative guidelines. The prevention and remediation of over-stretching grid cells are critical components of elasticity-based adaptive mesh methods. The inclusion of torsional springs (Farhat et al., 1998) is an example of a quintessential preventative measure. Since CFD methods tolerate mesh discontinuity as a matter of course, a discontinuous mesh update is the generic remediation, once the benefits of the way the elastic structure is formulated, are exhausted. Giving up on the no-slip conditions, and the use of actuation modes counterparts, is generally not a viable option in CFD contexts. That said, a closer, localized look at the remeshing step would typically reveal the conceptual partition into a sliding grid component and a correction that resolve the residual slip velocity, i.e., the approach presented here as a global strategy. That analogy is explicit even in the very title of the Shear-Slip mesh update method of Tezduyar (2001). That said, some CFD methods do allow the mesh to slide over moving boundaries (Demirdžić et al., 1997).

We also note that while the removal of the no-slip condition will resolve the adverse effect of rotational stretching, it will not address the impact of large scale translational motion. Methods to address this challenge are based on multi-domain approach: A moving body is surrounded by a local subdomain that is locked to the body's geometry, and moved together with the body. The methods described here will then apply to grid adaptation within that local subdomain. Velocity fields on the local and global subdomains are then reconciled in a subsequent step which is less challenging since it does not involve unsteady geometries. Several authors have addressed the issue of large scale translational motion in CFD contexts (Tezduyar, 2001; Murman et al., 2003).

The last comment concerns the very of solid, rather than fluid mechanics to derive the mesh adaptation scheme. The motivation is clear: Even when a fluid flow is considered reversible, this applies only to the velocity

field, and not necessarily to the induced Lagrangian particle motion. That said, generic examples such as the substantial oscillations of a flexible airfoil can be handled by use of highly viscous (Stokes) simulations to define the auxiliary mappings $\mathcal{S}$ and $\mathcal{T}$. The auxiliary Stokes flow is determined by boundary motion, as is derived from the original fluid simulations. In the generic case of (quasi) periodic oscillations, boundary motion can be expanded by a short harmonic expansion. Expanding the induced particle motion within the domain by a truncated harmonic expansion of the same length is a linear operation that does not affect incompressibility and defines domain (and grid) deformation that obeys the imposed boundary unsteadiness.

Example: A continuously deforming cylinder. Yet a third variant of the cylinder wake flow provides a very simple illustration of the Lagrangian-Eulerian approach to LOGMs of flows over unsteady boundaries. In this example the cylinder undergoes forced periodic deformations, and the fluid flow domain, $\Omega(\alpha)$, is parametrized by the phase, $\alpha \in [0,\, 2\pi] =: \mathcal{A}$, of these deformations:

$$\Omega(\alpha) := \{\mathbf{x} \in [-5, 15] \times [-5, 5] : \|\mathbf{x}\| \geq 0.5 + \epsilon \sin(\alpha) \cos(3\theta),\, \theta = \angle\mathbf{x}\}.$$

(The notation $\theta = \angle\mathbf{x}$ is interpreted by $\mathbf{x} = (x, y) = \|\mathbf{x}\|(\cos(\theta),\, \sin(\theta))$.) The deformations are illustrated by the top-left plot in Figure 12, where $\epsilon = 0.1$.

This example does not include rotational motion, and boundary unsteadiness is fully addressed by the transition to the canonical domain, defined by $\Omega_c := \Omega(0)$, or equivalently, by a transition to a Lagrangian grid. Domain deformation, i.e., the mappings ψ and Ψ, were computed both by an elasticity based adaptation and by the filtered Stokes simulation, as described in the preceding comment. As illustrated by the top-right plot in Figure 12, the maximum stroke of grid motion subsides rapidly as a function of the distance from the deforming cylinder, and is negligible near the far field boundary. A reference simulation was initiated by the steady NSE solution. As in the previous two cases, the amplitude of periodic vortex shedding oscillations grows along a transient, reaching a periodic attractor. Interestingly, following a brief alignment period, the evolution of the shedding frequency, ω, also shown in Figure 12, is quite similar to what is observed for the wake of a steady, rigid cylinder; i.e., starting with a low frequency at the early transient, and increasing as the flow approaches the attractor. That is the case even though the actuation frequency is held constant, at roughly the natural attractor shedding frequency of the flow over the rigid cylinder, which is the dominant frequency over the very near

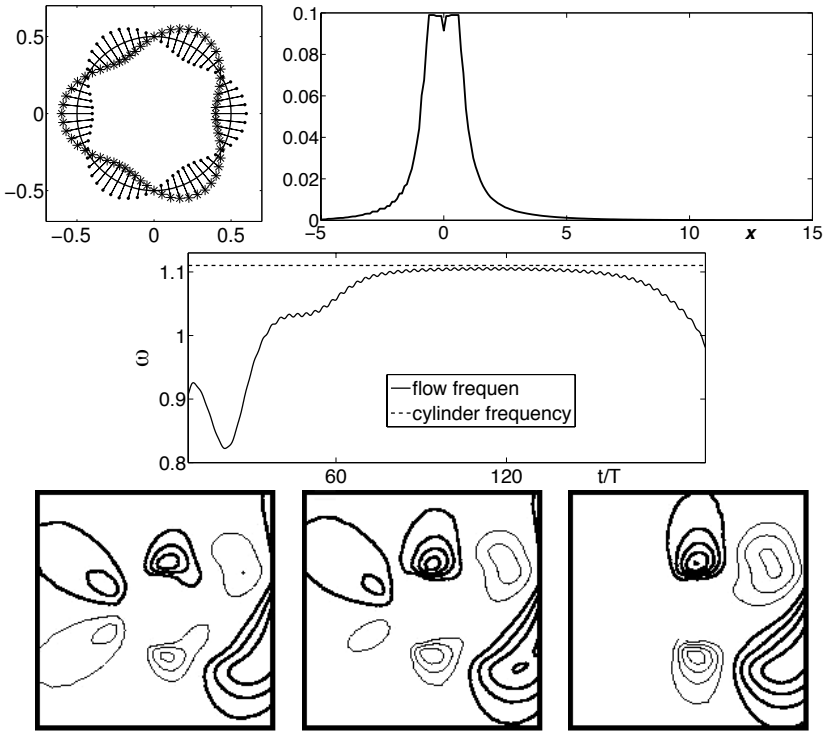

Figure 12. The periodically deforming cylinder. Top left: Grid points along the circular circumference are forced into sinusoidal fluctuations between the values indicated by bullets and asterisks. Top right: The maximal fluctuation of grid points $\{\mathbf{x}_i : |x_i(0) - x| < 0.2\}$, plotted as a function x. Center: Transient values of the instantaneous shedding frequency (solid), compared with the attractor shedding frequency of the rigid cylinder (dashed). Bottom: Near field zoom on 3 "physical domain" snapshots of the first harmonic mode $\mathbf{u}_1(\,\cdot\,\alpha)$, as it varies along an attractor period. The far field evaluation of $\mathbf{u}_1(\,\cdot\,\alpha)$ is nearly constant and similar to its counterpart over the attractor of the static cylinder wake.

field. Also noticed is the imperfect lock in of the shedding frequency onto the actuation frequency, evidenced by the dip in ω towards the end of the data stretch.

The velocity snapshots were mapped by the appropriate Ψ to equivalent snapshots over Ω_c, with a steady inflow velocity, and zero velocity over the cylinder wall. Harmonic expansion modes $\mathbf{u}_{c,i}$ were computed for the velocity field over $\Omega_c = \Omega(0)$. These modes where computed with respect to the instantaneous shedding frequency, and remain essentially constant over the attractor. The harmonic modes were pulled back to each $\Omega(\alpha)$ in the "physical domain", using the inverse mapping, Ψ^{-1}, according to (60). This defines $(\alpha, \dot{\alpha})$-dependent modes $\mathbf{u}_i$, over $\Omega(\alpha)$. (We shall revisit the revisit the general form of modes defined this way shortly; cf. (69)–(71), below.) While the harmonic modes are very similar to their rigid cylinder counterparts over the far field, the dependence on the oscillatory parameter variations is reflected by near field unsteadiness of each $\mathbf{u}_i$. The three plots at the bottom of Figure 12 illustrate this fact by a zoom on a streamline depiction of harmonic mode $\mathbf{u}_1$ over the immediate neighborhood of the cylinder, at three different points along a period.

7.4 Actuation Modes for Deforming Boundaries

The construction of actuation modes. As we have seen earlier, the need to construct actuation modes at this point arises from two types of sources: The slip velocity of grid points along walls of bodies immersed in the flow, and unsteady inflow conditions, including actuation and disturbances, global and local effects alike. The actuation modes are introduced in order to absorb these components of the boundary velocity, by an expansion of the form (56).

It will be convenient to formalize this requirement, and to discuss the construction of actuation modes, considering the embedded flow over the canonical domain Ω_c. We start, rewriting the actuation modes expansion (56) in clear reference to the embedded flow over Ω_c:

$$\mathbf{u}_{h,c} := \mathbf{u} - \mathbf{u}_{c,\,act} = \mathbf{u}_c - \sum_{i=1}^{N_{act}} b_i \mathbf{u}_{act,\,c,\,i}, \tag{67}$$

Here $\mathbf{u}_c$ is the velocity field in the image of Ψ, as in (60). The notation of $\mathbf{u}_{h,c}$ indicates the velocity field obtained at the end of the transition process, satisfying traditional, steady boundary conditions: A zero velocity along solid walls and a steady inflow. The actuation modes $\mathbf{u}_{act,\,c,\,i}$ are required to be defined as incompressible velocity fields over Ω_c, they should be independent of α, but include in their span the boundary velocity that

needs to be removed from $\mathbf{u}_c$, which is denoted here as $\mathbf{u}_{c,act}$. The dependence on $(\alpha, \dot{\alpha})$, in (67), is delegated to the coefficients b_i, where α may parametrize both domain deformation and inflow unsteadiness.

We review two approaches for the construction of the actuation modes:

(i) Analysis of the primary data set, i.e., the simulation or experimental data intended for the computation of expansion modes:

• The first step is the identification of a restriction of the modal expansion in (67) to the boundary, Ω_c'. This task is trivial in the rotating and oscillating cylinder examples. In general, one may use the adaptation to the boundary, Ω_c', of the empirical mode extraction methods discussed earlier, including the computation of harmonic expansions and POD analysis.

• Both the definition of harmonic modes and of POD modes are as linear combinations of data snapshots. Applying the same linear combinations that were used over the boundary to the entire snapshots, over Ω_c, defines incompressible velocity fields that agree with the boundary modes and can be used as actuation modes.

(ii) Using auxiliary simulations. Arguably, actuation modes that are intended to be used in operating conditions that are not identical to those used in model extraction, should translate boundary conditions into global modes in a manner that captures only the largest and least detailed structures possible:

• An auxiliary Stokes simulation over Ω_c is run, subject to the unsteady boundary velocity that needs to be resolved[8].

• Expansion modes are obtained from the auxiliary flow data. These expansion modes are the sought actuation modes.

Method (i) is reminiscent of approaches that extract actuation models by comparing the actuated and un-actuated flows, e.g. in Kasnakoğlu et al. (2008). The simple actuation modes that were reviewed earlier for the oscillating and rotating cylinder fit method (ii). The simulation based derivation of actuation modes for the heaving and pitching (solid) airfoil,

[8] Note that this means that if the inflow is steady, to begin with, the inflow boundary condition for the auxiliary simulation is zero.

in the pioneering work by Lewin and Haj-Hariri (2005), is also belonging to this class.

7.5 LOGMs in flows over deforming geometries

The Galerkin approximation in deforming geometries. The fluid velocity field $\mathbf{u}_{h,c}$, in (67), is defined over the steady canonical domain Ω_c, satisfying steady boundary conditions, including zero velocity along body wall. It is therefore amenable to the computation of POD or harmonic expansion modes, with the familiar Galerkin approximation format:

$$\mathbf{u}_{h,c}(\mathbf{x}_c,\, t) \approx \mathbf{u}_c^B(\mathbf{x}) + \sum_{i=1}^{N} a_i(t)\mathbf{u}_{c,\,i}(\mathbf{x}_c). \tag{68a}$$

Equivalently,

$$\mathbf{u}_c(\mathbf{x}_c,\, t) \approx \mathbf{u}_c^B(\mathbf{x}_c) + \sum_{i=1}^{N} a_i(t)\mathbf{u}_{c,\,i}(\mathbf{x}_c) + \sum_{i=1}^{N_{act}} b_i(\alpha, \dot\alpha)\mathbf{u}_{act,\,c,\,i}(\mathbf{x}_c). \tag{68b}$$

Parametrized mode deformation, due to transient changes in the flow, can be included in this formulation, precisely as discussed in § 6, provided pertinent entries to the parametrization vector α.

Applying the inverse mapping, Ψ^{-1}, to the combined (68), one maps the base flow $\mathbf{u}_c^B$, the expansion modes $\{\mathbf{u}_{c,\,i}\}_{i=1}^N$, and the actuation modes $\{\mathbf{u}_{act,\,c,\,i}\}_{i=1}^N$, back to velocity fields over the deforming physical domain $\Omega(\alpha)$. The dependence of Ψ^{-1} on $(\alpha,\, \dot\alpha)$ implies the same, regarding the expansion modes over the physical domain, meaning that the $\Omega(\alpha)$–counterparts of the fields in (68b) will all be unsteady. We begin this discussion with the details of these fields.

In keeping with the convention that the base flow absorbs inhomogeneous terms, we define

$$\mathbf{u}^B(\mathbf{x},\, \alpha,\, \dot\alpha) := \mathbf{u}_p^B(\mathbf{x},\, \alpha) + \mathbf{u}_v^B(\mathbf{x},\, \alpha)\dot\alpha, \tag{69}$$

where

$$\mathbf{u}_p^B := J^{-1}_{\mathbf{x}_c,\mathbf{x}}\, \mathbf{u}_c^B \quad \text{and} \quad \mathbf{u}_v^B := -J^{-1}_{\mathbf{x}_c,\mathbf{x}} J_{\mathbf{x}_c,\alpha}. \tag{70}$$

The term $\mathbf{u}_p^B$, on the right hand side of (69), is in standard change of coordinate form. It is determined by the slowly varying $\mathbf{u}_c^B$, and its dependence on α is static, and does not involve $\dot\alpha$. The term $\mathbf{u}_v^B\dot\alpha$ reflects the velocity field of the Lagrangian grid, and therefore includes the dependence on $\dot\alpha$.

With this definition of the base flow, actuation modes and expansion modes depend on α, but not on $\dot\alpha$. Moreover, expansion modes will satisfy

homogeneous boundary conditions:

$$\mathbf{u}_i(\mathbf{x},\,\alpha) = J_{\mathbf{x}_c,\mathbf{x}}(\mathbf{x},\,\alpha)^{-1}\,\mathbf{u}_{c,\,i}(\psi(\mathbf{x},\,\alpha)) \tag{71}$$

$$\mathbf{u}_{act,\,i}(\mathbf{x},\,\alpha) = J_{\mathbf{x}_c,\mathbf{x}}(\mathbf{x},\,\alpha)^{-1}\,\mathbf{u}_{act,\,c,\,i}(\psi(\mathbf{x},\,\alpha)) \tag{72}$$

The Galerkin approximation, in the original domain, is therefore of the form

$$\begin{aligned}\mathbf{u}(\mathbf{x},\,t) \quad \approx \quad & \mathbf{u}_p^B(\mathbf{x},\,\alpha) + \mathbf{u}_v^B(\mathbf{x},\,\alpha)\dot{\alpha} + \textstyle\sum_{i=1}^{N} a_i(t)\mathbf{u}_i(\mathbf{x},\,\alpha) \\ & + \textstyle\sum_{i=1}^{N_{act}} b_i(\alpha,\dot{\alpha})\mathbf{u}_{act,\,i}(\mathbf{x},\,\alpha).\end{aligned} \tag{73}$$

The Galerkin Dynamical System. The Galerkin dynamical system can be computed now in two equivalent ways, working over the steady computational domain or over the physical domain. The first approach is to rewrite the NSE in terms of the vector field $\mathbf{u}_c$ over the spatial domain Ω_c. In that case, unsteady change of variables, dependent on $(\alpha,\,\dot{\alpha})$, must be included in the appropriately modified NSE, followed by the projection on the time invariant expansion set. Here we detail only the alternative computation over the physical, unsteady domain, where the NSE retains its original, time invariant form.

Following the standard Galerkin paradigm, the acceleration field is approximated as the time derivative of the Galerkin approximation of the velocity field:

$$\begin{aligned}\partial_t\mathbf{u}(\mathbf{x},\,t) \quad \approx \quad & \textstyle\sum_{i=1}^{N} \dot{a}_i\mathbf{u}_i \\ & + \textstyle\sum_{i=1}^{N_{act}} (\partial_\alpha b_i\cdot\dot{\alpha} + \partial_{\dot{\alpha}} b_i\cdot\ddot{\alpha})\mathbf{u}_{act,i} \\ & + \left(\partial_\alpha\mathbf{u}_p^B + \textstyle\sum_{i=1}^{N} a_i\partial_\alpha\mathbf{u}_i + \sum_{i=1}^{N_{act}} b_i\,\partial_\alpha\mathbf{u}_{act,\,i}\right)\dot{\alpha} \\ & + \partial_\alpha\mathbf{u}_v^B\dot{\alpha}^2 + \mathbf{u}_v^B\ddot{\alpha}.\end{aligned} \tag{74}$$

The first sum on the right hand side of (74) is the mainstay of the standard Galerkin system computation, the subsequent, $\dot{\alpha}$, $\dot{\alpha}^2$ and $\ddot{\alpha}$ terms reflect the changing geometry and the velocity and acceleration that this change induces along $\Omega(\alpha)$.

The Galerkin projection of the NSE on the expansion set will therefore

be of the following general form

$$\begin{aligned}\dot{a}_i \;=\; & c_i(\alpha) + \textstyle\sum_{j=1}^{N} l_{ij}(\alpha) a_j + \sum_{j,k=1}^{N} q_{ijk}(\alpha) a_j a_k \\ & \qquad + \textstyle\sum_{i=1}^{N_{act}} l_{act,\,ij}(\alpha, \dot{\alpha}) b_j \\ & + \Big(c_i'(\alpha) + \textstyle\sum_{j=1}^{N} l_{ij}'(\alpha) a_j \\ & \qquad + \textstyle\sum_{i=1}^{N_{act}} l_{act,\,ij}'(\alpha, \dot{\alpha}) b_j \Big)\, \dot{\alpha} \\ & + \Big(\textstyle\sum_{i=1}^{N_{act}} l_{act,\,ij}''(\alpha, \dot{\alpha}) b_j \Big)\, \ddot{\alpha} \\ & \qquad + c_{2,i}(\alpha) \dot{\alpha}^2 + c_{3,i}(\alpha) \ddot{\alpha}.\end{aligned} \tag{75}$$

7.6 Closing Comments

Let us recap the extensions of the Galerkin methodology outlined in this section. Our starting point is the observation of an inherent inconsistency between the traditional Galerkin method and the modeling needs of systems with unsteady boundaries. As noted towards the end of the section, aspects of that inconsistency are manifest also in systems with unsteady inflow conditions.

Whereas studies that employ LOGMs for systems with unsteady boundaries commonly avoid the difficulty under a simplifying, small fluctuations assumption, solution ideas that address the problem, head on, have been proposed by a number of authors, over more than a decade. These ideas invariably include the transition to a steady computational domain, and where needed, the use of actuation modes. Methods for the transition to a canonical domain varied from very simple transformations, applicable to rigid body motion, to emulation of the string analogy, which is commonly used in CFD simulations.

The presentation of this section aimed to incorporate and extend these ideas, in a systematic, broadly applicable and computationally efficient framework, that meshes seamlessly with the formulation of LOGMs on parameterized manifolds, that was developed in § 6. Guidelines for the generation of elasticity-based, parameterized Lagrangian grids, include both the delineation of the properties required from such definitions in LOGM contexts, and the equally important highlights of the significant differences between these requirements, and the needs and implementations of Lagrangian grids in CFD simulation models.

A central theme in Lagrangian grid methods, in computational aeroelasticity, concerns the detrimental effects of excessive stretching of the fictitious

network of springs that control grid dynamics. Specifically, over-stretching may hinder the representation of grid cells by positive volume polyhedra, and requires a remeshing, a step we wish to avoid in parameterized grids used in LOGMs. To avoid this obstacle, the proposed framework removes the no-slip condition from the requirements used to define the Lagrangian grid, thus necessitating the complementary use of actuation modes, to absorb the residual wall-tangent velocity. Actuation modes are also needed to absorb unsteady boundary velocity due to actuation and or disturbances. We reviewed two alternative computations of actuation modes: One utilizes the same simulation data that is also used for mode extraction, in the derivation of the LOGM. The other utilizes auxiliary high viscosity (Stokes) fluid simulations, driven by the residual boundary conditions.

The two-step method is an enabler for a systematic, analytically derived modeling framework that is equally applicable to internal and external flows over moving boundaries, subject to unsteady inflows, allowing multiple, independently moving, immersed elastic bodies.

Finally, the singularity of boundary forcing has been a persistent impediment to the analytic incorporation of important actuation mechanisms in LOGMs. It necessitated the use of ad hoc, and often fragile calibration based substitutes, to include control mechanisms in the model. A significant aspect of the proposed framework is therefore in removing this obstacle. Indeed, the representation of forces along the boundary by global volume forces, proportional to $\ddot{\alpha}$ in (75), is analytically derived as an integral part of the Galerkin projection of the NSE, in the extended framework.

8 Feedback Design

Feedback flow control design may be characterized by a comparison of targeted response time scales to the time scales of dominant flow structure:

The regulation of a turbulent flow at rates that are much longer than those dominating flow unsteadiness is generically limited to statistical properties of the flow. The role of feedback is that of a slow adaptation of an otherwise open loop actuation, such as the amplitude and frequency of a pulsating synthetic jets (King, 2010; Becker et al., 2005; Pastoor et al., 2008; Little et al., 2009; Williams et al., 2009). Actuation is often at frequencies that are different than that of the dominant flow instability and feedback gains are not synchronized with the phase of flow oscillations. The models that are used to design control mechanisms in this class are therefore required to track and predict only the slowly varying statistical quantities of interest: The turbulent energy level of the flow or its sensed surrogates,

the aerodynamic forces acting on an airfoil, etc. Transfer functions are commonly used in such contexts, as well the mere implicit monotonicity assumption used in[9] *model-free* designs, such as in extremum-seeking control (Ariyur and Krstić, 2003; Wiederhold et al., 2010). Referring to the discussion in the chapter by Noack et al., the control of modal energy statistics, using FTT models Noack et al. (2008, 2010) belongs in this category as well.

Feedback flow control that acts at the flow's time scale is typically geared to attenuate, or to otherwise regulate, an oscillatory instability. This class of control tasks an oscillatory actuation to be tightly choreographed with the flow. The demands from design models are escalated accordingly, to providing accurate phase predictions of flow unsteadiness. In addition to analytical PDE and high dimensional numerical models (Aamo and Krstic, 2003; Bewley, 2001; Kim and Bewley, 2007; Vazquez and Krstic, 2007), reduced order models used in here cover the gamut, from simple sine-wave tracking (Pastoor et al., 2006, 2008; Joe et al., 2008), through state-space and transfer function linear time invariant and adaptive models Kegerise et al. (2007); Cattafesta et al. (2008) and vortex models Protas (2007, 2008) to LOGMs, the subject of the current discussion.

With that focus in mind, our objective here is not to review the range of design methods that have been, or that can be employed in feedback flow control. Rather, our goal is to highlight some key issues that have been identified as critical to the successful use of LOGMs in feedback flow control design, regardless of the underlying design philosophy. We shall illustrate these issues by the simple volume force actuated cylinder wake benchmark, as described in § 2.

8.1 Volume Force Actuation of the Cylinder Wake

A volume force actuator represents, e.g., a regulated magnetic field in the domain of a magnetohydrodynamic flow. Flow dynamics in the immediate vicinity of a plasma actuators is an example of this class of actuated flows (Moreau, 2007; Little et al., 2009). For convenience we repeat here the notations of a volume force actuated Galerkin model, which have been set in (7). Actuation is included in the NSE (6) as a distributed force field, $\mathbf{f}(\mathbf{x},\, t)$. The Galerkin projection of the NSE on an orthonormal set of expansion modes, includes an explicit representation of the volume force by terms

$$f_i(t) \,=\, (\mathbf{f}(\,\cdot\,,t),\, \mathbf{u}_i)_\Omega, \quad i = 1, \ldots, N. \tag{76a}$$

[9] Arguably, *any* feedback design requires a model that predicts the response of the system to actuation or disturbance. The term "model-free" is used when the model is restricted to such rudimentary properties as an assumed continuity, monotonicity and slow response.

Modifications for non-orthogonal expansions are straightforward. The i^{th} equation in the Galerkin system is thus of the form

$$\dot{a}_i = c_i + \textstyle\sum_{j\geq 1} l_{ij} a_j + \sum_{j,l\geq 1} q_{ijk} a_j a_k + f_i, \quad i \geq 1. \tag{76b}$$

We focus here on periodically dominated flows, where the volume force oscillates at harmonics of the dominant flow frequency. Suppressing space and time dependencies, the harmonic expansion of the actuation is

$$\mathbf{f} = B_0 \mathbf{g}_0 + \sum_{i=1}^{N} B_{2i-1} \cos(\phi_i)\, \mathbf{g}_{2i-1} + B_{2i} \sin(\phi_i)\, \mathbf{g}_{2i}. \tag{77}$$

The amplitudes B_i are treated here as slowly varying control commands. Explicit expressions are derived in these terms for the forcing terms in the *amplitude Galerkin system*, (18b):

$$\begin{aligned} F_{2i-1}(t/\tau) &= \tfrac{2}{t_p} \int_{-\frac{t_p}{2}}^{\frac{t_p}{2}} (\mathbf{f}(\,\cdot\,, t+r),\, \mathbf{u}_{2i-1})_\Omega \cos(\phi_i(t+r))\, dr \\ &= (\mathbf{g}_{2i-1},\, \mathbf{u}_{2i-1})_\Omega\, B_{2i-1}(t/\tau) \\ F_{2i}(t/\tau) &= (\mathbf{g}_{2i},\, \mathbf{u}_{2i})_\Omega\, B_{2i}(t/\tau). \end{aligned} \tag{78}$$

These expressions translate to forcing terms in the corresponding differential equations for a_{2i-1} and a_{2i}:

$$\begin{aligned} f_{2i-1}(t) &= F_{2i-1}(t/\tau)\, \cos(\phi_i(t)) \\ f_{2i}(t) &= F_{2i}(t/\tau)\, \sin(\phi_i(t)). \end{aligned} \tag{79}$$

As in the case of (15)-(18), the expressions (78) and (79) do not require mutual orthogonality of the harmonic modes.

8.2 Direct and Indirect Design Objectives

A single, vertical force field is specified in (3) as

$$\mathbf{f}(\mathbf{x}, t) = b(t)\, \mathbf{g}(\mathbf{x}),$$

where $\mathbf{g}$ is a unit amplitude vertical force field, supported over the disc Ω_{vf}, and where b is the control command.

The formal design objective, as stated in § 2, is engineering driven, with the goal to avoid the deleterious effects of cylinder oscillations:

1. Attenuate vortex shedding.

From a physical perspective, our objective is to use the actuator as a distributed deceleration force, applied to the vertical component of the velocity oscillations over the domain Ω_{vf}. An ideal selection would be at an *anti-phase* to the averaged vertical velocity field:

$$b(t) = -\kappa(t)\,(\mathbf{u}(\,\cdot\,,t),\,\mathbf{g})_\Omega = -\kappa(t)\int_{\Omega_{vf}} d\,\mathbf{x}\,v(\mathbf{x},t), \tag{80}$$

where v is the vertical component of the velocity $\mathbf{u} = (u, v)$, and where $\kappa > 0$ is a selected gain. Using the nomenclature of energy dynamics, in (21), this selection defines the *actuation power* as $G = -\kappa|(\mathbf{u},\,\mathbf{g})_\Omega|^2$, ensuring a negative contribution to the TKE; i.e., (80) defines a *dissipative control*. When κ is selected large enough, the actuation power will dominate all other contributions to the power equation (21), and ensure that the TKE will be driven to zero. This option can be easily demonstrated by DNS implementation (Gerhard et al., 2003; Lehmann et al., 2005).

In fact, the fact that feedback stabilization of flow oscillations by synchronous actuation needs to be dissipative, is generic. It is implied by the very nature of this design objective, and is therefore independent of the control theoretical approach used for solving the specific design problem. Our simple example is therefore representative of a very wide class of flow control problems, as is the ideal formulation of a dissipative control, in (80). Alas, access to the the distributed flow state, as required in (80), is available only in DNS simulations. Control decisions need to be based on realtime processing of sensor readings. In line with the focus of this chapter, this means:

2. Feedback design should be based on reduced order model based state estimates and control design.

The bulk of this section was dedicated to model development, motivated by this objective. Implicit in it is the onus on the designer to maintain the controlled flow within the validity envelope of the design model. Surely, model based state estimation, and predictions of control effects, will have little value, once the flow exits that envelope:

3. Model based feedback design should maintain the flow within the validity envelope of the reduced order model.

The purpose of the ensuing discussion is to highlight the implications of this indirect, but truly critical requirement, put in the generic context of

dissipative control design. The model we intend to use here is the least order, three state model (36). the generic property of this model is its very limited dynamic range. Regardless of any other aspect, it is valid only when the flow is characterized by periodic vortex shedding, when the shedding occurs at the frequency predicted by the model, and when the dominated coherent structures in the flows are those used as expansion modes in (36). As the discussion progresses, we shall review the options of using a fixed expansion set, comprising of the leading attractor POD modes and a shift mode, and the alternative of using the parameterized variant of this model.

The discussion will be focused, in the most part, on control and modeling related issues. To the limited degree at which state estimation issues will be discussed, that discussion will concern a broadly applicable issues, and will not relate to issues of specific observer design methods. It is therefore assumes that some text-book standard methods such as a Luenberger observer, an extended Kalman filter, and extensions thereof, are ample for the estimation task (Grewal and Andrews, 1993; Meurer et al., 2002; Åström and Murray, 2008; Crassidis, 2006). Otherwise, the assumption is that a dynamic state estimation has already been designed, producing reliable estimates of the Galerkin model's state, $\mathbf{a}$, and that this estimate has been reliably translated to estimates of the amplitude $A := A_1 = A_2$ and of the oscillations' phase ϕ.

8.3 Modeling Periodic Actuation

The implication of Objective 3 is that the shedding frequency will continue to dominate the dynamics, and will vary slowly, as the oscillation amplitude declines. It is therefore natural to define an actuation force that oscillates at the shedding frequency:

$$b = B\cos(\phi + \Delta\phi) = B\left(\cos(\Delta\phi)\cos(\phi) - \sin(\Delta\phi)\sin(\phi)\right). \qquad (81)$$

Here ϕ is the phase of oscillatory states of (36), as in the counterpart of the Fourier expansion (19). The phase shift, $\Delta\phi$, determines the relationship between the oscillations of the unknown full state $\mathbf{u}$ and the actuation force $\mathbf{f}$. In particular, it determines whether the negative forcing power (dissipativity) requirement (80) is satisfied. A wrong selection of $\Delta\phi$ may not only render the actuation ineffectual, but it may actually become destabilizing. In what follows we shall analyze this condition in terms of the actuated version of the LOGM (36). Our first task is therefore to compute the forcing term in that equation.

We have two options to explore the response: One is in terms of a direct appeal to the Galerkin projection, in the time domain. The other option

is an appeal to the expressions(78) and (79). This second option is based on the stipulation of periodic dominance, in line with Objective 3. We now review both options:

The forcing terms: A Direct Galerkin Projection. This computation is facilitated by the fact that, in this particular example, the three modes used in (36) are mutually orthogonal (Noack et al., 2003). The respective forcing terms are thus defined as in (76): $f_\Delta := (\mathbf{f},\, \mathbf{u}_\Delta)_\Omega$, is the actuation force in the shift mode equation, and $f_i := (\mathbf{f},\, \mathbf{u}_i)_\Omega$, $i = 1, 2$, are the respective forces for the two oscillatory states. Theses definitions lead to the following values:

• $f_\Delta = 0$. The symmetry of the shift mode and the anti-symmetry of the force field $\mathbf{g}$ with respect to the x-axis[10] causes $(\mathbf{g},\, \mathbf{u}_\Delta)_\Omega = 0$.

• To define the forcing terms acting on the oscillatory state we introduce the notations of $g_i := (\mathbf{g},\, \mathbf{u}_i)_\Omega$, $i = 1, 2$, The projection of the force field $\mathbf{f}$ is defined in these terms as:

$$\begin{aligned} f_1 &= (\mathbf{f},\, \mathbf{u}_1)_\Omega = b\,(\mathbf{g},\, \mathbf{u}_1)_\Omega = R_g\, B\, \cos(\theta)\cos(\phi + \Delta\phi) \\ &= R_g\, B\, \cos(\theta)(\cos(\Delta\phi)\cos(\phi) - \sin(\Delta\phi)\sin(\phi)), \\ f_2 &= (\mathbf{f},\, \mathbf{u}_2)_\Omega = b\,(\mathbf{g},\, \mathbf{u}_2)_\Omega = R_g\, B\, \sin(\theta)\cos(\phi + \Delta\phi) \\ &= R_g\, B\, \sin(\theta)(\cos(\Delta\phi)\cos(\phi) - \sin(\Delta\phi)\sin(\phi))\,. \end{aligned} \tag{82}$$

We note that the angle θ, in these expressions, is a function of g_1 and g_2, hence of the expansion modes $\mathbf{u}_1$ and $\mathbf{u}_2$. It remains constant if mode deformation is not accounted for, and it varies along with the expansion modes, when parameterized models are used.

Amplitude and phase equations are derived in terms of the polar coordinates representation of the oscillatory Galerkin states, $a_1 = A\cos(\phi)$ and $a_2 = A\sin(\phi)$. Explicitly, these equations are computed by substituting these expressions in the actuated variant of (36b) followed by an

[10] We say that a 2D vector field $\mathbf{u} = (u, v)$ is symmetric with respect to the x-axis when $u(x, y) = u(x, -y)$ and $v(x, y) = -v(x, -y)$. The vector field is anti-symmetric with respect to the x-axis when $u(x, y) = -u(x, -y)$ and $v(x, y) = v(x, -y)$.

inner-product with $\begin{bmatrix}\cos(\phi)\\ \sin(\phi)\end{bmatrix}$ and $\begin{bmatrix}-\sin(\phi)\\ \cos(\phi)\end{bmatrix}$, respectively:

$$\begin{aligned}
\dot{a}_\Delta &= -\sigma^B a_\Delta + \beta^B \left(a_1^2 + a_2^2\right), && \text{(83a)}\\
\dot{A} &= \left(\sigma^C - \beta^C a_\Delta\right) A + B R_g \cos(\phi-\theta)\cos(\phi+\Delta\phi) && \text{(83b)}\\
\dot{\phi} &= \omega - \frac{R_g B}{A}\sin(\phi-\theta)\cos(\phi+\Delta\phi). && \text{(83c)}
\end{aligned}$$

The forcing terms: A phasor equation derivation. Here the starting point of the computation is the assumption of harmonic dominance of the flow and the dynamic phasor equations (18b). Deriving the forcing terms for the phasor amplitude equations from the general formulae (78) leads to the following equalities:

$$\begin{aligned}
F_1 &= (\mathbf{g},\, \mathbf{u}_1)_\Omega B\cos(\Delta\phi) = R_g\, B\cos(\theta)\cos(\Delta\phi)\\
F_2 &= -(\mathbf{g},\, \mathbf{u}_2)_\Omega B\sin(\Delta\phi) = -R_g\, B\sin(\theta)\sin(\Delta\phi).
\end{aligned} \qquad (84)$$

Dynamic equations for the oscillations amplitudes are obtained by adding the forcing terms (84) to the homogeneous amplitude equation, (18b). We recall that the precise form of the homogeneous equation for the linear cylinder wake model, (8), has already been computed in (20). An obvious adaptation to a model that includes the shift model, leads to the equations:

$$\begin{aligned}
\frac{d}{dt}A_1 &= (\sigma^C - \beta^C a_\Delta)\, A_1 + F_1\\
&= (\sigma^C - \beta^C a_\Delta)\, A_1 + R_g\, B\cos(\theta)\cos(\Delta\phi) && \text{(85a)}\\
\frac{d}{dt}A_2 &= (\sigma^C - \beta^C a_\Delta)\, A_2 + F_2\\
&= (\sigma^C - \beta^C a_\Delta)\, A_2 - R_g\, B\sin(\theta)\sin(\Delta\phi). && \text{(85b)}
\end{aligned}$$

Examining these equation, one observes an apparent discrepancy: The two oscillation amplitudes are essentially identical, $A_1 = A_2$, in our phase averaged system. In contrast, eq:act:pgap suggests the possibility of two distinct dynamic rules. We shall revisit this issue shortly.

The tasks ahead includes the derivation of guidelines for the selection of the control parameters B and $\Delta\phi$, and the reconciliation of the two sets of equations, i.e., (82) and (83), which were derived by direct projection, and (84) and (85), which were derived in a dynamic phasor formulation. In addition, the observed mismatch between the two equations in (85), needs to be addressed. The analysis of these issues will reveal important modeling and design aspects of the generic scenario where the goal of flow control is

the stabilization of oscillatory flow instabilities. Indeed, our motivation for employing the dual formulation is precisely as an opportunity to unveil and illustrate these issues.

8.4 Detailed Design Guidelines

Dissipative actuation phase. We examine the requirement that actuation will have a dissipative, stabilizing effect in each of the presented formulations.

Let us start with the amplitude equation (83b). Here the requirement is that the oscillatory forcing term be (maximally) negattive:

$$\cos(\phi - \theta)\cos(\phi + \Delta\phi) < 0.$$

This objective is achived with the selection of

$$\Delta\phi = \pi - \theta \quad \Rightarrow \quad \cos(\phi - \theta)\cos(\phi + \Delta\phi) = -\cos(\phi - \theta)^2. \tag{86a}$$

A by product of this selection is that this selection creates an oscillatory forcing term in the phase equation (83c):

$$-\sin(\phi - \theta)\cos(\phi + \Delta\phi) = \frac{1}{2}\sin(2(\phi - \theta)). \tag{86b}$$

We shall revisit this added term shortly.

Next, let us consider the effect of the same selection on the two phasor based amplitude equations, in (85). Indeed, here too, both forcing terms become negative when $\Delta\phi = \pi - \theta$:

$$\cos(\theta)\cos(\Delta\phi) = -\cos(\theta)^2, \quad -\sin(\theta)\sin(\Delta\phi) = -\sin(\theta)^2. \tag{87}$$

While the assignment of $\Delta\phi$ has the desired dissipative effects in each of the two settings, the expressions we computed appear to include several inherent inconsistencies:

Creating an oscillatory frequency in (86b)**.** The validity envelope characterized by a slowly varying frequency. The actual frequency now second harmonic sinusoidal fluctuation in ω, which is modulated by the growing inverted amplitude, $1/A$, in the closed loop (83c).

An imbalance in (87)**.** Unless $\theta = \frac{2k+1}{4}\pi$ and $g_1 = \pm g_2$, the closed loop forcing terms in the two equations, in (87), are not identical. (In the extreme, either g_1 or $g_2 = 0$.) In particular there appears to be a possibility of driving the values of A_1 and A_2 apart, thus violating the characterization

$A = A_1 = A_2$ of the model's validity envelope.

An inconsistency between (86a) ***and either of the two expressions in*** (87)**.** The directly derived forcing term in the amplitude equation is oscillatory, whereas the alternative counterparts in the phasor description are constant (or slowly varying).

It is left to the reader to observe that a joint root cause for these issues is the fact that the benchmark under consideration stipulates the use of only a single actuator. Two independent control inputs, would have enabled the independent regulation of a_1 and a_2, and similarly, of A and of ω. That extra degree of freedom could have been used to ensure that, indeed, the forcing in (83b) be slowly varying, that it will agree with both forcing terms in (87), and that not actuation effects will be felt by ω. Under actuation, however, is the reality one faces in fluid flow systems, and at least in this sense, the difficulties observed here are generic. In fact, there generic in yet another aspect, which we discuss next.

Time scale separation as an inherent design guideline. A requirement that closed loop stabilization adhere to a time scale separation between the shedding half-period and the attenuation of the oscillations amplitude, emerges as a common solution to the apparent inconsistencies listed above: As long as changes in $1/A$ are small over a half period, the net forcing effect on ω over a shedding period, will be small. The same time scale separation ensures that the period averaged contribution of the periodic fluctuations in $-\cos(\phi-\theta)^2$ to the amplitude dynamics, under (86a), will also be negligible. The net effect of the actuation in (83b) will therefore be nearly equivalent to that of the slowly varying input $\frac{1}{2}\,B\,R_g$.

Phase averaging requirement in phasor models actuation. To understand the case of $g_1 \neq \pm g_2$ we refer to the FTT terminology (Noack et al., 2008) that was introduced in the chapter by Noack et al., and used in our discussion of energy dynamics. The dynamic role of the skew symmetric component of the original matrix coefficient in (36b), is precisely the continuous exchange of TKE between the two oscillatory states, a_1 and a_2, leading to equal time averages of the respective K_1 and K_2, hence of A_1 and A_2. In fact, this implicit energy redistribution is an essential property of harmonically dominant systems and of their models, and is equivalent to a generalized weighted variant of the phase averaging property, allowing, e.g. elliptical limit cycles.

An inherently implied property of a system that maintains a constant

(or slowly varying) ratio between the TKE contents of oscillatory state-pairs, is that the energy redistribution that is mediated by the oscillations, occur at substantially higher rates than the actuated or natural transient changes in these TKE levels. In effect, harmonic dominance implies that the actuation inputs into each such pair of states will be phase averaged in the same manner as the said states. The upshot of this discussion is that the use of the "raw" g_i in the phasors of the forcing terms, in (84), and subsequently, in (85), constitutes a contradiction in terms. The correct gains in the phasor dynamics formulation are, indeed, $g_i = \pm\frac{1}{\sqrt{2}}R_g$, $\theta = \frac{2k+1}{4}\pi$ and the identical actuation terms in the two equations, in (85), are $\frac{1}{2}\,R_g\,B$. That is, these equations are precisely the period averaged variants of (83b). For convenience we rewrite this equation here:

$$\dot{A} = (\sigma^C - \beta^C\, a_\Delta)\, A - \frac{1}{2}\, R_g\, B. \tag{88}$$

In summary, time scale separation between actuation and (half) the vortex shedding period justifies the suppression of nearly zero mean terms in the closed loop (85), as well as the corrected phase averaged modeling of the actuation term, in a dynamic phasor model.

Actuation amplitude, subject to dissipation and time scale separation constraints. The observations above lead to two requirements from the actuation amplitude, B: It needs to be high enough, to overcome the instability in (88), and yet low enough, to ensure the required time scale separation between the oscillations period and the rate of decay in the actuated flow. This dual requirement is simply formulated a a two sided inequality, on B:

$$\left(\frac{\sigma^C - \beta^C\, a_\Delta}{R_g} + \epsilon\right) A < B < \left(\frac{\sigma^C - \beta^C\, a_\Delta}{R_g} + \delta\right) A. \tag{89}$$

The values of ϵ and δ, in (89), represent the minimal and the maximal acceptable decay rates, with corresponding time constants $\tau_\epsilon := 1/\epsilon$ and $\tau_\delta := 1/\delta$.

8.5 Performance Limitations

Like many nonlinear control problems, flow control is often subject to performance limitations that stem from the very structure of the system. Here we highlight two types of generic limitations, illustrated by our running example.

Stability of the operating point: An amplitude perspective. The expressions on both sides of (89) involve both a_Δ and A. Simplifying these expressions for the purpose of this discussion, let us slave a_Δ to A^2. The two expressions bounding B are then cubic polynomials in A, defining the normalized destabilizing force in (88). The solid curve in Figure 13 is a schematic representation of the amplitude of that destabilizing force, drwan as a function of A. Considering this representation, we observe that a constant actuation amplitude, B, would balance the destabilizing force in (88), at two distinct values of A, illustrated by the examples of A_{low} and A_{high}, in Figure 13. The fixed point at A_{high} is dynamically stable: Oscillations

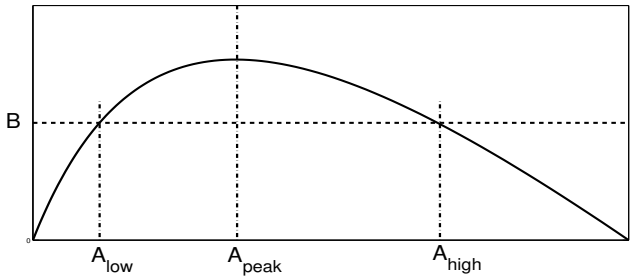

Figure 13. A schematic illustrating the existence of two oscillating amplitudes, A_{low} and A_{high}, at which an actuation level, B, balances the destabilizing force (solid curve) in (88). The fixed point at A_{low} is dynamically unstable, whereas that at A_{high} is dynamically stable.

at an amplitude $A > A_{high}$ create a destabilizing force that is lower than the actuation force, and will be attenuated. Oscillations at an amplitude $A < A_{high}$ generate a destabilizing force that is higher than the actuation force, and will grow. In contrast, the same reasoning shows that the fixed point at A_{low} is dynamically unstable and is therefore intrinsically more difficult to enforce. Furthermore, the reasoning we have just provided also applies to the slow feedback stabilization, as the system traverses a slowly decaying actuated transient $A(t)$. That threshold for dynamic instability is the value A_{peak}, at which the destabilizing force, on the right hand side of (88), reaches its maximal value.

This observation reveals an important root cause of the observed phenomenon, whereby controllers designed to stabilize an oscillatory instability, seem to "loose their grip", once the fluctuations level has been reduced below a certain threshold. At that point, the flow begins to displays chaotic

oscillations. Careful design may nonetheless succeed in maintaing a low averaged TKE. In other cases, the emerging oscillations stimulate new instabilities which are not covered by the model, leading to a return higher oscillation levels.

Stability of the operating point: A phase perspective. The exact definition of the phase ϕ requires knowledge of the distributed velocity field, $\mathbf{u}$. This information is not available and a observer is needed to produces an estimate $\hat{\phi}$ of ϕ. That estimate is then used instead of ϕ, in the applied actuation force:

$$b = B\cos(\hat{\phi} + \Delta\phi) = -B\cos(\hat{\phi} - \theta). \tag{90}$$

We us consider this actuation command, using the assignment (86) for $\Delta\phi$. Later we shall comment also on the issue of the correct evaluation of $\Delta\phi$.

We shall now illustrate the growing difficulty in maintaining a good estimate in the closed loop actuated system, as the shedding instability is increasingly attenuated. To do so, we consider the closed loop actuated dynamics of ϕ. The use of $\hat{\phi}$ instead of ϕ brings (83c) to the following period averaged form:

$$\dot{\phi} = \omega - \frac{R_g B}{A}\overline{\sin(\theta - \phi)\cos(\hat{\phi} - \theta)} \approx \omega - \frac{R_g B}{2A}\sin(\hat{\phi} - \phi). \tag{91}$$

In this formulation an overline indicates period average. The approximation is justified when the phase estimated error, denoted $\tilde{\phi} := \phi - \hat{\phi}$, is sufficiently small to make $\phi + \hat{\phi} - 2\theta$ close to $2(\phi - \theta)$, allowing to neglect the period averaged contribution of $\cos(\phi + \hat{\phi} - 2\theta)$. As noted earlier, this equation coincides with the un-actuated phase dynamics, in (18a), in the ideal case of a precisely known phase.

To illustrated the estimation difficulty, let us consider a dynamic observer of ϕ, with a correction term h

$$\dot{\hat{\phi}} = \omega + h. \tag{92}$$

As a simplifying hypothesis, we implicitly assumed in this formulation that the slowly varying (effective) ω is known. The purpose of this analysis is to reveal the growing demands on a stabilizing h.

Following the standard derivation of the estimation error dynamics, we subtract (92) from (91), followed by a linearization, justified for small values of $\tilde{\phi}$.

$$\dot{\tilde{\phi}} = \frac{R_g B}{2A}\sin(\tilde{\phi}) - h \approx \frac{R_g B}{2A}\tilde{\phi} - h. \tag{93}$$

Indeed, not only is this equation anti-stable, but its growth rate is reversely proportional to the oscillations amplitude, A. The correction term h therefore needs to overcome this instability, a task that becomes ever harder, as A approaches zero.

An interesting observation concerns the stability of dynamic phase estimation in the closed loop system, under the reversed objective, of feeding energy into the instability. Backtracking on our computations, above, the ideal selection of the actuation phase shift is $\Delta\phi = -\theta$, precisely an anti-phase to the stabilizing selection. In that case, however, the sign of the right hand side of (93) will be reversed, and the homogeneous component of this equation will become stable. Indeed its small signal stability will only increase for small values of A!

This simple analysis is aligned with the observation of a generic tendency of a fluid flow system to extract energy from an active external source that is coupled with the flow, till the coupled system reaches an equilibrium.

The role of mode deformation. Both the analysis of the actuation amplitude and of the actuation phase reveals the dependence of an effective actuation on the exact *definition* and correct estimation of the flow phase ϕ and of the values of the projections g_i, hence of the amplitude R_g and phase θ. A dynamic observer used to translate sensor readings into state estimates is also dependent on the phase shifts and amplitude relations between sensor oscillations and the oscillations of the time coefficients a_i, $i = 1, 2$ in the actuated flow. The deformation of the leading oscillatory modes along natural and actuated transients lead to growing discrepancies between the correct relations between the required quantities and those predicted by a model based on a constant mode set. These facts were illustrated by the observations in Figures 2, 3 and 9. The deleterious effects of using constant modes in model based control have been clearly demonstrated, in this example, in Gerhard et al. (2003); Lehmann et al. (2005); Luchtenburg et al. (2006). These studies showed that the feasible closed loop TKE attenuation is meager, and can be improved several folds when control design employs a parameterized mode set. This observation is aligned with similar observations by numerous investigating teams. References to some pertinent literature can be found in § 6.

9 Concluding Remarks

The evolution of the field of fluid flow control has been driven by significant and still growing engineering needs, and by an accumulating body of experimental and numerical studies. The adaptation of control design

and related modeling methods to the needs of fluid flow applications, have been by a potpourri of pioneering theoretical investigations and ad-hoc experimentation with diverse methods and ideas, borrowed from a similarly diverse ensemble of fields.

Of the many types of models used in the design of feedback flow control, the Galerkin paradigm is clearly a dominant presence. It has the advantage of allowing a more direct contact between the reduced order model and the constitutive equations than black-box identified linear models, while maintaing manageable complexity, when compared with CFD models, or even with the often unruly, Lagrangian vortex models. The use of Galerkin models have been further popularized by the efficient approximation offered by POD mode sets. Within this vibrant realm, observations of fundamental discrepancies between ends and means, methods and needs, have been made early on, and are now widely recognized by the flow control community.

Building on our presentations in the previous two chapters (i.e., by Morzyński et al. and by Noack et al.), our goal here is to systematically identify the root causes of a number of persistent obstacles, and to propose an equally systematic enhancement of the Galerkin paradigm, that is geared, by design to remove these obstacles. Issues covered included the mean field and subgrid models, mode deformation and unsteady boundaries. At the model development level we have also reviewed a useful framework based on temporal harmonics, that is especially suitable for the generic task of controlling periodically dominated instabilities.

We closed the discussion with an illustration of generic feedback design issues that arise specifically, because of the use of low and least order models.

Bibliography

O. Aamo and M. Krstic. *Flow Control by Feedback Stabilization and Mixing.* Springer Verlag, 2003.

B. Adams, M. Ovsjanikov, M. Wand, H.-P. Seidel, and L. J. Guibas1. Meshless modeling of deformable shapes and their motion. In M. Gross and D. James, editors, *Eurographics / ACM SIGGRAPH Symposium on Computer Animation*, 2008.

S. Ahuja, C. W. Rowley, I. G. Kevrekidis, M. Wei, T. Colonius, and G. Tadmor. Low-dimensional models for control of leading-edge vortices: Equilibria and linearized models. In *45th AIAA Aerospace Sciences Meeting and Exhibit*, 2007. AIAA Paper 2007-709.

A. Amanatiadis and I. Andreadis. A survey on evaluation methods for image interpolation. *Meas. Sci. Technol.*, 20(104015), 2009.

D. Amsallem and C. Farhat. Interpolation method for adapting reduced-

order models and application to aeroelasticity. *AIAA J.*, 46:1803–1813, 2008.

D. Amsallem, J. Cortial, K. Carlberg, and C. Farhat. A method for interpolating on manifolds structural dynamics reduced-order models. *Int. J. Numer. Meth. Engng.*, 80:1241–1257, 2009.

P. B. Andersen, M. Gaunaa, C. Bak, and M. H. Hansen. A dynamic stall model for airfoils with deformable trailing edges. In J. N. Sørensen, M. O. L. Hansen, and K. S. Hansen, editors, *The Science of Making Torque from Wind*, volume 75 of *J. Phys.: Conference Series*, 2007.

S. A. Ansari, R. Żbikowski, and K. Knowles. Aerodynamic modelling of insect-like flapping flight for micro air vehicles. *Prog. Aerospace Sci.*, 42: 129–172, 2006.

A. Antoulas. *Approximation of Large-scale Dynamical Systems*. SIAM press, 2005.

J. S. R. Anttonen, P. I. King, and Beran P. S. POD-based reduced-order models with deforming grids. *Math. Comp. Modeling*, 38:41–62, 2003.

J. S. R. Anttonen, P. I. King, and P. S. Beran. Applications of multi-pod to a pitching and plunging airfoil. *Math. Comp. Modeling*, 42:245–259, 2005.

H. Aref, M. Brøns, and M. A. Stremler. Bifurcation and instability problems in vortex wakes. *J. of Phys.: Conf. Series*, 64(012015), 2007. 2nd Int. Symp. on Instability and Bifurcations in Fluid Dynamics.

E. Arian, M. Fahl, and E. W. Sachs. Trust-region proper orthogonal decomposition for flow control. Technical Report A283773, ICASE, NASA, May 2000.

K. B. Ariyur and M. Krstić. *Real-time optimization by extremum-seeking control*. Wiley & Sons, Inc., 2003.

K. J. Åström and R. M. Murray. *Feedback Systems: An Introduction for Scientists and Engineers*. Princeton University Press, 2008.

P. J. Attar, E. H. Dowell, J. R. White, and J. P. Thomas. Reduced order nonlinear system identification methodology. *AIAA J.*, 44:1895–1904, 2006.

N. Aubry, P. Holmes, J.L. Lumley, and E. Stone. The dynamics of coherent structures in the wall region of a turbulent boundary layer. *J. Fluid Mech.*, 192:115–173, 1988.

D. Barkley. Linear analysis of the cylinder wake mean flow. *Europhys. Letters*, 75:750–756, 2006.

T. K. Barlas and G. A. M. van Kuik. Aeroelastic modelling and comparison of advanced active flap control concepts for load reduction on the upwind 5MW wind turbine. In *Proc. European Wind Energy Conference & Exhibition (EWEC)*, 2009.

J. T. Batina. Unsteady euler airfoil solutions using unstructured dynamic meshes. *AIAA J.*, 28:381–1388, 1990.

R. Becker, M. Garwon, C. Gutknecht, G. Bärwolff, and R. King. Robust control of separated shear flows in simulation and experiment. *J. Processs Cont.*, 15:691–700, 2005.

D. E. Berg, D. G. Wilson, B. R. Resor, M. F. Barone, J. C. Berg, S. Kota, and G. Ervin. Active aerodynamic blade load control impacts on utility-scale wind turbines. In *Proc. of WindPower Conf. & Exhib.*, 2009.

M. Bergmann and L. Cordier. Optimal control of the cylinder wake in the laminar regime by trust-region methods and POD reduced-order models. *J. Comp. Phys.*, 227:7813–7840, 2008.

M. Bergmann, L. Cordier, and J.-P. Brancher. Optimal rotary control of the cylinder wake using POD reduced order model. *Phys. Fluids*, 17: 097101, 1–21, 2005.

M. Bergmann, L. Cordier, and J.-P. Brancher. Drag minimization of the cylinder wake by trust-region proper orthogonal decomposition. In R. King, editor, *Active Flow Control*, volume 95 of *Notes on Numerical Fluid Mechanics and Multidisciplinary Design*, pages 309–324. Springer Verlag, 2007.

T. R. Bewley. Flow control: new challenges for a new renaissance. *Progress in Aerospace Sciences*, 37:21–58, 2001.

I. Bijelonja, I. Demirdžić, and S. Muzaferija. A finite volume method for incompressible linear elasticity. *Comput. Methods Appl. Mech. Engrg.*, 195:6378–6390, 2006.

F. J. Blom. Considerations on the spring analogy. *Int. J. Numer. Meth. Fluids*, 32:647–668, 2000.

J. Borggaard, A. Hay, and D. Pelletier. Interval-based reduced order models for unsteady fluid flow. *Int. J. Num. Anal. & Modeling*, 4:353–367, 2007.

R. Bourguet, M. Braza, A. Sévrain, and A. Bouhadj. Capturing transition features around a wing by reduced-order modeling based on compressible navier-stokes equations. *Phys. Fluids*, 21(094104), 2009. Submitted.

M. P. Boyce. *Gas turbine engineering handbook*. Elsevier, Jordan Hill, Oxford, UK, 2006.

J. Braun, C. Thieulot, P. Fullsack, M. DeKool, C. Beaumont, and R. Huismans. DOUAR: A new three-dimensional creeping flow numerical model for the solution of geological problems. *Phys. Earth and Planetary Inter.*, 171:76–91, 2008.

A. C. Carruthers, A. L. R. Thomas, and G. K. Taylor. Automatic aeroelastic devices in the wings of a steppe eagle Aquila nipalensis. *J. Exp. Biology*, 210:4136–4149, 2007.

L. N. Cattafesta, Q. Song, D. R. Williams, C. W. Rowley, and F. S. Alvi. Active control of flow-induced cavity oscillations. *Prog. Aerospace Sci.*, 44:479–502, 2008.

X. Chen, I. M. Navon, and F. Fang. A dual-weighted trust-region adaptive POD 4D-VAR applied to a finite-element shallow-water equations model. *Int. J. Numer. Meth. Fluids*, 60:709–732, 2009.

M-C. Chiang, A.D. Leow, A.D. Klunder, R.A. Dutton, M. Barysheva, S.E. Rose, K.L. McMahon, G.I. de Zubicaray, A.W. Toga, and P.M. Thompson. Fluid registration of diffusion tensor images using information theory. *IEEE Trans. Medical Imaging*, 27:442–456, 2008.

R. Clark, E. H. Dowell, D. Cox, H. C. Curtiss, J. W. Edwards, K. C. Hall, D. A. Peters, T. W. Strganac, R. H. Scalan, E. Simiu, and F. Sisto. *A Modern Course In Aeroelasticity.* Springer Verlag, 2004.

L. Cordier, B. Abou El Majd, and J. Favier. Calibration of POD reduced-order models using Tikhonov regularization. *Int. J. Numer. Meth. Fluids*, 63:269–296, 2010.

M. Couplet, C. Basdevant, and P. Sagaut. Calibrated reduced-order pod galerkin system for fluid flow modeling. *J. Comput. Phys.*, 207:192–220, 2005.

J. L. Crassidis. Sigma-point Kalman filtering for integrated GPS and inertial navigation. *IEEE Transactions on Aerospace and Electronic Systems*, 42: 750–756, 2006.

J. D'Adamo, R. Sosa, A. Cammilleri, and G. Artana. Reduced order models for EHD controlled wake flow. *J. of Phys.: Conf. Series*, 166(012014), 2009. X Meeting on Recent Advances in the Physics of Fluids and their Applications.

M. J. de C. Henshaw, K. J. Badcock, G. A. Vio, C. B. Allen, J. Chamberlain, I. Kaynes, G. Dimitriadis, J. E. Cooper, M. A. Woodgate, A. M. Rampurawala, D. Jones, C. Fenwick, A. L. Gaitonde, N. V. Taylor, D. S. Amor, T. A. Eccles, and C. J. Denley. Non-linear aeroelastic prediction for aircraft applications. *Prog. Aerospace Sci.*, 43:63–137, 2007.

E. de Langre. Effects of wind on plants. *Ann. Rev. Fluid Mech.*, 40:141–168, 2008.

A.E. Deane, I.G. Kevrekidis, G.E. Karniadakis, and S.A. Orszag. Low-dimensional models for complex geometry flows: Application to grooved channels and circular cylinders. *Phys. Fluids A*, 3(10):2337–2354, 1991.

J. D. DeLaurier. An aerodynamic model for flapping-wing flight. *Aeronaut. J.*, 97:125–130, 1993.

C.L. DeMarco and G.C. Verghese. Bringing phasor dynamics into the power system load flow. In *North American Power Symposium*, pages 463–469, 1993.

L. Demasi and E. Livne. Dynamic aeroelasticity of structurally nonlinear configurations using linear modally reduced aerodynamic generalized forces. *AIAA J.*, 47:70–90, 2009.

I. Demirdžić, S. Muzaferija, M. Perić, and E. Schreck. Numerical method for simulation of flow problems involving moving and sliding grids. In *Proc. 7th Int. Symp. Comp. Fluid Dyn.*, pages 359–364, 1997.

R. Diziol and J. Bender D. Bayer. Volume conserving simulation of deformable bodies. In *Proc. Eurographics*, 2009. computer graphics, spring analogy,elastic body,numerical methods.

H. Dong, M. Bozkurttas, R. Mittal P. Madden, and G. V. Lauder. Computational modelling and analysis of the hydrodynamics of a highly deformable fish pectoral fin. *J. Fluid Mech.*, 645:345–373., 2010.

E. H. Dowell and K. C. Hall. Modeling of fluid-structure interaction. *Ann. Rev. Fluid Mech.*, 33:445–490, 2001.

Q. Du and M. Gunzburger. Centroidal voronoi tessellation based proper orthogonal decompositon analysis. In *Control and Estimation of Distributed Parameter Systems*, volume 143 of *International Series of Numerical Mathematics*, pages 137 –150. Birkhauser, 2003.

A. Edelman, T. A. Arias, and S. T. Smith. The geometry of algorithms with ortogonality constraints. *SIAM J. Matrix Anal. Appl.*, 20:303–353, 1998.

B. I. Epureanu, E. H. Dowell, and K. C. Hall. Mach number influence on reduced-order models of inviscid potential flows in turbomachinery. *J. Fluids Engineering*, 124:977–987, 2002.

M. Fahl. *Trust-region methods for flow control based on reduced order modelling*. PhD thesis, Universität Trier, 2000.

C. Farhat, C. Degand, B. Koobus, and M. Lesoinne. Torsional springs for two-dimensional dynamic unstructured fluid meshes. *Comput. Meth. Appl. Mech. Enrgrg.*, 163:231 – 245, 1998.

Z. Feng and A. Soulaïmani. Nonlinear aeroelasticity modeling using a reduced order model based on proper orthogonal decomposition. In *ASME Pressure Vessels and Piping Division Conference*, 2007. Paper PVP2007-26006.

FFAST. Ffast: Future fast aeroelastic simulation technologies. Technical report, European South Africa Science and Technology Advancement Programme (ESASTAP), 2010.

F. E. Fish and G. V. Lauder. Passive and active flow control by swimming fishes and mammals. *Ann. Rev. Fluid Mech.*, 38:193–224, 2006.

K. Fitzpatrick, Y. Feng, R. Lind, A. J. Kurdila, and D. W. Mikolaitis. Flow control in a driven cavity incorporating excitation phase differential. *J. Guidance, Control, and Dynamics*, 28:63–70, 2005.

C. Foiaş, O. Manley, and R. Temam and. Modelling of the interaction of small and large eddies in two dimensional turbulent flows. *RAIRO - Modél. math. et anal. numér*, 22:93 – 118, 1988.

C. Foias, G. R. Sell, and R. Temam. Inertial manifolds for nonlinear evolutionary equations. *J. Diff. Eqs.*, 73:309–353, 1988.

B. D. O. Anderson G. Obinata. *Model Reduction for Control System Design*. Springer Verlag, 2000.

B. Galletti, A. Bottaro, C.-H. Bruneau, and A. Iollo. Accurate model reduction of transient and forced wakes. *Eur. J. Mech., B/Fluids*, 26:354–366, 2007.

J. Gerhard, M. Pastoor, R. King, B.R. Noack, A. Dillmann, M. Morzyński, and G. Tadmor. Model-based control of vortex shedding using low-dimensional Galerkin models. In *33rd AIAA Fluids Conference and Exhibit*, 2003. AIAA Paper 2003-4262.

A. Glezer and M. Amitay. Synthetic jets. *Annu. Rev. Fluid Mech.*, 34: 503–529, 2002.

M. Goman and A. Khrabrov. State space representation of aerodynamic characteristics of an aircrat at high angles of attack. *J. Aircraft*, 31 (1109–1115), 1994.

A.N. Gorban, N. K. Kazantzis, I. G. Kevrekidis, H.C. Öttinger, and C. Theodoropoulos, editors. *Model Reduction and Coarse-Graining Approaches for Multiscale Phenomena*. Springer Verlag, 2006.

W. R. Graham, J. Peraire, and K. Y. Tang. Optimal control of vortex shedding using low order models - Part I Open loop model development. *Int. J. Numer. Meth. Fluids*, 44:945–972, 1999a.

W. R. Graham, J. Peraire, and K. Y. Tang. Optimal control of vortex shedding using low order models - Part II model based control. *Int. J. Numer. Meth. Fluids*, 44:973–990,, 1999b.

M. S. Grewal and A. P. Andrews. *Kalman Filtering: Theory and Practice*. Prentice Hall, 1993.

J. Guckenheimer and P. Holmes. *Nonlinear Oscillations, Dynamical Systems, and Bifurcation of Vector Fields*. Springer Verlag, 6th printing edition, 2002.

B. Günther, F. Thiele, R. Petz, W. Nitsche, J. Sahner, T. Weinkauf, and H.C. Hege. Control of separation on the flap of a three element high-lift configuration'. In *45th AIAA Aerospace Sciences Meeting and Exhibit*, 2007. Paper AIAA-2007–0265.

K. C. Hall, R. E. Kielb, and J. P. Thomas, editors. *Unsteady aerodynamics, aeroacoustics and aeroelasticity of turbomachines*. Springer Verlag, 2006.

A. Hay, J. Borggaard, and D. Pelletier. Local improvements to reduced-order models using sensitivity analysis of the proper orthogonal decomposition. *J. Fluid Mech.*, 629:41–72, 2009.

S. Ho, H. Nassef, N. Pornsinsirirak, Y.-C. Taib, and C.-M. Hoa. Unsteady aerodynamics and flow control for flapping wing flyers. *Prog. Aerospace Sci.*, 39:635–681, 2003.

C. A. Holmes. Bounded solutions of the nonlinear parabolic amplitude equation for plane Poiseuille flow. *Proc. Roy. Soc. London A*, 402:299–322, 1985.

P. Holmes, J.L. Lumley, and G. Berkooz. *Turbulence, Coherent Structures, Dynamical Systems and Symmetry.* Cambridge University Press, 1998.

C. Homescu, L. R. Petzold, and R. Serban. Error estimation for reduced-order models of dynamical systems. *SIAM J. Numer. Anal.*, 43:1693–1714, 2005.

M. Hong, S. Jung, M.-H. Choi, and S. W.J. Welch. Fast volume preservation for a mass-spring system. *IEEE Comp. Graph. Appl.*, 26:83–91, 2006.

S.-Y. Hsu and C.-L. Chang. Mesh deformation based on fully stressed design: The method and two-dimensional examples. *Int. J. Numer. Meth. Engng.*, 72:606–629,, 2007.

G.-H. Hu, D.-J. Sun, X.-Y. Yin, and B.-G. Tong. Hopf bifurcation in wakes behind a rotating and translating circular cylinder. *Phys. Fluids*, 8: 1972–1974, 1996.

G. Irving, C. Schroeder, and R. Fedkiw. Volume conserving finite element simulations of deformable models. *Int. Conf. Comp. Graphics and Interactive Techniques (ACM SIGGRAPH)*, 2007.

D. Ishihara and S. Yoshimura. A monolithic approach for interaction of incompressible viscous fluid and an elastic body based on fluid pressure Poisson equation. *Int. J. Numer. Meth. Fluids*, 64:167–203, 2005.

W.-T. Joe and T. Colonius. Feedback control of vortex shedding from an inclined flat plate. *Theor. Comp. Fluid Dyn.*, 2010.

W.-T. Joe, K. Taira, T. Colonius, D. G. MacMynowski, and G. Tadmor. Closed-loop control of vortex shedding on a two-dimensional flat-plate airfoil at a low Reynolds number. In *46th AIAA Aerospace Sciences Meeting and Exhibit*, 2008. AIAA P-2008-634.

K. Kaepernick, L. Koop, and K. Ehrenfried. Investigation of the unsteady flow field inside a leading edge slat cove. In *11th AIAA/CEAS Aeroacoustics Conference*, 2005. AIAA Paper 2005-2813.

R. Kamakoti and W. Shyy. Fluid–structure interaction for aeroelastic applications. *Prog. Aerospace Sci.*, 40:535–558, 2004.

C. Kasnakoğlu, A. Serrani, and M. Ö. Effe. Control input separation by actuation mode expansion for flow control problems. *Int. J. Control*, 81: 1475–1492, 2008.

C. Kasnakoğlu, R. C. Camphouse, and A. Serrani. Reduced-order model-based feedback control of flow over an obstacle using center manifold methods. *ASME J. Dyn. Sys. Meas. Cotr.*, 131(011011), 2009.

N. Kato and S. Kamimura. *Bio-mechanisms of Swimming and Flying*. Springer Verlag, 2008.

M. A. Kegerise, R. H. Cabell, and L. N. Cattafesta. Real-time feedback control of flow-induced cavity tones—Part 1: Fixed-gain control, Part 2: Adaptive control. *J. Sound and Vibration*, 3007:906–923, 924–940, 2007.

J. Kim and T. R. Bewley. A linear systems approach to flow control. *Ann. Rev. Fluid Mech.*, 39:383–417, 2007.

R. King (editor) *Active Flow Control II*. Number 108 in Lecture Notes on Numerical Fluid Mechanics and Interdisciplinary Design. Springer Verlag, Berlin, 2010.

S. Kota, R. Osborn, G. Ervin, D. Maric, P. Flick, and D. Paul. Mission adaptive compliant wing–design, fabrication and flight test. In *Morphing Vehicles*, number RTO-MP-AVT-168-18 in . NATO Research and Technology Organization, 2009.

I. Lasiecka and R. Triggiani. *Control theory for partial differential equations: continuous and approximation theories*. Cambridge University Press, 2000.

E. Lauga and T. R. Powers. The hydrodynamics of swimming microorganisms. *Rep. Prog. Phys.*, 72(096601), 2009.

O. Lehmann, M. Luchtenburg, B.R. Noack, R. King, M. Morzynski, and G. Tadmor. Wake stabilization using POD Galerkin models with interpolated modes. In *44th IEEE Conference on Decision and Control and European Control Conference ECC, Seville, Spain*, pages 500–505, 2005.

J. G. Leishman. *Principles of helicopter aerodynamics*. Cambridge University Press, 2006.

H. Lev-Ari and A. Stanković. Phasor-banks: Customizable filter banks for robust dynamic time-frequency analysis. In *40th North American Power Symposium (NAPS)*, 2008.

G. C. Lewin and H. Haj-Hariri. Reduced-order modeling of a heaving airfoil. *AIAA J.*, 43:270–283, 2005.

Y. Liang, Y. Yuga, and M. Taya. Design of membrane actuator based on ferromagnetic shape memory alloy composite for synthetic jet applications. *Sens. Act. A: Physical*, 125:512–518, 2006.

E. Liberge and A. Hamdouni. Reduced order modelling method via proper orthogonal decomposition (POD) for flow around an oscillating cylinder. *J. Fluids and Structures*, 26:292–311, 2010.

E. Liberge, M. Benaouicha, and A. Hamdouni. Proper orthogonal decomposition investigation in fluid structure interaction. *Euro. J. Comp. Mech.*, 16:401–418, 2008.

J. Little, M. Nishihara, I. Adamovich, and M. Samimy. High-lift airfoil trailing edge separation control using a single dielectric barrier discharge plasma actuator. *Exps. Fluids*, 48:521–537, 2009.

E. Livne. Future of airplane aeroelasticity. *J. Aircraft*, 40:1066–1091, 2003.

D. Lo Jacono, J. N. Sørensen, M. C. Thompson, and K. Hourigan. Control of vortex breakdown in a closed cylinder with a small rotating rod. *J. Fluids and Structures*, 24:1278–1283, 2008.

I. Lopez and N. Sarigul-Klijn. A review of uncertainty in flight vehicle structural damage monitoring, diagnosis and control: Challenges and opportunities. *Prog. Aerospace Sci.*, 46:247–273, 2010.

M. Luchtenburg, G. Tadmor, O. Lehmann, B. R. Noack, R. King, and M. Morzynski. Tuned POD Galerkin models for transient feedback regulation of the cylinder wake. In *44th AIAA Aerospace Sciences Meeting and Exhibit*, 2006. Paper AIAA-2006-1407.

M. Luchtenburg, B. R. Noack, B. Günther, R. King, and G. Tadmor. A generalised mean-field model of the natural and high-frequency actuated flow around a high-lift configuration. *J. Fluid Mech.*, 623:283–316, 2009.

M. Manhart. Energy transfer between coherent structures in the wake of a hemisphere. In J.N. Sorensen, E.J. Hopfinger, and N. Aubry, editors, *Simulation and Identification of Organized Structures in Flows*, pages 499–508. Kluwer Academic Publishers, 1998.

J. E. Marsden and M. McCracken. *The Hopf Bifurcation and Its Applications*. Springer Verlag, 1976.

L. Mathelin and O. P. Le Maitre. Robust control of uncertain cylinder wake flows based on robust reduced order models. *Computers & Fluids*, 38: 1168–1182, 2009.

W. J. McCroskey. Unsteady airfoils. *Ann. Rev. Fluid Mech.*, 14:285–311, 1982.

T. Meurer, K. Graichen, and E.-D. Gilles, editors. *Control and observer design for nonlinear finite and infinite dimensional Systems*, volume 322 of *Lecture Notes in Control and Information Sciences*. Springer Verlag, 2002.

I. Mezić. Spectral properties of dynamical systems, model reduction and decompositions. *Nonlinear Dynamics*, 41:309–325, 2005.

A. Mishra, G. Tadmor, and Z. Rusak. The dynamics of the axisymmetric vortex breakdown in a pipe. In *38th AIAA Fluid Dynamics / 4th Flow Control Conference and Exhibit*, 2008. AIAA Paper 2008-3799.

A. Mishra, G. Tadmor, and Z. Rusak. Bifurcation analysis of the axisymmetric vortex breakdown in a pipe. In *39th AIAA Fluid Dynamics Conference / 27th AIAA Applied Aerodynamics Conference*, 2009. AIAA Paper-2009-3709.

S. Mittal and B. Kumar. Flow past a rotating cylinder. *J. Fluid Mech.*, 476:303–334, 2003.

P. Mokhasi and D. Rempfer. Sequential estimation of velocity fields using episodic proper orthogonal decomposition. *Physica D*, 237:3197–3213, 2008.

P. Mokhasi, D. Rempfer, and S. Kandala. Predictive flow-field estimation. *Phys. D*, 238:290–308, 2009.

E. Moreau. Airflow control by non-thermal plasma actuators. *J. Phys. D: Appl. Phys.*, 40:605–636, 2007.

M. Morzyński, W. Stankiewicz, B. R. Noack, R. King, F. Thiele, and G. Tadmor. Continuous mode interpolation for control-oriented models of fluid flow. In R. King, editor, *Active Flow Control*, volume 95 of *Notes on Numerical Fluid Mechanics and Multidisciplinary Design*, pages 260–278. Springer Verlag, Berlin, Germany, 2007.

S. M. Murman, M. J. Aftosmis, and M. J. Berger. Implicit approaches for moving boundaries in a 3-D Cartesian method. In *41st AIAA Aerospace Sciences Meeting*, 2003. AIAA Paper 2003-1119.

I. M. Navon. Data assimilation for numerical weather prediction : A review. In S. K. park and L. Xu, editors, *Data Assimilation for Atmospheric, Oceanic, and Hydrologic Applications*, pages 21–66. Springer Verlag, I. M. Navon.

H. Nijmeijer and A.J. van der Schaft. *Nonlinear Dynamical Control Systems*. Springer–Verlag, New York, 1990.

B. R. Noack, M. Schlegel, M. Morzyński, and G. Tadmor. System reduction strategy for Galerkin models of fluid flows. *Int. J. Numer. Meth. Fluids*, 63:231–248, 2010. doi: 10.1002/fld.2049.

B.R. Noack and H. Eckelmann. A low-dimensional Galerkin method for the three-dimensional flow around a circular cylinder. *Phys. Fluids*, 6(1): 124–143, 1994.

B.R. Noack, P. Papas, and P.A. Monkewitz. Low-dimensional Galerkin model of a laminar shear-layer. Technical Report 2002-01, Laboratoire de Mécanique des Fluides, Département de Genie Mécanique, Ecole Polytechnique Fédérale de Lausanne, Switzerland, 2002.

B.R. Noack, K. Afanasiev, M. Morzyński, G. Tadmor, and F. Thiele. A hierarchy of low-dimensional models for the transient and post-transient cylinder wake. *J. Fluid Mech.*, 497:335–363, 2003.

B.R. Noack, G. Tadmor, and M. Morzyński. Actuation models and dissipative control in empirical Galerkin models of fluid flows. In *The 2004 American Control Conference*, volume 6, pages 5722 –5727, Boston, MA, U.S.A., 2004a. Paper **FrP15.6**.

B.R. Noack, G. Tadmor, and M. Morzyński. Low-dimensional models for feedback flow control. Part I: Empirical Galerkin models. In *2nd AIAA Flow Control Conference*, 2004b. AIAA Paper 2004-2408.

B.R. Noack, P. Papas, and P.A. Monkewitz. The need for a pressure-term representation in empirical Galerkin models of incompressible shear flows. *J. Fluid Mech.*, 523:339–365, 2005.

B.R. Noack, M. Schlegel, B. Ahlborn, G. Mutschke, M. Morzyński, P. Comte, and G. Tadmor. A finite-time thermodynamics of unsteady flows. *J. Nonequilibrium Thermodynamics*, 33:103–148, 2008.

T. E. Noll, S. D. Ishmael, B. Henwood, M. E. Perez-Davis, G. C. Tiffany, J. Madura, M. Gair, J. H. Brown, and T. Wierzbanowski. Technical findings, lessons learned, and recommendations resulting from the helios prototype vehicle mishap. In *RTO Applied Vehicle Technology Panel (AVT) Workshop*, volume RTO-MP-AVT-145 of *UAV Design Processes / Design Criteria for Structures*. NATO Research and Technology Organisation, 2007.

M. Pastoor, R. King, B.R. Noack, and G. Tadmor. Observers & feedback control for shear layer vortices. In *44th IEEE Conference on Decision and Control and European Control Conference ECC, Seville, Spain*, 2005.

M. Pastoor, B. R. Noack, R. King, and G. Tadmor. Spatiotemporal waveform observers and feedback in shear layer control. In *44th AIAA Aerospace Sciences Meeting and Exhibit*, 2006. Paper AIAA-2006-1402.

M. Pastoor, L. Henning, B. R. Noack, R. King, and G. Tadmor. Feedback shear layer control for bluff body drag reduction. *J. Fluid Mech.*, 608: 161–196, 2008.

M. J. Patil. Nonlinear gust response of highly flexible aircraft. In *Proc. 48th AIAA , Structural Dynamics, and Materials Conf.*, 2007. AIAA Paper 2007-2103.

E. Pendleton. Back to the future: How active aeroelastic wings are a return to aviation's beginnings and a small step to future bird-like wings. In *RTO AVT Symposium on Active Control Technology for Enhanced Performance Operational Capabilities of Military Aircraft, Land Vehicles and Sea Vehicles*, 2000.

P.-O. Persson and J. Peraire. Curved mesh generation and mesh refinement using Lagrangian solid mechanics. In *47th AIAA Aerospace Sciences Meeting and Exhibit*, 2009. AIAA Paper 2009-949.

D. A. Peters, M.-C. Hsieh, and A. Torrero. A state-space airloads theory for flexible airfoils. *J. Amer. Helicopter Soc.*, 51:329–342, 2007.

R. D. Prabhu, S. Scott Collis, and Y. Chang. The influence of control on proper orthogonal decomposition of wall-bounded turbulent flows. *Phys. Fluids*, 13:520—-537, 2001.

B. Protas. Center manifold analysis of a point-vortex model of vortex shedding with control. *Phys. D*, 228:179–187, 2007.

B. Protas. Vortex dynamics models in flow control problems. *Nonlinearity*, 21:R203–R250, 2008.

B. Raghavan and M. J. Patil. Flight control for flexible, high-aspect-ratio flying wings. *AIAA J. Guidance, Control, and Dynamics*, 33:64, 2010.

S. S. Ravindran. Reduced-order adaptive controllers for fluid flows using POD. *J. Scientific Computing*, 15:457–478, 2000.

D. Rempfer. *Kohärente Strukturen und Chaos beim laminar-turbulenten Grenzschichtumschlag (transl.: Coherent structures and chaos of the laminar-turbulent boundary-layer transition)*. PhD thesis, Fakultät Verfahrenstechnik der Universität Stuttgart, 1991. (Part of this work has been published by Rempfer, D. and Fazle, F.H. (1994) in J. Fluid Mech. 260 & 275).

R. Roszak, P. Posadzy, W. Stankiewicz, and M. Morzyński. Fluid structure interaction for large scale complex geometry and non-linear properties of structure. *Archives of Mechanics*, 61:1–24, 2009.

C. W. Rowley, I. G. Kevrekidis, J. E. Marsden, and K. Lust. Reduction and reconstruction for self-similar dynamical systems. *Nonlinearity*, 16: 1257–1275, 2003.

C.W. Rowley. Model reduction for fluids, using balanced proper orthogonal decomposition. *Int. J. on Bifurcation and Chaos*, 15:997–1013, 2005.

A. E. Russell. Some factors affecting large transport aeroplanes with turboprop engines: The thirteenth Wright brothers lecture. *J. Aeronautical Sciences*, 17:67–93, 1950.

R. Sánchez-Peña and M. Sznaier. *Robust Systems Theory and Applications*. Wiley & Sons, Inc., 1998.

T. P. Sapsis and P. F. J. Lermusiaux. Dynamically orthogonal field equations for continuous stochastic dynamical system. *Phys. D*, 238:2347–2360, 2009.

M. Schatz, B. Günther, and F. Thiele. Computational investigation of separation control over high-lift airfoil flows. In R. King, editor, *Active Flow Control*, volume 95 of *Notes on Numerical Fluid Mechanics and Multidisciplinary Design*. Springer Verlag, Berlin, 2007.

W. H. A. Schilders, H. A. van der Vorst, and J. Rommes, editors. *Model Order Reduction: Theory, Research Aspects and Applications*, volume 13 of *The European Consortium for Mathematics in Industry*. Springer Verlag, 2008.

D. M. Schuster, D. D. Liu, and L. J. Huttsell. Computational aeroelasticity: Success, progress, challenge. *J. Aircraft*, 40:843–856, 2003.

W. Shyy, H. Aono, S. K. Chimakurthi, P. Trizila, C.-K. Kang, C. E. S. Cesnik, and H. Liu. Recent progress in flapping wing aerodynamics and aeroelasticity. *Prog. Aerospace Sci.*, 2010.

S. Siegel, K. Cohen, J. Seidel, M. Luchtenburg, and T. McLaughlin. Low dimensional modelling of a transient cylinder wake using double proper orthogonal decomposition. *J. Fluid Mech*, 2008. accepted for publication.

W. A. Silva, V. N. Vasta, and R. T. Biedron. Development of unsteady aerodynamic and aeroelastic reduced-order models using the FUN3D code. In *Int. Forum on Aeroelasticituy and Structural Dynamics (IFASD)*, 2009.

W. Stankiewicz, M. Morzyński, R. Roszak, B. R. Noack, and G. Tadmor. Reduced order modelling of flow around an airfoil with a changing angle of attack. *Archives of Mechanics*, 60:509–526, 2008.

T. Stathopoulos and C. C. Baniotopoulos, editors. *Wind Effects on Buildings and Design of Wind-Sensitive Structures*. Springer Verlag, 2007.

E. Strømmen. *Theory of Bridge Aerodynamics*. Springer Verlag, 2006.

G. Tadmor. On approximate phasor models in dissipative, bilinear systems. *IEEE Transaction on Circuits & Systems I: Fundamental Theory*, 49: 1167–1179, 2002.

G. Tadmor and B.R. Noack. Dynamic estimation for reduced Galerkin models of fluid flows. In *The 2004 American Control Conference*, volume 1, pages 746 –751, Boston, MA, U.S.A., 2004. Paper **WeM18.1**.

G. Tadmor, B.R. Noack, M. Morzyński, and S. Siegel. Low-dimensional models for feedback flow control. Part II: Controller design and dynamic estimation. In *2nd AIAA Flow Control Conference*, 2004. AIAA Paper 2004-2409.

G. Tadmor, M. D. Centuori, B. R. Noack, M. Luchtenburg, O. Lehmann, and M. Morzyński. Low Order Galerkin Models for the Actuated Flow Around 2-D Airfoils. In *45th AIAA Aerospace Sciences Meeting and Exhibit*, 2007a. AIAA Paper 2007-1313.

G. Tadmor, J. Gonzalez, O. Lehmann, B. R. Noack, M. Morzyński, and W.Stankiewicz. Shift Modes and Transient Dynamics in Low Order, Design Oriented Galerkin Models. In *45th AIAA Aerospace Sciences Meeting and Exhibit*, 2007b. Paper AIAA 2007-111.

G. Tadmor, D. Bissex, B. R. Noack, M. Morzyński, T. Colonius, and K. Taira. Temporal-harmonic specific POD mode extraction. In *4th Flow Control Conference / 38th AIAA Fluid Dynamics Conference and Exhibit*, 2008. AIAA Paper 2008-4190.

G. Tadmor, O. Lehmann, B. R. Noack, and M. Morzyński. Mean field representation of the natural and actuated cylinder wake. *Phys. Fluids*, 22(034102), 2010.

T. E. Tezduyar. Finite element methods for flow problems with moving boundaries and interfaces. *Arch. of Comp. Methods in Eng.*, 2001.

T. Theodorsen. General theory of aerodynamic instability and the mechanism of flutter. Technical Report 496, National Advisory Commitee for Aeronautics (NACA), 1935.

R. Vazquez and M. Krstic. A closed-form feedback controller for stabilization of the linearized 2-D Navier–Stokes Poiseuille system. *IEEE Trans. Autom. Contr.*, 52:2298–2312, 2007.

T. von Kármán and H. Rubach. über den mechanismusdes fl"ussigkeits-und luftwiderstandes. *Phys. Z.*, 13:49–59, 1912.

O. Wiederhold, R. King, and B. R. Noack. Robust control in turbumachinary configurations. In R. King, editor, *Active Flow Control II*, volume 108 of *Lecture Notes on Numerical Fluid Mechanics and Interdisciplinary Design*, pages 187–201. Springer Verlag, 2010.

D. R. Williams, G. Tadmor, T. Colonius, W. Kerstens, V. Quach, and S. Buntain. The lift response of a stalled wing to pulsatile disturbances. *AIAA J.*, 47:3031–3037, 2009.

C.H.K. Williamson. Vortex dynamics in the cylinder wake. *Annu. Rev. Fluid Mech.*, 28:477–539, 1996.

D. G. Wilson, D. E. Berg, M. F. Barone, J. C. Berg, B. R. Resor, and D. W. Lobitz. Active aerodynamic blade control design for load reduction on large wind turbines. In *Proc. Euro. Wind Energy Conf. and Exhibit. (EWEC)*, 2009.

X. Xie, L. C. Musson, and M. Pasquali. An isochoric domain deformation method for computing steady free surface flows with conserved volumes. *J. Comp. Phys.*, 226:398–413, 2007.

H. Yu, M. Leeser, G. Tadmor, and S. Siegel. Real-time particle image velocimetry for feedback loops using FPGA implementation. *AIAA J. Aerospace Computing, Information, and Communication*, 3:52–56, 2006.